TECHNISCHE UNIVERSITÄT MÜNCHEN

Fachgebiet für Experimentelle Radioonkologie

Determination of the dynamics of tumor hypoxia during radiation therapy using biological imaging on mouse xenograft tumors

Constantin Alin Maftei

Vollständiger Abdruck der von der Fakultät Wissenschaftszentrum Weihenstephan für Ernährung, Landnutzung und Umwelt der Technischen Universität München zur Erlangung des akademischen Grades eines

Doktors der Naturwissenschaften

genehmigten Dissertation.

Vorsitzender: Univ.-Prof. Dr. B. Küster

Prüfer der Dissertation: 1. Univ.-Prof. Dr. G. Multhoff

2. Univ.-Prof. Dr. P. Vaupel (i.R.)
Johannes Gutenberg Universität Mainz

Die Dissertation wurde am 08.01.2013 bei der Technischen Universität München eingereicht und durch die Fakultät Wissenschaftszentrum Weihenstephan für Ernährung, Landnutzung und Umwelt am 02.04.2013 angenommen.

Erklärung

Ich, Constantin Alin Maftei erkläre an Eides statt, dass ich die der Fakultät Wissenschaftszentrum Weihenstephan für Ernährung, Landnutzung und Umwelt (WZW) der Technischen Universität München zur Promotionsprüfung vorgelegte Arbeit mit dem Titel:

„Determination of the dynamics of tumor hypoxia during radiation therapy using biological imaging on mouse xenograft tumors“

in Experimentelle Radioonkologie der Klinikum rechts der Isar der TU München, unter der Anleitung und Betreuung durch Univ.-Prof. Dr. Gabriele Multhoff, ohne sonstige Hilfe erstellt und bei der Auffassung nur die gemäß § 6 Abs. 5 angegebenen Hilfsmittel benutzt habe.

Ich habe keine Organisation eingeschaltet, die gegen Entgelt Betreuerinnen und Betreuer für die Anfertigung von Dissertation sucht, oder die mit obliegenden Pflichten hinsichtlich der Prüfungsleistungen für mich ganz oder teilweise erledigt.

Ich habe die Dissertation in dieser oder ähnlicher Form in keinem anderen Prüfungsverfahren als Prüfungsleistung vorgelegt.

Ich habe den angestrebten Doktorgrad noch nicht erworben und bin nicht in einem früheren Promotionsverfahren für den angestrebten Doktorgrad endgültig gescheitert.

Die Promotionsordnung der Technischen Universität München ist mir bekannt.

München, den 08.01.2013 ……

Unterschrift

This cumulative thesis is based on the following consecutive publications on chronic and acute hypoxia in xenografted tumors. The original publications are included in the appendix.

1. Maftei CA, Bayer C, Shi K, Astner ST, Vaupel P. Quantitative assessment of hypoxia subtypes in microcirculatory supply units of malignant tumors using (immuno-)fluorescence techniques. Strahlenther Onkol 2011;187:260-6.

2. Maftei CA, Bayer C, Shi K, Astner ST, Vaupel P. Changes in the fraction of total hypoxia and hypoxia subtypes in human squamous cell carcinomas upon fractionated irradiation: Evaluation using pattern recognition in microcirculatory supply units. Radiother Oncol 2011;101:209-16.

3. Maftei CA, Shi K, Bayer C, Astner ST, Vaupel P. Comparison of (immuno-)fluorescence data with serial [^{18}F]Fmiso PET/CT imaging for assessment of chronic and acute hypoxia in head and neck cancers. Radiother Oncol 2011;99:412-7.

4. Maftei CA, Bayer C, Shi K, Vaupel P. Intra- and intertumor heterogeneities in total, chronic, and acute hypoxia in xenografted squamous cell carcinomas: Detection and quantification using (immuno-)fluorescence techniques. Strahlenther Onkol 2012;188:606-615.

Abbreviations

AFN	Atipamezole Flumazenil Naloxone
aHF	Acute Hypoxic Fraction
cHF	Chronic Hypoxic Fraction
CI	Confidence Interval
CT	Computer Tomography
DMEM	Dulbecco's Modified Eagle Medium
DMSO	Dimethyl Sulphoxide
DPBS	Dulbecco's Phosphate Buffered Saline
^{18}F-Fmiso	^{18}F-Fluoromisonidazole
FCS	Fetal Calf Serum
H&E	Hematoxylin & Eosin
IF	(Immuno-)fluorescence
Mab	Monoclonal Antibody
MCSU	Microcirculatory Supply Unit
MMF	Medetomidine Midazolam Fentanyl
NEAA	Non-Essential Amino Acids
PBS	Phosphate Buffered Saline
PET/CT	Positron Emission Tomography & Computer Tomography
PAD	Primary Antibody Diluent
P/S	Penicillin & Streptomycin
SEM	Standard Error of the Mean
SCCHN	Squamous Cell Carcinoma of the Head and Neck
SPSS	Statistical Package for the Social Sciences
SUV	Standard Uptake Volume
TCD_{50}	Tumor Control Dose 50%
ZPF	Center for preclinical research (Zentrum für Präklinische Forschung)

SUMMARY

Determination of the dynamics of tumor hypoxia during radiation therapy using biological imaging on mouse xenograft tumors

Background: Hypoxia is a characteristic of solid tumors that can favor the development of a more aggressive tumor phenotype and can lead to treatment resistance. Traditionally, hypoxia is classified into two different subtypes: *chronic* and *acute.* Chronic hypoxia is mostly caused by diffusion limitations, while acute hypoxia is mainly caused by transient disruptions in perfusion. A third and less studied subtype of hypoxia, termed hypoxemic hypoxia, has been identified recently. Hypoxemic hypoxia can be either chronic or acute. The purpose of this thesis was to shed light on the exact role of these three subtypes of hypoxia for radiation therapy. Additionally, the distribution of intra- and inter-tumoral hypoxia was investigated in FaDu tumors before irradiation.

Material & Methods: Xenograft tumors were established from squamous cell carcinoma of the head and neck. For *ex-vivo* studies on the existence of total hypoxia and hypoxia subtypes in tumors, cryosections were prepared and stained. H&E staining was performed for visualization of vital and necrotic tissue areas and an (immuno-)fluorescence method was developed to assess the fractions of chronic, acute and hypoxemic hypoxia before and after fractionated irradiation. For the non-invasive detection and classification of hypoxia, tumor-bearing mice were injected with the clinically used hypoxia marker ^{18}F-FMISO and scanned via PET/CT. Afterwards, the hypoxia fraction was quantified using the mathematical Wang model. These results were compared to the results derived by (immuno-)fluorescence analysis.

Results: The fraction of total hypoxia decreased in larger tumors and increased in smaller tumors from the apical to the basal part of the tumors. Chronic hypoxia was the most abundant hypoxia subtype, followed systematically by acute and hypoxemic hypoxia. Upon fractionated irradiation, the hypoxic fraction decreased in all tumor lines apart from one. The fraction of acute hypoxia was higher after non-invasive detection of hypoxia with ^{18}F-FMISO PET/CT (Wang Model) than after quantification using the (immuno-)fluorescence method.

Conclusions: Chronic hypoxia is the predominant subtype before and upon fractionated irradiation in all tumors, followed systematically by acute and hypoxemic hypoxia. The Wang Model is a promising non-invasive method for the detection and quantification of acute versus chronic hypoxia. Thus, further preclinical investigations will be necessary before implementation of the Wang model into the clinic.

ZUSAMMENFASSUNG

Bestimmung der Dynamik von Tumorhypoxie unter Bestrahlung mittels biologischer Bildgebungsverfahren in einem xenograft Tumormausmodell

Grundlage: Tumorhypoxie begünstigt bei soliden Tumoren die Ausbildung eines aggressiveren Phänotyps, der zu Therapieresistenz gegenüber Strahlentherapie führen kann. Traditionell wird die Hypoxie in zwei unterschiedliche Subtypen eingeteilt, die *chronische* und *akute Hypoxie*. Die chronische Hypoxie ist überwiegend durch eine limitierte Diffusion verursacht, während die akute Hypoxie eine Folge von vorübergehenden Perfusionsunterbrechungen ist. Ein dritter, weniger untersuchter, Subtyp der Hypoxie, die sogenannte hypoxämische Hypoxie, wurde vor kurzer Zeit beschrieben. Dieser dritte Hypoxiesubtyp kann sowohl chronisch als auch akut auftreten. Das Ziel dieser Doktorarbeit war es, die exakte Rolle dieser drei Hypoxiesubtypen in Bezug auf eine Strahlentherapie zu erarbeiten. Zudem wurde die intra- und intertumorale Verteilung der Tumorhypoxie in nicht bestrahlten FaDu Tumoren untersucht.

Material & Methoden: Xenografttumoren wurden aus Plattenepithelkarzinomen von Kopf und Hals generiert. Für die ex-vivo Untersuchungen des Auftretens von gesamter Hypoxie und den Hypoxiesubtypen in Tumoren wurden Kryoschnitten hergestellt und gefärbt. HE-Färbungen wurden durchgeführt, um vitale und nekrotische Geweberegionen zu visualisieren. Eine (Immun-)Fluoreszenzmethode wurde entwickelt um die Anteile an akuter, chronischer und hypoxämischer Hypoxie vor und nach der Bestrahlung in den Tumoren zu identifizieren. Für die nicht-invasive Untersuchung und Klassifizierung der Hypoxie wurden tumortragende Mäuse mit dem klinisch verwendeten Hypoxiemarker ^{18}F-FMISO injiziert und anschließend mittels PET/CT gescannt. Danach wurde der Hypoxieanteil mit Hilfe eines mathematischen Models (Wang Model) quantifiziert. Diese Ergebnisse wurden mit den aus der (Immun-)Fluoreszenz gewonnenen Ergebnissen verglichen.

Ergebnisse: Der Anteil an gesamter Hypoxie sinkt von der apikalen bis zur basalen Tumorseite in größeren Tumoren, steigt aber in selbiger Richtung in den kleineren Tumoren an. Die chronische Hypoxie war der am häufigsten vorhandene Hypoxiesubtyp, gefolgt von akuter und hypoxämischer Hypoxie. Der Hypoxieanteil sank nach fraktionierter Bestrahlung mit einer Ausnahme in allen Tumorlinien. Der Anteil akuter Hypoxie wurde von der nicht-invasiven Methode (^{18}F-FMISO PET/CT, Wang Model) im Vergleich zur invasiven (Immun-)Fluoreszenzanalyse als höher eingeschätzt.

Schlussfolgerung: Die chronische Hypoxie ist der in allen Tumoren am meisten vorhandene Hypoxiesubtyp vor und nach fraktionierter Bestrahlung, gefolgt von akuter und

hypoxämischer Hypoxie. Mit Hilfe des Wang Models kann man die Anteile von akuter und chronischer Hypoxie nach einer nicht invasiven ^{18}F-FMISO PET/CT Untersuchung quantifizieren. Zusammenfassend kann man sagen, dass das Wang-Model weiterer präklinischer Verbesserungen bedarf bevor es in die Klinik eingeführt werden kann.

1 INTRODUCTION

1.1 Tumor formation (Carcinogenesis)

Tumor formation is induced by somatic events leading to alterations in oncogenes, tumor-suppressor genes and microRNA genes [Croce 2008]. Thus, it is widely accepted that carcinogenesis is a multistep process [López-Lázaro M, 2010], which begins with carcinogenic factors (chemical, physical, mechanical etc), followed by a series of DNA alterations (mutations, epigenetic changes, aneuploidy and genetic instability) and ends with formation of neoplastic cells (cancer). These neoplastic cells respond abnormally to signals regulating cell growth and death. In the very early stages, tumors are mostly composed of avascular cell aggregates, which are provided with oxygen and nutrients from the surrounding tissue via diffusion. In advanced stages, (beginning at 1-2 mm in diameter), tumors begin to form stroma and vessels [Folkman 1976].

1.2 Tumor vascularity and oxygenation

Tumor vascularisation begins with the co-operation of pre-existing normal blood vessels from the surrounding tissue, and newly formed, mostly immature blood vessels (neo-angiogenesis) [Vaupel et al. 1989, Höckel and Vaupel 2001, Vaupel et al. 2001]. This type of vascular supply can be emphasized as a maximally stimulated system, which hardly fulfills the metabolic need of the growing tumor [Hirst and Flitney 1997]. The preexisting normal host vasculature undergoes a series of morphological and physiological changes. Eventually, the tumor microvessels become tortuous, elongated and dilated, but do not increase in number, leading to a reduction in exchange area for oxygen, nutrients, hormones, growth factors etc. Moreover, they can disintegrate, become obstructed or compressed. Excessive branching is also a characteristic of tumor microvessels, often accompanied by blind ending. Neovascularisation usually originates from preexisting venules in the tumor mass or from the adjacent host tissue. The vascular buds begin to form lumen and anastomose, these being the events leading to blood perfusion [Osinsky et al. 2011].

Tumor growth beyond 1-2 mm in diameter requires a supply of oxygen and nutrients via blood vessels [Folkman 1976]. Chaotic vascularisation represents a hallmark of solid tumors. This characteristic reflects not only the spatial distribution of vessels but also structural and functional abnormality. For instance, in the normal rat colon, (Fig. 1) capillaries within the

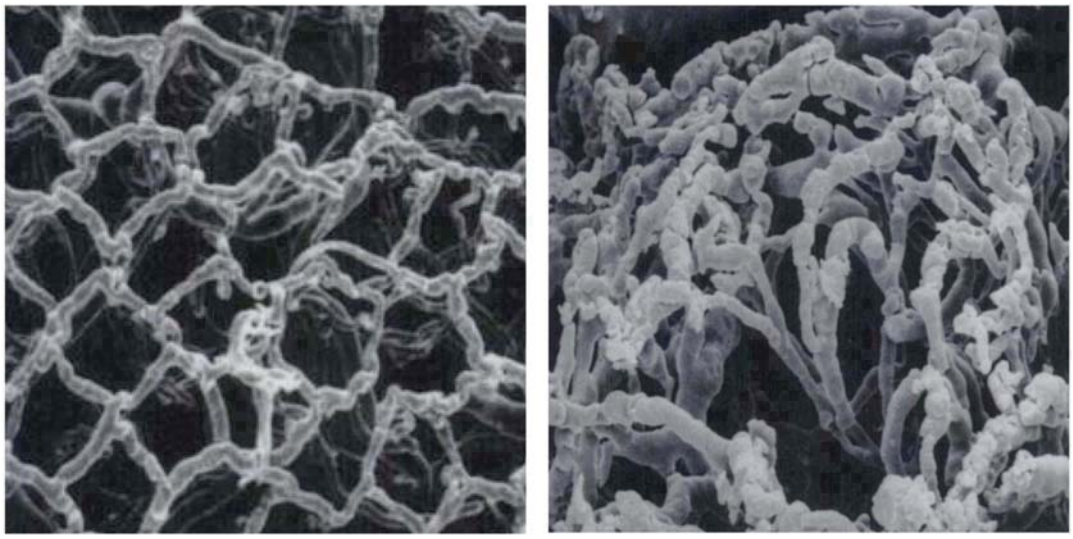

Fig. 1. Scanning electron microscopy of a vascular cast. The left picture shows a normal rat colon viewed from the luminal side. The right picture shows a moderately differentiated adenocarcinoma of the rat colon viewed from the surface of the tumor [modified from Skinner et al. 1990].

mucosa are quite uniform in size and are arranged in a regular honeycomb-like pattern around the mucosa glands [Skinner et al. 1990]. On the other hand, in a moderately differentiated adenocarcinoma of the rat colon, the capillaries are highly irregular in form and dimension and the honeycomb-like pattern is no longer present. Other studies [Vaupel et al. 1989, Margaritescu et al. 2008] show that vessels from oral squamous cell carcinoma are mostly aberrant in morphology without clear lumen, without pericytes and smooth muscle cells. In addition, variability in thickness, discontinuities and loose adherence of endothelial cells on their basal membrane often results in leaky vessels. Abnormal vascularisation eventually will lead to areas of reduced oxygenation (hypoxia), nutrient supply and waste removal. Tumor hypoxia occurs as a result of a disturbed balance between oxygen supply and its consumption at the cellular level. This disturbance creates a deficiency in oxygen concentration that compromises biologic functions [Vaupel et al. 1989]. Thus, tumor hypoxia is often associated with vital functional deficits that can be found in tumors at microscopic or macroscopic levels [Osinsky et al. 2011]. Oxygen levels are commonly measured as pO_2, (e. g., via Eppendorf pO_2 histography). This technique is minimally invasive and allows a reliable measurement of oxygen partial pressures (pO_2) [Vaupel et al. 2007]. In this thesis, the term hypoxia refers to a critical oxygen level below which clinical, biological and molecular effects are observed, and the binding of hypoxic markers occurs.

In normal tissues, the median pO_2 spans from 24 to 66 mm Hg, whereas in malignant tumors the median pO_2 usually reaches levels under 10 mm Hg. Higher pO_2 levels have only been registered at the periphery of tumors [Vaupel 1990, Vaupel et al. 2007].

1.3 Hypoxia subtypes

According to traditional classification, two subtypes of hypoxia exist: the chronic and the acute hypoxia (Fig. 3).

Chronic hypoxia, commonly known as diffusion-limited hypoxia was first described by Thomlinson and Gray [Thomlinson and Gray 1955]. This phenomenon is primarily attributed to a critical limitation in oxygen diffusion from tumor microvessels into the surrounding tumor tissue. The tissue volume supplied by oxygen from a central microvessel resembles a truncated cone with continuously decreasing diffusion distances from the arterial to the venous side. The duration of chronic hypoxia varies depending on the experimental approach. However, it is generally accepted to last longer than the acute form [Bayer et al. 2012]. Chronic hypoxia is a known source of radiation resistance. However, this subtype can lead to a proliferation stop, G_1 arrest, and cell death if no reoxygenation occurs, and finally to less aggressive tumor growth. [Vaupel et al. 2004, 2008, Pires et al. 2010].

Acute hypoxia was first postulated by Brown and experimentally verified by Chaplin et al. [Brown 1979, Chaplin et al. 1986]. According to these authors, acute hypoxia, (also called perfusion-limited hypoxia) is mainly caused by temporary, local disturbances in blood perfusion through microvessels or by strong fluctuations in the red blood cell fluxes. This hypoxia subtype generates more aggressive, radioresistant phenotypes and can cause metastases.

Based on pathogenetic and pathophysiological mechanisms, a third hypoxia subtype, termed *hypoxemic hypoxia*, has been identified. Hypoxemic hypoxia can be acute, caused by transient plasma flow, or chronic, caused by long term reduction of oxygen content in the blood (e. g., in anemic patients). This less commonly discussed subtype can have drastic pathophysiological consequences [Bayer et al. 2011]. The existence of such a subtype in experimental tumors has been previously shown using the window chamber method [Dewhirst et al. 1999, Erickson et al. 2003]. Nevertheless, in the clinic, hypoxemic hypoxia in tumors has not been investigated although it might play a major role in outcome.

1.4 Detection of hypoxia

The detection of tumor hypoxia in experimental settings and in human tumors can be assessed using various techniques [Tatum et al. 2006, Vaupel et al. 2007, Bache et al. 2008, Arabi et al. 2010, Astner et al. 2010, Chitneni et al. 2011] such as the use of O_2-sensitive microsensors, detection of nitroimidazole adducts in tissue sections and PET-imaging using radioactive tracers (e. g., nitroimidazoles and copper compounds). The bioreductive hypoxia

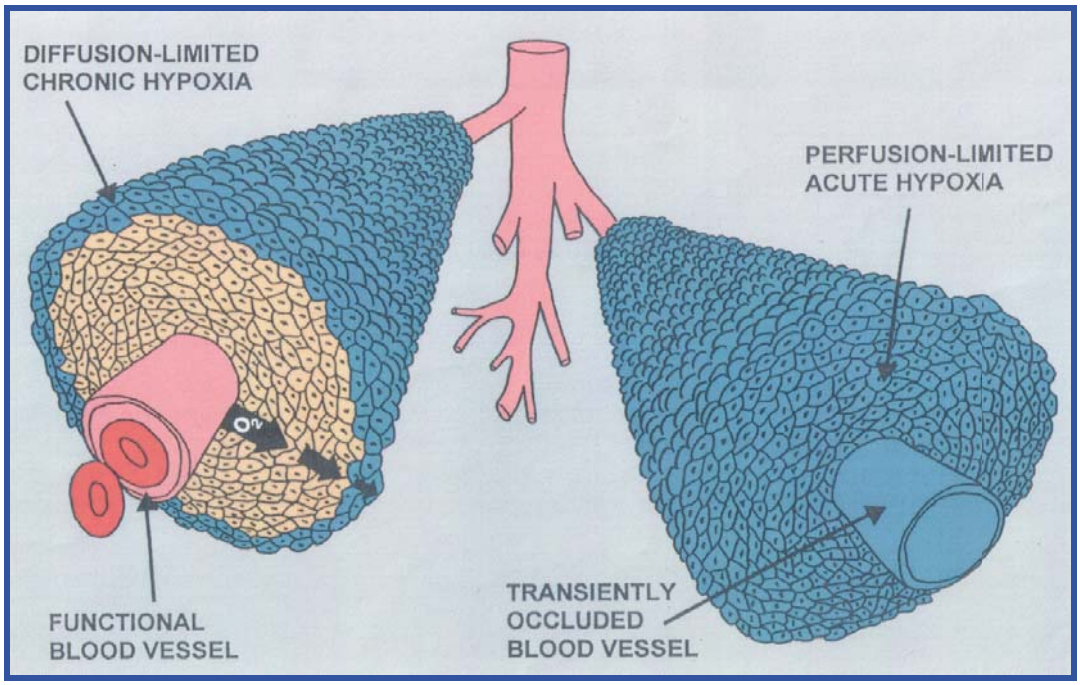

Fig. 2. Chronic and acute hypoxia. Diffusion-limited (chronic) hypoxia is depicted on the left side. The functional blood vessel (in pink) allows red blood cells (in red) to flow through. The tumor cells close to the functional blood vessel (yellow) are then supplied with oxygen via diffusion, whereas the tumor cells at a certain distance from the functional blood vessel (in blue) are hypoxic due to critically reduced oxygen diffusion. Perfusion-limited (acute) hypoxia is depicted on the right side. The transiently occluded blood vessel (in blue) does not allow red blood cells to pass through, and all the surrounding tumor cells (in blue) become hypoxic due to the absence of oxygen-carrying red blood cells [Horsman 1998].

marker misonidazole is able to bind at pO_2 levels ≤ 10 mm Hg *in vivo* [Gross et al. 1995]. The hypoxia marker pimonidazole used in this study is a derivate of mizonidazole, so that the hypoxia detected reflects pO_2 levels ≤ 10 mm Hg. Pimonidazole at low pO_2 levels follows a reduction pathway and is covalently bound to thiol-containing proteins in hypoxic cells [Varia et al. 1998, Raleigh et al. 1999], whereas at high oxygen levels, it follows the oxygenation pathway (Fig. 3). The reduced form of pimonidazole is covalently bound to cellular proteins and can be detected by incubation with a fluorescently labeled anti-pimonidazole antibody [Artel et al. 1995, Ljungkvist et al. 2002]. Experimental and clinical trials to distinguish between acute and chronic hypoxia have already been performed using different methods. Some of these methods include the window chamber preparation [Reinhold et al. 1977], FACS analysis after dual perfusion marker injection [Chaplin et al. 1986], laser Doppler flowmetry [Vaupel et al. 1988], paired survival curve analysis [Rofstad et al. 1999], electron paramagnetic resonance imaging (EPRI) [Yasui et al. 2010] and ^{19}F MRI (magnetic resonance imaging) [Magat et al. 2010]. The experimental approach used in this thesis utilizes serial [^{18}F]Fmiso PET/CT imaging combined with mathematical modeling

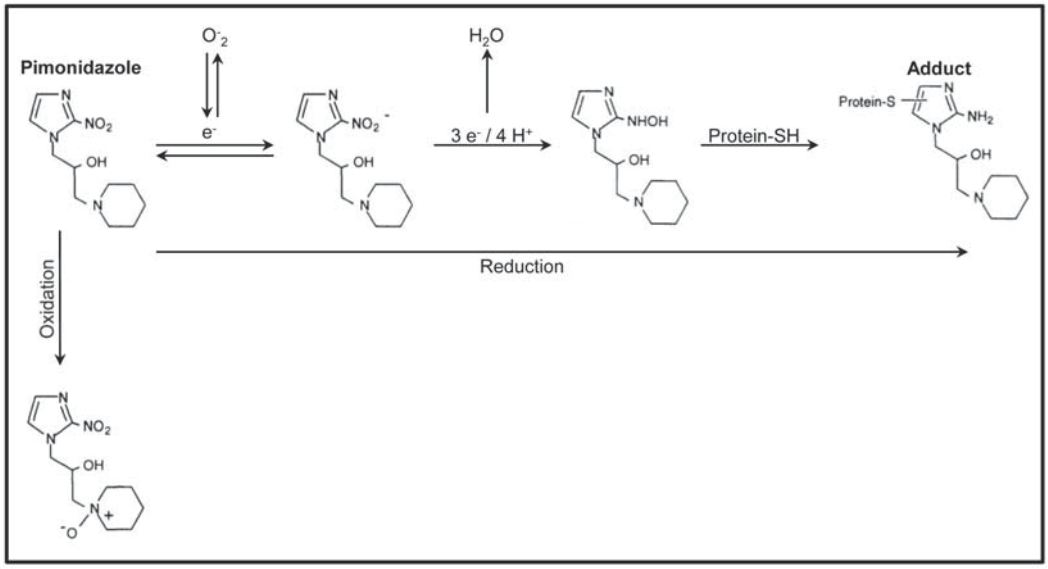

Fig. 3. Scheme of the reduction and oxidation pathway of pimonidazole *in vivo*. The reductive pathway is followed in the absence of oxygen (pO_2 under 10 mm Hg) and the reduced form will bind to proteins leading to the adduct. The oxidative pathway shows the pimonidazole metabolism in the presence of oxygen (pO_2 above 10 mm Hg [modified from Varia et al. 1998, Raleigh et al. 1999]).

[Wang et al. 2009] and (immuno-)fluorescence techniques to distinguish between acute and chronic hypoxia. Partially similar approaches were previously used to detect tumor hypoxia in an animal model by Cho et al. [Cho et al. 2009]. PET/CT has the advantage of being a non-invasive method that could be integrated into the clinic in the future.

1.5 Intra- and inter-tumor heterogeneity

The microenvironment (vascularisation, perfusion, oxygenation status etc.) of solid tumors exhibit certain heterogeneities. In experimental tumors, it has been shown that microvessel density, perfusion, hypoxia and necrosis are tumor line dependent. [Yaromina et al. 2006, 2011]. Head and neck tumors are known to contain hypoxic regions, which are unevenly distributed over the tumor mass [Höckel et al. 1991, Vaupel et al. 1991, Stadler et al. 1999, Nordsmark et al. 2005, Grosu et al. 2007, Vaupel et al. 2007]. Also a heterogenous distribution of the neovasculature has been reported and seems to be a characteristic of almost all solid tumors [Schor et al. 1998, Weidner et al. 1991, Wyss et al. 2007]. This heterogeneity leads to differences in treatment response, which makes prediction of treatment outcome difficult.

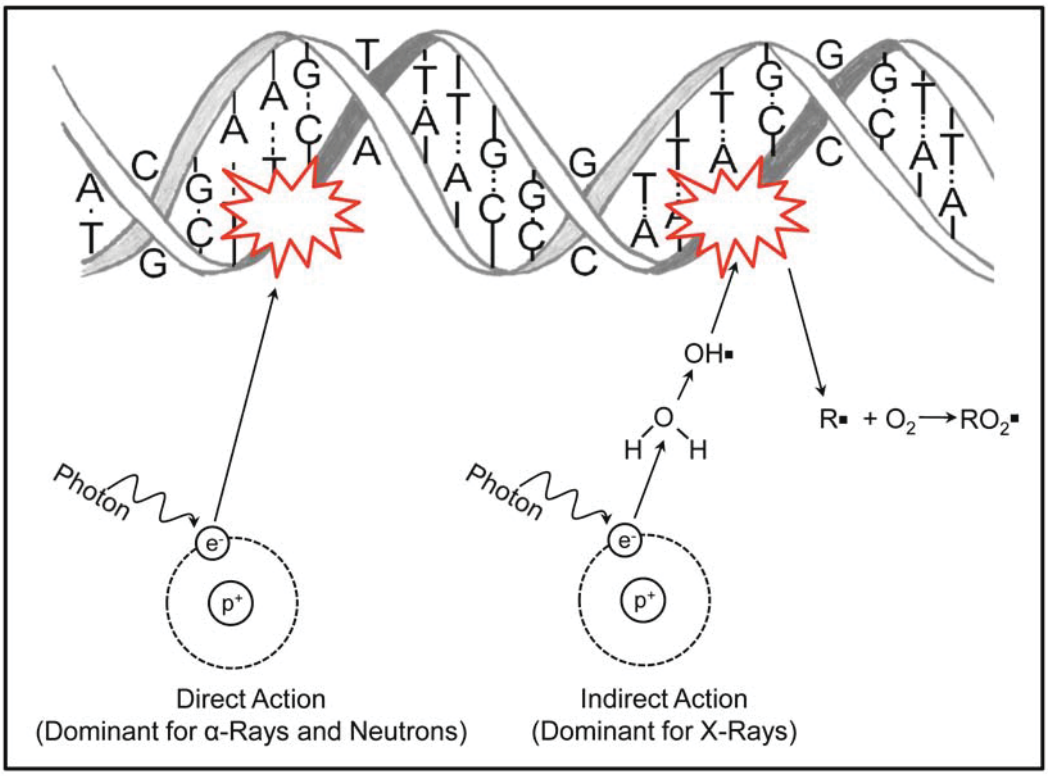

Fig. 4. Mechanisms of different radiation-induced DNA damages. α-rays and neutrons mostly produce DNA damages via direct action. X-rays mostly produce DNA damages via indirect action, whereas free radical formation (R·) plays an intermediate role. For details see the text [modified from Hall and Giaccia 2006].

1.6 Hypoxic tumors and resistance to radiotherapy

The fact that hypoxic tumor cells are more radioresistant than normoxic cells has been known for 57 years [Thomlinson and Gray 1955]. Early publications show that the extent of X-ray damage is strongly dependent on the level of oxygen [Barendsen et al. 1966, Broerse et al. 1968]. Thus, the increase in dose needed to achieve the same biological effect under hypoxia as under normoxia has been defined as the oxygen enhancement ratio (OER). The OER in the case of X-rays is approximately 2.5 x. This means that biological material of the same nature requires a 2.5 times higher dose under hypoxic conditions than under well-oxygenated conditions to achieve equivalent damages. On the other hand the OER is very low for densely ionizing radiation such as α-particles (≈1.0) and for neutrons (≈1.6), because they directly cause DNA damages. The mechanism proposed to explain the enhancement of radiation damage by oxygen is called “the oxygen fixation hypothesis” and is illustrated in Fig. 4. [Hall and Giaccia 2006, Stewart et al. 2010]. Most DNA damage from X-rays is caused by indirect action. In this situation, a secondary electron interacts with a water molecule to form hydroxyl radicals (OH·), which react with DNA to form R·. In the presence of

oxygen, R· reacts with O_2 to form RO_2·. As soon as RO_2· is formed, the radiation-induced damages are irreversibly and chemically fixed. However, in hypoxic medium, R· can react with H^+, so that the original form will be restored and the radiation-induced damages will be repaired (Fig. 4).

2 MATERIALS AND METHODS

2.1 Tumor lines and mice

Materials / Devices	Company
Atipamezole	Pfizer, Berlin, Germany
BBD 6220 CO_2 incubator	Thermo Scientific, Langenselbold, Germany
Ciprofloxacin	Fresenius Kabi, Bad Homburg, Germany
DMEM	Gibco, Paisley, UK
DMSO	Sigma-Aldrich, Steinheim, Germany
DPBS	Gibco, Paisley, UK
Fentanyl	Jansen-Cilag, Neuss, Germany
FCS	PAA Laboratories, Pasching, Austria
Flumazenil	Insera Arzneimittel, Freiburg, Germany
Gulmay RS225A	Gulmay Medical Ltd, Camberley, UK
Logiq-5	GE Healthcare, Solingen, Germany
Midazolam	Ratiopharm, Ulm, Germany
Medetomidine	Pfizer, Berlin, Germany
Naxolone	Insera Arzneimittel, Freiburg, Germany
NEAA	PAA Laboratories, Pasching, Austria
NMRI (nu/nu) mice	Charles River, Sulzfeld, Germany
P/S	Gibco, Paisley, UK
Trypsin	PAN Biotech, Aidenbach, Germany
T_{75} flasks	Corning, New York, USA

Six established human squamous cell carcinomas of the head and neck (UT-SCC-5, UT-SCC-14, UT-SCC-15, FaDu, SAS and CAL-33) of varying radiation resistance as assessed by TCD_{50} (radiation dose in Gy necessary to locally control 50% of tumors) were investigated (see Tab. 1). [1 Gy is defined as the enhancement of 1 joule per kg body weight (1 Gy= 1J/kg)].

The tumor lines were cultured in standard DMEM containing 10% FCS and supplements (1% NEAA and 1% P/S) in a BBD 6220 CO_2 incubator at 37 °C and 5% CO_2. Cells were cultured in T_{75} flasks (75 cm^2 cell culture flasks) and were split twice a week when they reached a density of about 90%. For harvesting, the cells were washed with DPBS, treated

with trypsin for 5 minutes at 37°C until they became detached. Trypsin was stopped by adding FCS-containing medium, followed by cell collection via centrifugation and DPBS washing. The cell pellet was resuspended at a concentration of $1x10^6$ cells/100 µl cold DPBS, and used for transplantation into nude mice NMRI (nu/nu).

NMRI (nu/nu) mice are characterized by the absence of the thymus and of hair due to basic defects in the embryonic ectoderm. As a result, they have virtually no T-cells but in "compensation", an increased level of NK-cell activity. This genetic disturbance (immune deficiency) qualifies this strain as a valuable tool for studying tumor xenografts, because transplants in the presence of a normal immune system would be rejected from the body.

The experiments were performed using 7–14-week-old female NMRI (nu/nu) mice in the ZPF of the Klinikum rechts der Isar, TU Munich. The animal rooms provided a 12 h light – 12 h dark cycle (light-on time 7 a.m.), a constant temperature of 26.8°C and a relative humidity of 50–60%. The animals were fed commercial laboratory animal diet and water ad libitum.

Tab. 1. Tumor lines, description of their origin, delivery source and radiosensitivity (TCD_{50}).

Tumor line	Origin	Delivery source	In vivo TCD_{50} (Gy) with CI
UT-SCC-15	Recurrent SCCHN of the mobile part of the tongue. [Grenman et al. 1991, Krause et al. 2007]	Professor Reidar Grénman Dept of Otorhinolaryngology - Head and Neck Surgery, Turku University Hospital PO Box 52, FI-20521, Turku, Finland	37.7 (14;49)
UT-SCC-14	Primary SCCHN of the tongue. [Grenman et al. 1991, Hessel et al. 2004]	Professor Reidar Grénman Dept of Otorhinolaryngology - Head and Neck Surgery, Turku University Hospital PO Box 52, FI-20521, Turku, Finland	44.2 (35;49)
FaDu	Primary hypopharyngeal SCCHN	American Type Culture Collection, Rockville, MD, USA	61.5 (30;53)
SAS	Primary SCCHN of the tongue.	Japan Health Sciences Foundation, Health Science Research Resources Bank, Japan	99.1 (91;108)
UT-SCC-5	Primary pharyngeal SCCHN [Grenman et al. 1991, Pekkola-Heino et al. 1994]	Professor Reidar Grénman Dept of Otorhinolaryngology - Head and Neck Surgery, Turku University Hospital PO Box 52, FI-20521, Turku, Finland	101.8 (88;117)
CAL-33	Primary SCCHN of the tongue	Deutsche Sammlung von Mikroorganismen und Zellkulturen, Braunschweig, Germany	105 (90;141)

Initially, xenografted tumors from SCCHN tumor lines (UT-SCC-5, UT-SCC-14, UT-SCC-15, FaDu and SAS) generated in Dresden [Yaromina et al. 2005], were used as biological material to develop a method (MCSU method) for assessing the fraction of chronic and acute hypoxia *ex vivo* before and upon fractionated irradiation [see goal A from results and Maftei et al. 2011(a), 2011(b)]. In all subsequent experiments, the xenografted tumors FaDu and CAL-33 were generated in Munich. These tumors were used as biological basis for developing a non-invasive method to distinguish between chronic and acute hypoxia and to determine the inter- and intratumor heterogeneity between tumors [see goals B, C and D from results and Maftei et al. 2011(c), 2012]. The mouse experiments described here have been approved according to German animal welfare regulation (approval # 55.2-1-54-2531-35-11, district government of Upper Bavaria).

2.2 Whole body irradiation

In order to guaranty complete depletion of the residual immune system, mice were whole-body irradiated 2-3 days before tumor transplantation with 4 Gy (200 kV X-rays, 0.5 mm Cu filter, 1 Gy/min) using the Gulmay RS225A device. For this, mice (maximum 10) were placed in an in-house designed irradiation cage (Fig. 5). For ensuring a homogenous dose

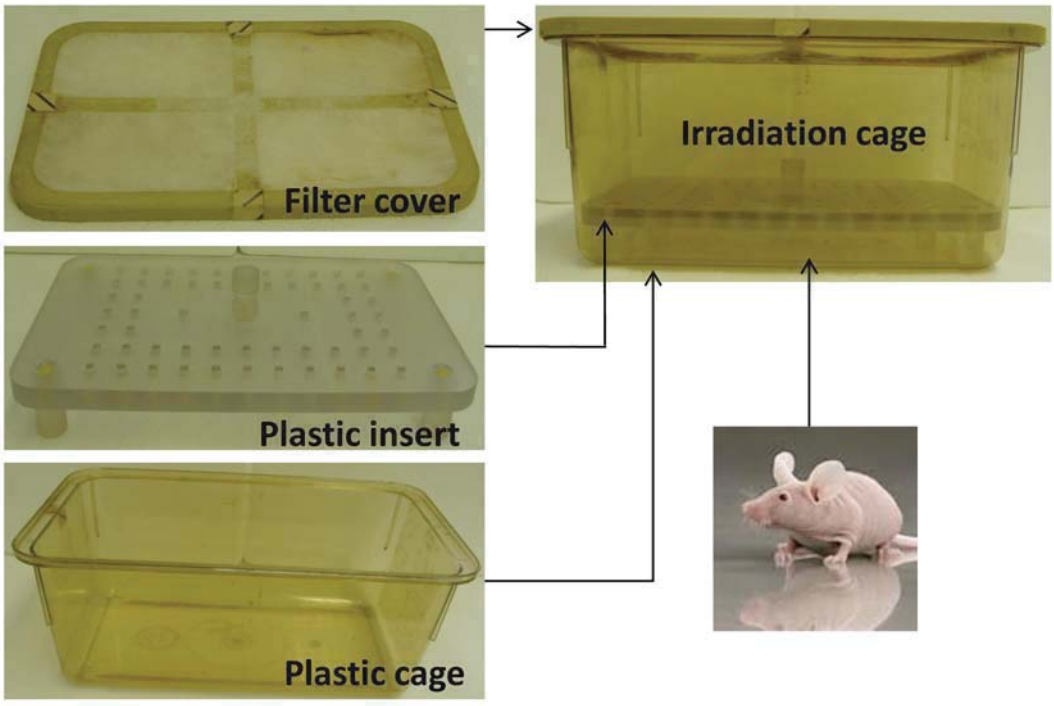

Fig. 5. Configuration of the irradiation cage: Mice (maximum number of 10) are placed in the plastic cage followed by addition of the plastic insert and filter cover.

distribution over the entire mouse body, a plastic insert was placed in the cage to delimit a space at the bottom of the irradiation cage at a designated height equivalent to that of a mouse. This plastic insert restricts movement of the mice only in the vertical direction. A filter cover was added on top of the plastic cage to maintain sterile conditions during irradiation. The whole irradiation cage (including the mice) was then placed in the irradiation field for 252 sec.

2.3 Tumor generation (for cryostocks and hypoxia assessment)

To prevent any bacterial infection, mice received the antibiotic ciprofloxacin at 40 mg/l in the drinking water for 10 days, starting on the day of whole-body irradiation. Mice were anesthetized with MMF and antagonized with AFN (Tab. 2), both via i.m. injection.

2.3.1 Tumor cryostocks:

For generating tumor cryostocks, 1 x 10^6 freshly harvested cells (in 0.1 ml DPBS) were injected into the right axilla of anesthetized mice 2 or 3 days after whole-body irradiation. Immediately after tumor cell injection, the mice were antagonized. The tumors were allowed to grow to a maximum size of 12 mm in diameter (3-5 weeks) at which time the animal was sacrificed and the tumor excised. Vital tumor tissue was then separated from necrosis and cut into small pieces (about 1 mm^3), placed in freezing medium (DMEM + 10% FCS, + 10% DMSO, + 1% P/S, + 1% NEAA) and stored in liquid nitrogen until use.

2.3.2 Tumors for hypoxia investigation:

Generally, a single tumor piece from the cryostocks was transplanted subcutaneously into one right hind-leg of each anaesthetized mouse. A small number of mice were transplanted on both hind-legs. Using a surgical scissor, a small incision was made into the skin and a subcutaneous pocket was formed. A tumor piece was inserted with fine forceps ≈ 2 cm away from the incision. The transplanted tumor pieces were then allowed to form tumor xenografts up to a maximum size of 12 mm in diameter.

Tab. 2. Composition and doses of the anaesthetic and antagonist.

Anaesthetic (MMF)			Antagonist (AFN)	
Medetomidine	0.5 µg/g body weight		Atipamezole	2.5 mg/g body weight
Midazolam	5 µg/g body weight		Flumazenil	0.5 µg/g body weight
Fentanyl	0.05 µg/g body weight		Naloxone	1.2 µg/g body weight

The measurements of tumor volume were performed (in 3-dimensions) twice per week by ultrasound using a Logiq-5. Tumor volumes were calculated by the formula of a rotational ellipsoid: [$V = \pi/6 \times d_1 \times d_2 \times d_3$ (d = diameter)].

2.4 Local tumor irradiation

Local tumor irradiation was performed in Dresden (OncoRay Center) and has been described earlier [Yaromina et al. 2006]. These tumors were used as biological tissues for developing a method to assess the fractions of chronic and acute hypoxia *ex vivo* before and upon fractionated irradiation (Publication # 1). Briefly, 200 kV X-rays were applied (0.5 mm Cu filter, ≈ 1 Gy/min) at 2 Gy per fraction 5 times per week to all tumors, except SAS tumors, which received only 1.84 Gy per fraction due to technical reasons [Yaromina et al. 2011]. Mice for sham controls were handled in the same way as the irradiated tumors, except that they were not irradiated. The tumors were excised (for histological examination) 24 hours after 5 or 10 fractions of irradiation. All irradiations were performed on non-anesthetized animals. Mice entered the experiment when the tumors reached 7 mm in diameter.

2.5 Histology

Materials / Devices	**Company**
AlexaFluor 594 Goat anti-rat IgG	Invitrogen, Eugene, OR, USA
Aqueous Mount	Zytomed Systems, Berlin, Germany
AxioVision 4.7	Zeiss, Jena, Germany
Cover slip	Menzel, Braunschweig, Germany
Eosin	Merck, Darmstadt, Germany
Fluorescent mounting medium	DAKO, Glostrup, Denmark
Hematoxilin	Merck, Darmstadt, Germany
Hoechst 33342	Sigma, Deisenhofen, Germany
Mab FITC-labeled anti-pimonidazole antibody	Hypoxyprobe, Burlington, MA, USA
O.C.T. Compound	Sakura, Alphen aan den Rijn, Netherlands
Pimonidazole	Hypoxyprobe, Burlington, MA, USA
PAD	Serotec, Oxford, UK
PBS	Sigma-Aldrich, Steinheim, Germany
Rat anti-mouse CD31 antibody MEC 13.3	BD PharMingen, Heidelberg, Germany

The hypoxia marker pimonidazole and the perfusion marker Hoechst 33342 were injected into living animals. Pimonidazole dissolved in saline was administrated i.v. at a concentration of 80 µg/g body weight in 50-100 µl approximately 2 h before tumor excision. Hoechst 33342 was dissolved in saline and administrated i.v. at 15 µg/g body weight in 50 µl one min before sacrificing the tumor-bearing mice. Tumors located on one or both hind-legs were excised immediately upon animal sacrifice. Thereafter, tumors were embedded in O.C.T. compound, frozen on dry ice, and stored at -80°C. Each tumor was cut into blocks. Each block contained four or more consecutive 10 µm cryosections (Fig. 6). For all experiments (except those from Publication # 4), a single 10 µm cryosection from the middle of each tumor was analyzed. For the experiments described in Publication # 4, all 4 serial cryoslices from all three blocks were processed. Tumor cryoslices were fixed in cold (4°C) acetone, air dried and rehydrated in PBS. Pimonidazole was stained with the Mab FITC-labeled anti-pimonidazole antibody diluted 1:50 in PAD by incubating for 1 h at 37 °C in the dark [Arteel et al. 1995, Ljungkvist et al. 2002]. Microvessels were stained using the purified rat anti-mouse CD31 antibody MEC 13.3 diluted 1:100 in PAD. Anti-CD31 was detected using the secondary antibody, AlexaFluor 594 Goat anti-rat IgG diluted 1:200 in PBS for 1 h at 37°C in the dark.
The cryosections were then embedded in fluorescent mounting medium and stored at 4°C. Necrotic tissue areas were detected by H&E staining of adjacent or the same slices as used for IF staining and excluded from the analysis (Fig. 7). For H&E staining of the same cryosections as for IF staining, the cover slip was removed by keeping the slides in water for about 10 hours. Cryosections were rehydrated in PBS for 10 min, followed by drying. Finally, they were stained with H&E and embedded in aqueous mount.

2.6 Microcirculatory supply units (MCSU)

The IF staining was used to enable visualization of the four different MCSU patterns as depicted in Fig. 8 (Publication # 1). A MCSU is defined as a vital tumor tissue area (tissue cone) supplied by a central microvessel. According to its perfusion and oxygenation status, each MCSU can be categorized into normoxic, chronically hypoxic, acutely hypoxic or hypoxemically hypoxic based on the prediction (Fig. 8) and confirmed by the results (Fig. 12). Individual whole tumor cross-sections (Fig. 7) were scanned and photographed using the AxioVision 4.7 and the multi-dimensional and mosaix modules.
For calculation of the vital tissue fraction of whole tumor cross-sections, necrotic regions and overlaying skin regions (detected by H&E staining of the same slide or of adjacent slides) were outlined on (immuno-)fluorescence digital images as shown in Fig. 7 using the Windows PowerPoint Program (version 2007). The amount of pixels in the necrotic and total

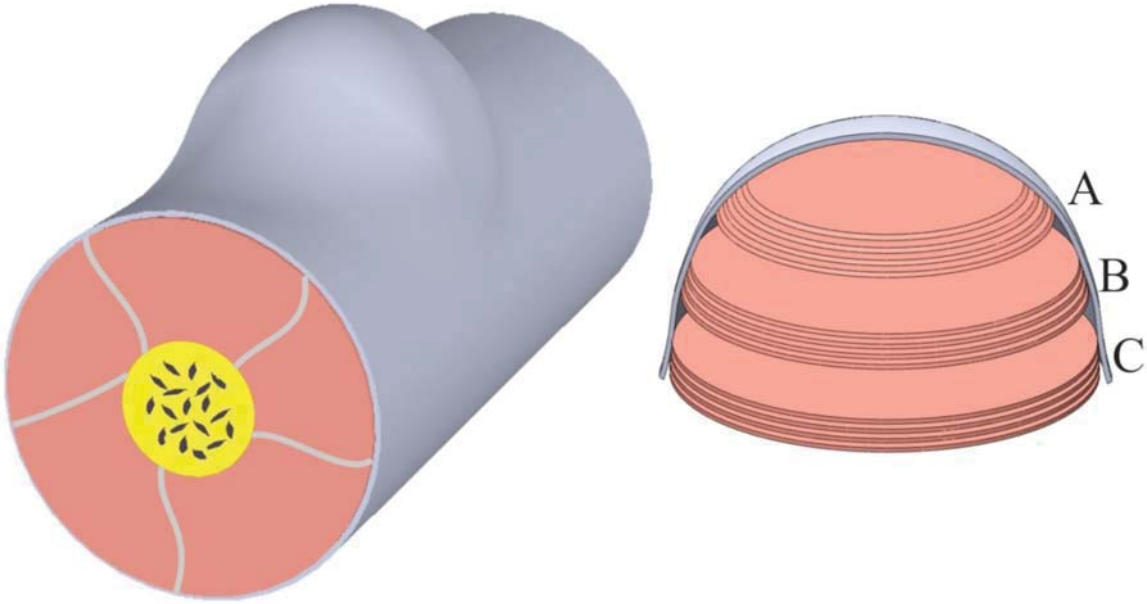

Fig. 6. Cartoon representing tumor location and tumor slicing. The left side shows a portion of the hind leg with the tumor located on it. The right side shows the tumor cryoslicing with the three tissue blocks: Block A represents the apical, block B the central, and block C the basal position (close to the muscle layer) within the tumor. Each block contains 4 serial cryosections [Maftei et al. 2012].

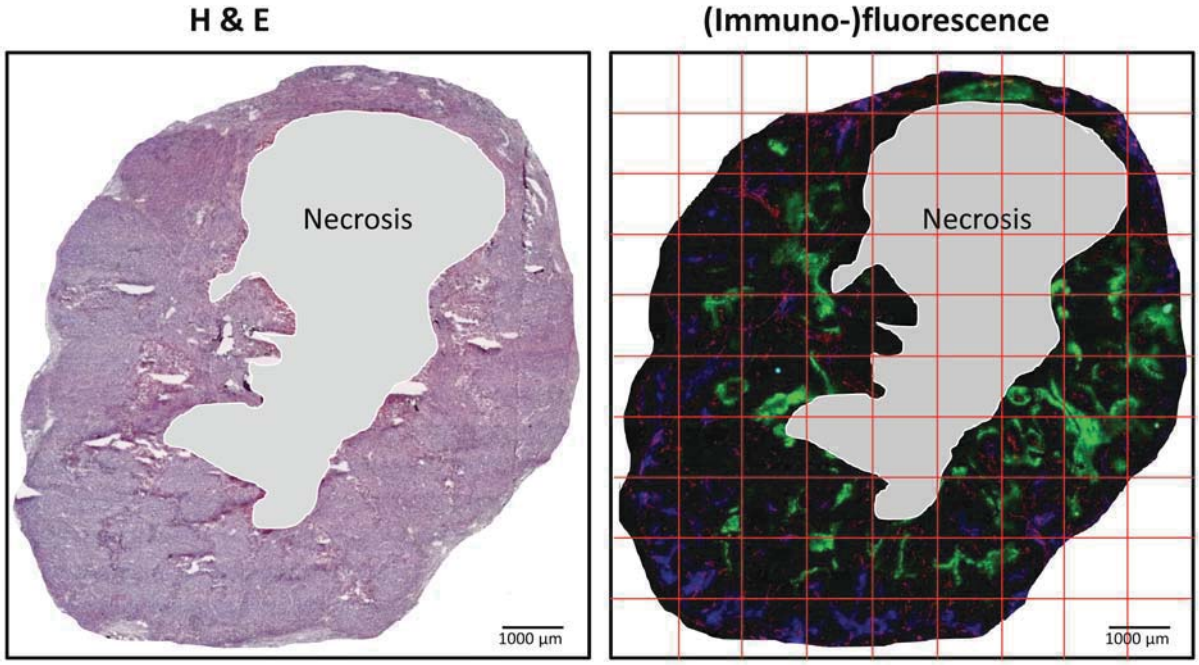

Fig. 7. Example of a H&E staining (left picture) performed on the same cryosection as for the IF staining (right picture) showing the tumor margins and the necrotic area. The red grid over the IF staining is used as a guideline for MCSU exploration.

tumor areas were calculated using Adobe Photoshop CS4 extended (version 11.0.1). The vital tumor tissue areas were calculated by subtracting the necrotic area from the total tumor area. The vital tumor fraction was calculated by dividing the vital tumor area by the total tumor area. Since only viable tissue areas were analyzed, necrotic and skin masks were overlaid onto the IF pictures and thereby excluded from the analysis. Next, a grid was placed over the (immuno-)fluorescence image (see Fig. 7) to facilitate counting, and the magnification was increased so that the MCSUs were easily recognizable (Fig. 12). The evaluation was visually done by two independent researchers by counting MCSUs after categorizing according to their perfusion and oxygenation status.

2.7 [^{18}F]Fmiso PET/CT imaging and the Wang model

Materials / Devices	**Company**
[^{18}F]Fmiso	IASON, Graz, Austria
Gamma-counter 1480 Wizard	PerkinElmer, Turku, Finland
Imeron 300	Bracco Imaging, Konstanz, Germany
Isoflurane	Abbott, Wiesbaden, Germany
MATLAB, Version R2010a	The Mathworks, Natick, MA, USA
PMOD software, version 3.1	PMOD Technologies, Zurich, Switzerland
Siemens Inveon microPET/CT	Siemens, Knoxville, TN, USA
SPSS	SPSS, Chicago, IL, USA

For these experiments mice underwent two dynamic [^{18}F]Fmiso PET/CT scans on consecutive days at an interval of 24 h using the Siemens Inveon microPET/CT. For coregistration of the two PET/CT measurements, the animals were immobilized on an in-house developed coordinated multi-point fixation system (Fig. 9). The grid was supplied with an electric heater for keeping a constant warm temperature for the mouse during measurements. During the entire experiment, the mice were kept anaesthetized by breathing isoflurane gas. The anaesthetized mouse was placed on the grid and the exact positioning of the tumor was achieved by placing fixation pins into the grid surrounding the tumor. Before starting the first PET/CT measurement (time = 0 h), the exact position of the mouse and tumor on the grid was photographed and used to guide the positioning for the second PET/CT measurement (time = 24 h). In addition, two external CT contrast lines were painted with Imeron 300 onto the tumor skin at the exact same location for the two scans. After each CT scan, 10 - 15 MBq [^{18}F]Fmiso was injected intravenously (using a catheter in the tail vein)

into the tumor-bearing mice anaesthetized with isoflurane, and dynamic PET data were acquired for 2 hours. Pimonidazole for the histological analysis was injected immediately before [^{18}F]Fmiso. At the end of the PET scanning, Hoechst 33342 was injected intravenously and each anaesthetized mouse was killed via cervical dislocation 1 min later. Two venous blood samples (2 - 7 µl each) were taken directly after scanning, weighed, and the activity of ^{18}F in the blood measured in a gamma-counter (1480 Wizard). The images were reconstructed using the filtered back-projection (FBP) algorithm (Ramp filter, cutoff frequency 0.5 cycles/pixel, 46 frames of varying durations from 1 - 900 s).

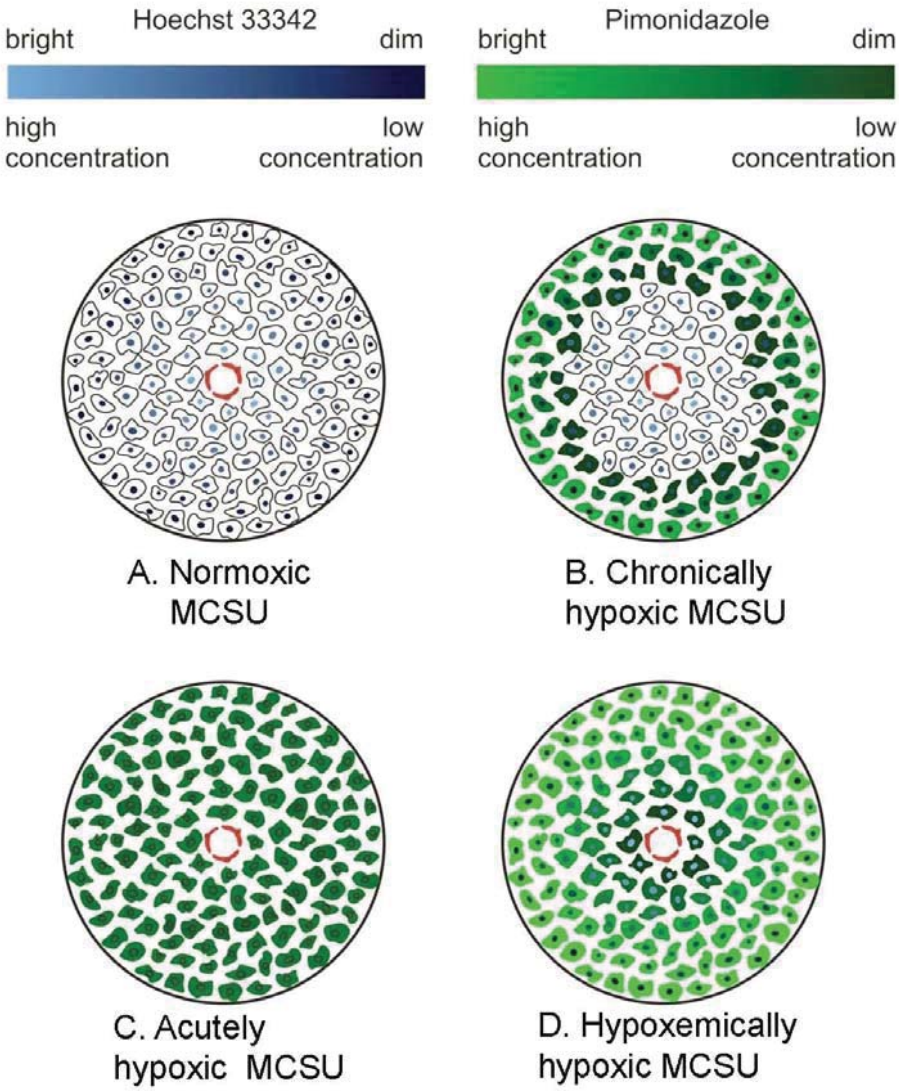

Fig. 8. Schematic diagrams representing microcirculatory supply units (MCSUs) with different oxygenation states: (A) normoxic MCSU = normoxia; (B) chronically hypoxic MCSU = chronic hypoxia; (C) acutely hypoxic MCSU = acute hypoxia; (D) hypoxemically hypoxic MCSU = hypoxemic hypoxia. The red circle in the center represents the microvascular endothelial lining. The color bars in the upper part of this figure indicate fluorescence intensities for Hoechst 33342 (blue) and pimonidazole (green); [Maftei et al. 2011(b)].

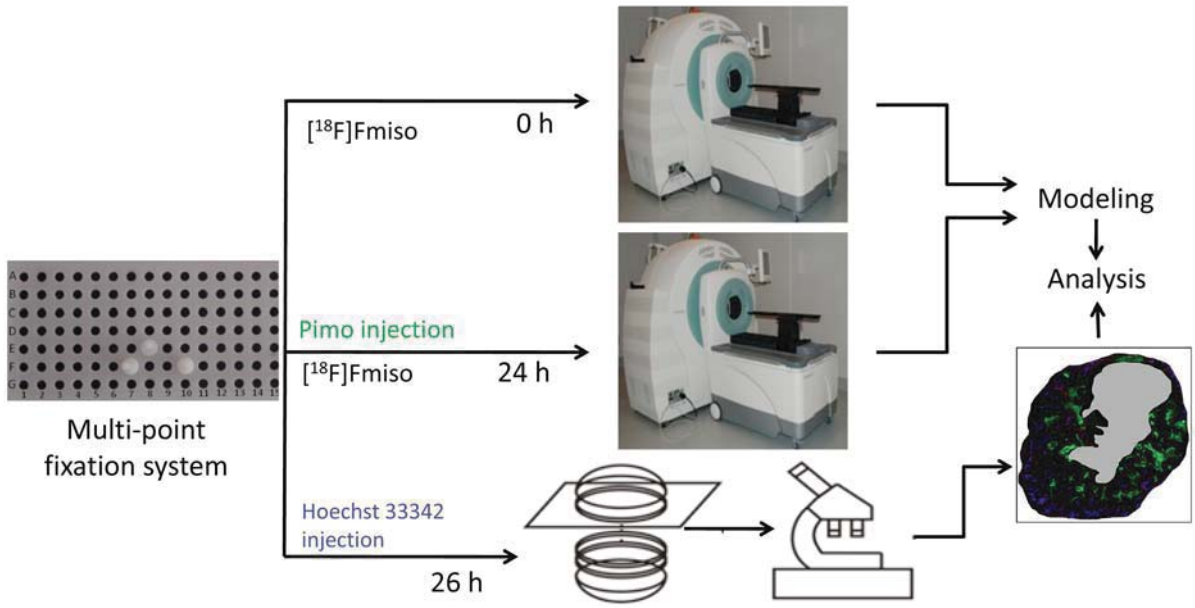

Fig. 9. Scheme of the dynamic [^{18}F]Fmiso PET/CT experiments. On the left side, the coordinated multi-point fixation system, with 3 fixation pins is shown. Time point 0 and 24 h indicate the start of the two consecutive PET/CT measurements. Data obtained from the 2 measurements were analyzed via modeling (Wang Model). The injection of Pimonidazole and Hoechst 33342 is indicated. Time point 26 h indicates the end of PET/CT measurements and excision of the tumor for cryoslicing [Maftei et al. 2011(c)].

The attenuation correction was applied based on the acquired CT data. Additionally, all measurements were corrected for physical decay, dead time and non-uniformity of microPET response. A measured system calibration factor was used to convert voxel count rates to activity concentrations. The voxel size of the reconstructed image data was 0.78 × 0.78 × 0.80 mm^3.

The images from two consecutive scans were co-registered based on the CT-visible fixation pins on the immobilization system. The registration accuracy was assessed based on the painted CT contrast lines on the tumor skin. Contours of the tumors were outlined manually based on CT images using PMOD software (version 3.1). The imaging data were then converted into SUV values and the total activity within the tumor area of the two scans was normalized by rescaling them to be the same.

To analyze the serial PET scans and estimate the fraction of acute hypoxia, the mathematical model described by Wang et al. [Wang et al. 2009] was applied. This model assumes that both chronic and acute hypoxia contribute to the [^{18}F]Fmiso images and the total uptake *H* in a voxel is the sum of the contributions

$$H = H_a + H_c$$

where H_a is the contribution of acute, and H_c is the contribution of chronic hypoxia. Then, the total uptake H_1 and H_2 from the two PET scans of the same voxel can be written as

$$H_1 = H_{a1} + H_c$$
$$H_2 = H_{a2} + H_c$$

which assumes that the "chronic" contribution, H_c, is unchanged in the two scans and resembles a Gaussian distribution. Therefore, a part of the uptake was extracted, which fits best to a Gaussian distribution. To do so, the uptakes H_1 and H_2 were sorted into high H_h and small H_s readings in the same voxel. The fraction of H_h is denoted $\omega = H_{ah} / H_h$ as due to acute hypoxia and defined as $x = \Delta H / H_h$, where ΔH is H_h - H_s. Finally, a relation between ω and x was assumed:

$$\omega = \rho x^{\beta} = \rho \frac{\Delta H^{\beta}}{H_h^{\beta}}.$$

For voxels with H_h, the chronic hypoxia was then calculated as

$$H_c = (1 - \rho x^{\beta}) H_h.$$

Here, β = 0.6 was derived from a Monte-Carlo simulation. To model the "chronic" contribution, the model iteratively adapted ρ until it achieved a best fit with the maximized R-square (R^2). The model was re-implemented in MATLAB, Version R2010a.

In addition to the expression of acute hypoxia $\omega = H_{ah} / H_h$ as described by Wang et al. [Wang et al. 2009], also the fraction of the average contribution $(H_{ah} + H_{as})/(H_h + H_s)$ for the assessment of the fraction of acute hypoxia (modified Wang model) was tested.

2.8 Statistical analyses

Statistical analyses were performed using the SPSS version 20 (T-test and Correlation). Linear regression analysis and Pearson´s correlation coefficient, r, were used to test correlation between variables. Data are presented as mean values ± SEM. p-values < 0.05 were considered to be statistically significant.

3 RESULTS

The planning of radiation treatment schedules and outcome can be influenced by the fractions of acute and chronic hypoxia in tumors [Rugierri et al. 2004]. Due to the fact that hypoxia in solid tumors is a dynamic phenomenon, and this dynamic process is also influenced by fractionated radiation therapy, an *in vivo* non-invasive detection method for the differentiation between chronic and acute hypoxia in tumors should provide better radiation treatment planning for the patients. Thus, the goals of this thesis were:

A. To develop a method to assess the fractions of chronic and acute hypoxia *ex vivo* before and upon fractionated irradiation. This was achieved by (immuno-)fluorescence staining of representative cryosections from the center of each tumor and application of a novel method to classify normoxia and hypoxia subtypes.

B. To develop a non-invasive method to distinguish between chronic and acute hypoxia using [^{18}F]Fmiso PET/CT and mathematical modeling (Wang Model).

C. To compare the fraction of acute hypoxia detected by *ex vivo* (immuno-)fluorescence staining of tumor cryosections to the fraction of acute hypoxia detected by *in vivo* serial dynamic [^{18}F]Fmiso PET/CT from non-irradiated xenografted tumors in mice.

D. To investigate the intra- and inter-tumor heterogeneity in total, chronic and acute hypoxia with respect to tumor volume in non-irradiated tumors.

3.1 Vital tissue fraction (VTF) before, during and after fractionated irradiation of tumors (Publication # 2)

Solid tumors become increasingly necrotic during growth and substantially necrotic after radiation treatment. In order to detect hypoxia in vital tumor tissue only, necrotic areas were detected before and after fractionated irradiation with H&E staining and excluded from the analysis.

Xenografted tumors of the 5 SCCHN tumor lines UT-SCC-5, UT-SCC-14, UT-SCC-15, FaDu and SAS at comparable volumes and identical transplantation site were analyzed (Fig. 10). Before irradiation, FaDu tumors had the highest (91.1 ± 3.6%) and UT-SCC-15 the lowest proportion of vital tissue (47.3 ± 5.8%) of the 5 tumor lines investigated (Fig. 10).

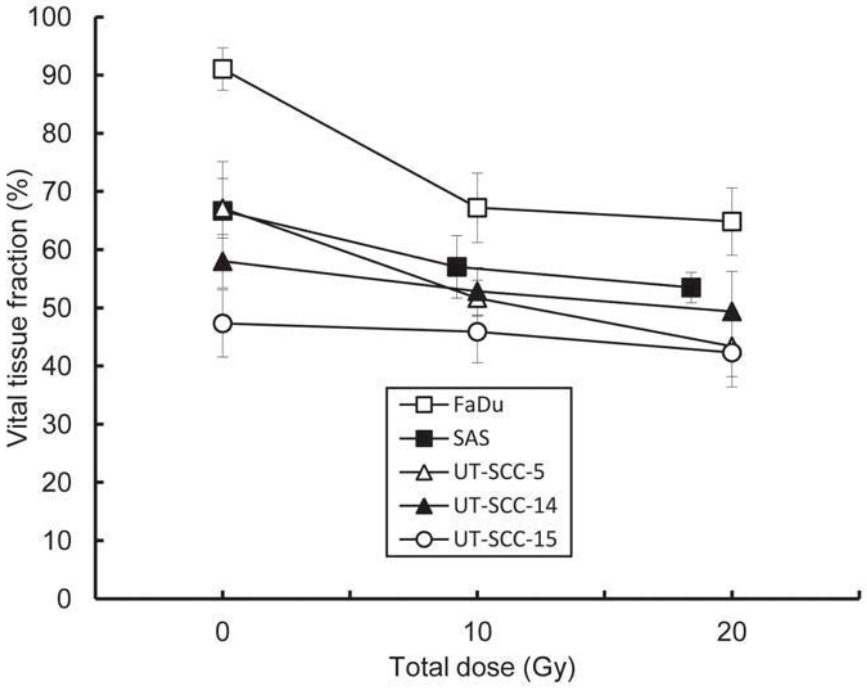

Fig. 10. Changes in the fraction of vital tissue (VTF, %) before, during and after fractionated irradiation with a total dose of 10 Gy (5 x 2 Gy) and 20 Gy (10 x 2 Gy) in 5 human xenograft hHNSCC lines (note: total dose in SAS tumors was 9.2 Gy, and 18.4 Gy, respectively). Significant reductions in VTF were observed for FaDu ($p < 0.001$) and UT-SCC-5 ($p = 0.006$) tumors. Mean values ± SEM are presented. [Maftei et al. 2011(b)].

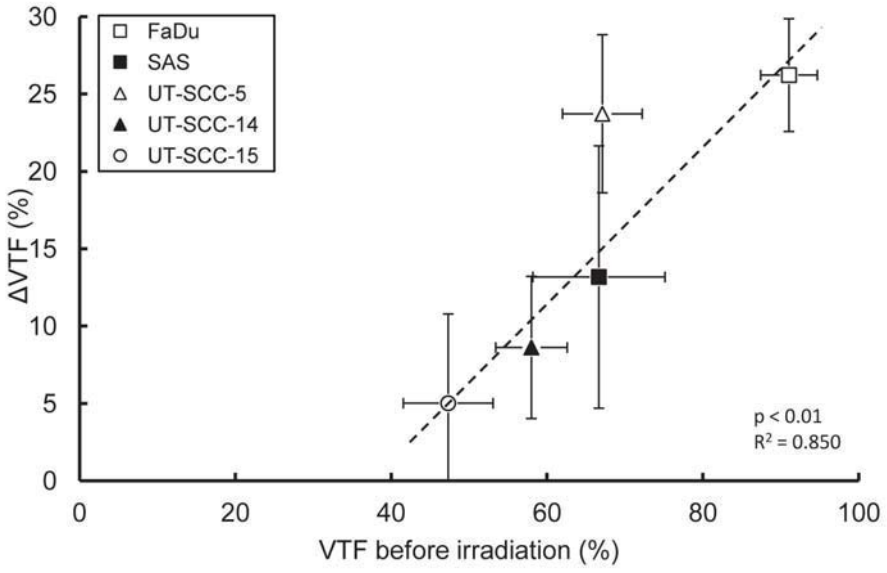

Fig. 11. Correlation between vital tissue fraction (VTF, %) before irradiation and ΔVTF, where ΔVTF is the vital tissue fraction before (control) minus vital tissue fraction following a total dose of 20 Gy (SAS: 18.4 Gy) in 5 human xenograft hHNSCC lines. Linear regression analysis and Pearson's coefficient of correlation (R) were used to examine the relationship between variables. Mean values ± SEM are presented [Maftei et al. 2011(b)].

Upon fractioned irradiation using 5 x 2 Gy, and 10 x 2 Gy, respectively, the fraction of vital tumor tissue significantly dropped in FaDu. UT-SCC-5 followed a significant decrease in vital tumor tissue fraction after treatment with a total dose of 20 Gy (Fig. 10). The other tumor lines also showed a trend for a decline in VTF upon fractionated irradiation. There was a correlation between higher VTF before irradiation, and a larger increase in necrotic areas upon irradiation with 10 x 2 Gy (Fig. 11).

3.2 Method for detection of normoxia and hypoxia subtypes (Publication # 1)

A novel method was developed for assessing the fractions of hypoxia subtypes *ex vivo* in cryosections of xenografted tumors. This method is based on the characteristics of individual hypoxia subtypes. As described in Material and Methods, it was hypothesized that specific patterns for normoxia, chronic hypoxia, acute hypoxia and hypoxemic hypoxia could be visually detected after (immuno-)fluorescence staining of hypoxia (pimonidazole), perfusion (Hoechst 33342) and microvessels (CD31). Such patterns were defined in Microcirculatory Supply Units (MCSUs). Each MCSU is defined as a vital tumor area supplied by a microvessel. Microscopic images of tumor cryosections from the five tumor lines SAS, FaDu, UT-SCC-5, UT-SCC-14, UT-SCC-15 confirmed the existence of these MCSUs (Fig. 12).

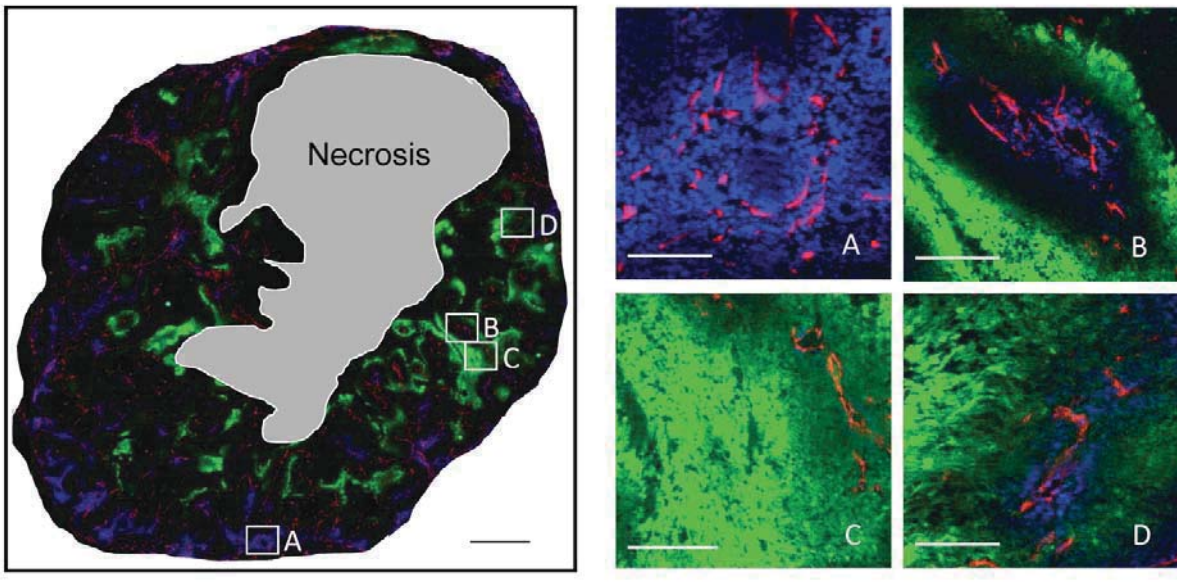

Fig. 12. Tissue sections showing examples of the 4 patterns as suggested in Fig. 8: (A) normoxia (B) chronic hypoxia; (C) acute hypoxia; (D) hypoxemic hypoxia. Hoechst 33342 fluorescence of perfused areas is shown in blue, pimonidazole staining of hypoxia in green, and CD31 staining for micro vascular endothelial cells in red. The white bars represent 200 µm and the black bar represents 1000 µm [modified from Maftei et al. 2011(b), 2011(c)].

The 4 different MCSUs were as follows:
(A) *Normoxia:* the microvessel in red is perfused, which is denoted Hoechst 33342 blue fluorescence surrounding it, but there is no hypoxia detected as seen by the absence of green pimonidazole staining. (B) *Chronic hypoxia*: the microvessel in red is perfused, which is denoted by Hoechst blue fluorescence surrounding it, but at a certain distance (100 – 150 µm) hypoxia can be seen as a green pimonidazole staining. (C) *Acute hypoxia:* the microvessel in red is not perfused with the absence of Hoechst 33342 blue fluorescence around it. Hypoxia can be seen as a green pimonidazole staining close to the microvessel. (D) *Hypoxemic hypoxia:* the microvessel in red is perfused, denoted by the presence of blue Hoechst 33342 fluorescence around it and concomitantly hypoxia can be seen as a green pimonidazole staining close to the microvessel.

3.3 Quantitative assessment of normoxia and hypoxia subtypes before and upon fractionated irradiation (Publication # 2)

Using this MCSU method, normoxia and hypoxia subtypes were quantitatively assessed in tumor cryosections from the center of the tumor. This was accomplished by assigning each MCSU in a tumor cryosection to one of the four categories (Fig. 12) and then calculating the fraction relative to the total number in vital tumor tissue. The number of analyzed tumors (n) and the average number of MCSUs per tumor line analyzed are shown in Tab. 3.
The fraction of normoxia and total hypoxia were calculated in the total vital tumor area and are depicted in Fig. 13, left column of each block. The fractions of chronic, acute and hypoxemic hypoxia were calculated relative to the fraction of total hypoxia and are depicted in Fig. 13, right column of each block. The fractions of normoxia, total hypoxia and hypoxia subtypes (chronic, acute and hypoxemic hypoxia) of unirradiated (sham) tumors can be seen in Fig. 13, Block A. In unirradiated tumors, the fraction of total hypoxia is larger than normoxia only in UT-SCC-15 (56.9 ± 2.76%).

Tab. 3. Number of analyzed MCSUs, and tumors

Tumor line	Average number of analyzed MCSUs per tumor			Number of analyzed tumors (n)		
	0 Gy	10 Gy	20 Gy	0 Gy	10 Gy	20 Gy
UT-SCC-15	207	323	388	5	7	5
UT-SCC-14	404	357	292	8	8	4
FaDu	529	426	735	7	7	7
SAS	300	269	442	7	9	7
UT-SCC-5	411	368	283	8	10	8

In the other 4 tumor lines, normoxia predominates (range from 50.1 ± 4.08% to 72.8 ± 3.03%). Concerning hypoxia subtypes, chronic hypoxia is the most abundant in all tumor lines (range from 65.4 ± 4.95% to 85.9 ± 2.70%), followed by acute hypoxia (range from 12.9 ± 2.03% to 29.8 ± 4.11%). The fraction of hypoxemic hypoxia is consistently small (range from 1.20 ± 1.23% to 6.40 ± 3.21%).

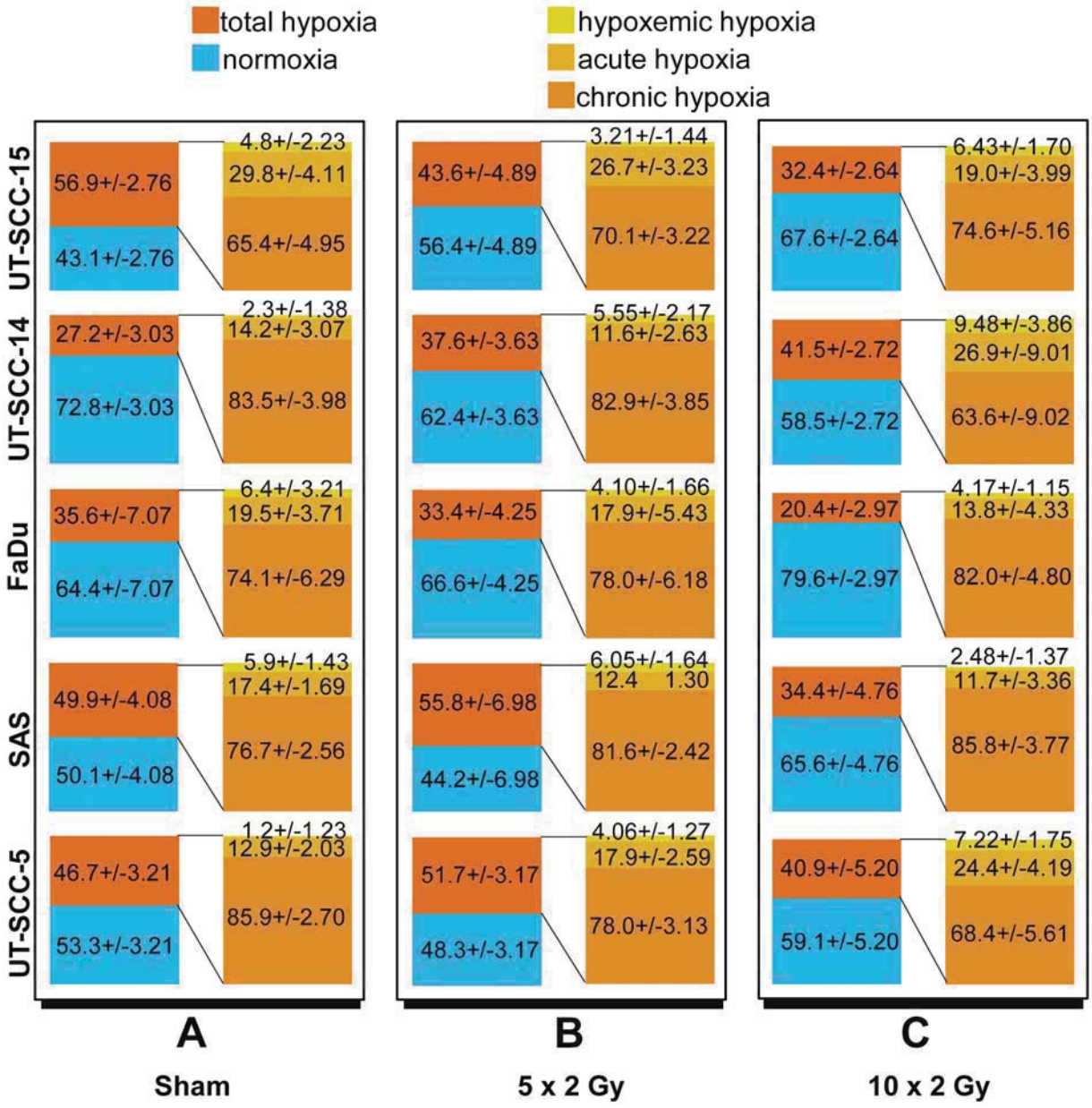

Fig. 13. Quantitative analysis of normoxia and hypoxia in 5 different hSCC tumor lines. Block A, Sham; block B, 5 x 2 Gy, block C, 10 x 2 Gy. In each block, the left column shows the fraction of normoxia and total hypoxia, and the right column exhibits the fraction of the three different subtypes of hypoxia (chronic, acute and hypoxemic). Data are shown as mean ± SEM [Modified from Maftei et al. 2011(a), 2011(b)].

When considering changes in total hypoxia upon fractionated irradiation, UT-SCC-14 was the only tumor line to undergo a regular increase in hypoxia upon all irradiation steps (5 x 2 Gy or 10 x 2 Gy, see Fig. 13). The other 4 tumor lines exhibited an opposite trend (decrease in total hypoxia upon irradiation). The tumor lines SAS and UT-SCC-5 showed a slight deviation from this trend (increase in total hypoxia at 5 x 2 Gy, see Fig. 13). Chronic hypoxia continued to be the most abundant subtype of hypoxia followed by acute and hypoxemic hypoxia.

3.4 Assessment of chronic and acute hypoxia *in vivo* using [^{18}F]Fmiso PET/CT imaging and the Wang model (Publication # 3)

In order to distinguish between chronic and acute hypoxia *in vivo*, serial dynamic [^{18}F]Fmiso PET/CT scans were performed on FaDu and CAL-33 SCCHN xenograft tumors. Since non-invasive PET/CT imaging can be used on patients, these experiments are relevant for clinical diagnostics. Based on the literature data on the dynamics of acute hypoxia [Dewhirst et al. 1996, 1999, Bayer et al. 2011], our PET/CT scans were implemented 24 h apart. Importantly, only very few studies exist validating the use of nitroimidazole-PET for hypoxia detection in animals and humans. Therefore, the goal was to investigate the potential of the Wang model in predicting the fraction of total hypoxia and hypoxia subtypes in tumors. The Wang Model is a mathematical algorithm that assumes that the intensity of ^{18}F-Fmiso signal in a PET voxel represents the composite uptake of a spectrum of microscopic regions, ranging from normoxic to anoxic. In order to analyze individual voxels of serial PET images, precise co-registration of serial CT images is essential.

Tab. 4. Co-registration error values, curve fitting values (R^2), and volumes of all tumors analyzed after serial [^{18}F]Fmiso PET/CT.

Tumor line	Co-registration error (ε)	R^2 Gaussian distribution	R^2 Poisson distribution	Tumor volume (mm^2)
FaDu (1)	0.65	0.97	0.82	1255
FaDu (2)	0.50	0.73	0.76	1626
FaDu (3)	0.34	0.86	0.90	776
FaDu (4)	0.39	0.91	0.90	849
FaDu (5)	0.71	0.88	0.82	522
FaDu (6)	0.41	0.90	0.80	431
FaDu (7)	0.54	0.95	0.87	418
CAL33 (1)	0.91	0.94	0.70	140
CAL33 (2)	0.50	0.87	0.88	300
CAL33 (3)	0.84	0.97	0.95	122
CAL33 (4)	0.85	0.97	0.95	189
CAL33 (5)	0.51	0.93	0.71	99.3

For this, an immobilization device with pins was developed for the mice, and CT contrast solution was applied to the tumor and used as external markers (see Material and Methods). It was possible to achieve good co-registration error values, curve fitting values and tumor volumes (Tab. 4). In Fig. 14, an example of the co-registration results is shown, where (A) is the CT image at 0 h in gray scale, (B) is the CT image at 24 h in color scale and (C) is the overlap of the two serial CT images. Detailed co-registration of the tumor at 0 and 24 h for serial CT and PET images are shown in (D) and (E), respectively.

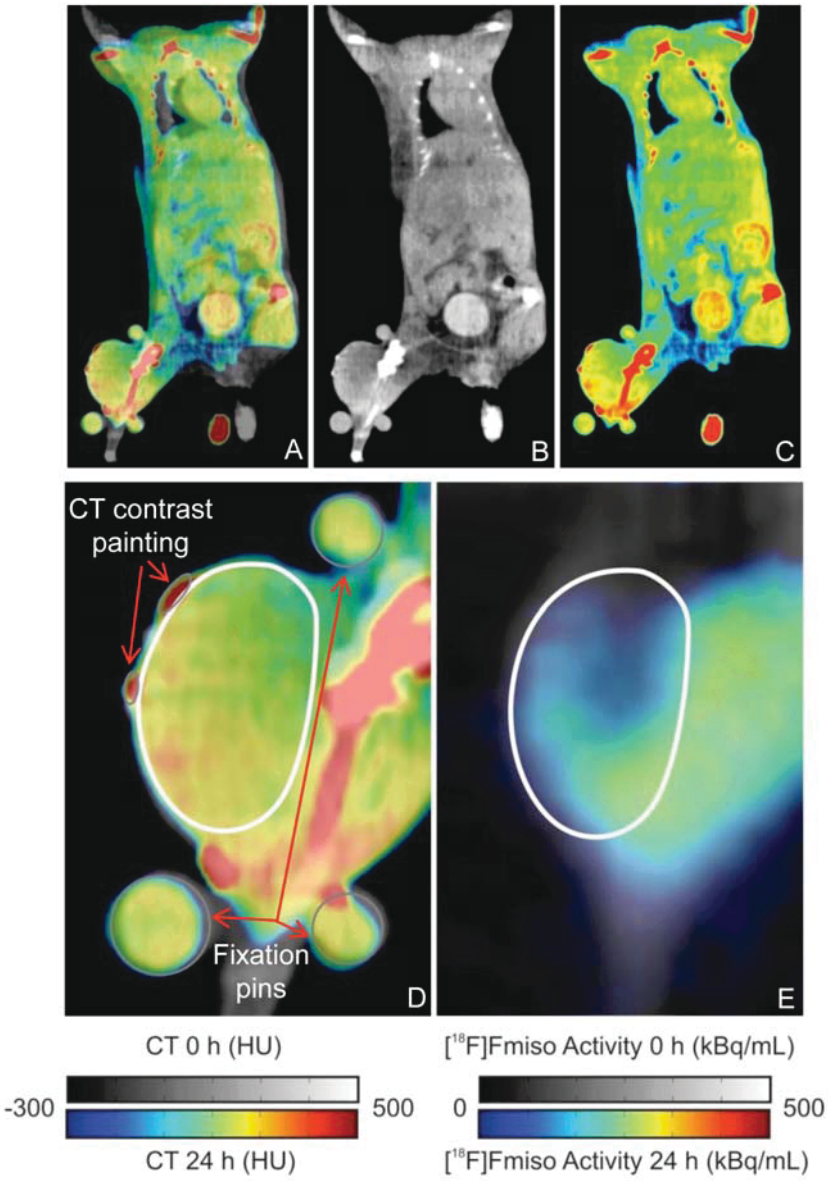

Fig. 14. Example of a co-registration between 0 and 24 h for a FaDu tumor. (A) Shows the fusion of the two serial CT images (0 and 24 h), (B) is the CT image at 0 h (gray scale) and (C) is the CT image at 24 h (color scale). Detailed views of the acquired over-lapped CT (D) and PET (E) images of the investigated tumor area are represented in the bottom panels. The gray contours indicate the external fixation pins and tumor skin painted with CT contrast solution, the white contour denotes the investigated tumor area [Maftei et al. 2011(c)].

Based on patient data, chronic hypoxia generates a SUV distribution that can be described by Gaussian statistics, and acute hypoxia is an operational definition, denoting voxels in which variation in ^{18}F-Fmiso uptake is observed [Wang et al. 2009]. Fig. 15 shows an example of data derived from SUV (% injection dose/g) of [^{18}F]Fmiso at 0 and 24 h that were analyzed using the original Wang model for the fraction of chronic (A) and acute hypoxia (B). The quality of fitting to a Gaussian distribution for the contribution of chronic hypoxia in this example is 0.88, while the fitting of a Poisson distribution for the contribution of acute hypoxia is 0.82. The quality of primary fitting (R^2 of the Gaussian distribution) for all tumors ranged from 0.62 to 0.97 (Tab. 4).

For comparison, cryosections taken from the central part of the tumor from the same mice used for the serial [^{18}F]Fmiso PET/CT study were stained and analyzed for the fraction of acute hypoxia (aHF). Since the total of the aHF and the cHF equals 100%, the trend for the aHF is exactly opposite of cHF. The aHF based on MCSUs was similar for both tumor lines at 25.3 ± 3.69% for FaDu and 22.4 ± 2.50% for CAL33 (Fig. 16). The estimated mean aHF using the original and modified Wang model analysis of serial [^{18}F]Fmiso PET/CT was higher than data based on the MCSU method: 40.5 ± 3.13% for FaDu and 45.4 ± 3.06% for CAL33 because of differences in the two methods. Using the modified Wang Model, the mean aHF was 34.1 ± 2.69% for FaDu and 38.4 ± 2.60% for CAL33 (Fig. 16). The aHF assessed using the MCSU method in cryosections showed a better trend (FaDu: r = 0.68, p = 0.21 and CAL33: r = 0.71, p = 0.18) with the modified than the original Wang Model (FaDu: r = 0.52, p = 0.23 and CAL33: r = 0.56, p = 0.19), however, this was not significant.

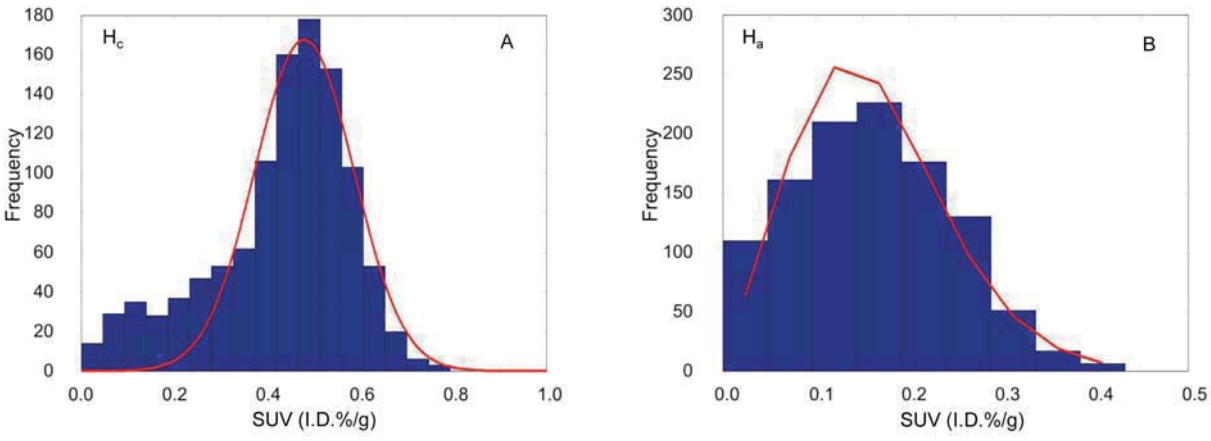

Fig. 15. Example of the Wang model fitting for a FaDu tumor. The distribution of the contributed SUV uptake by chronic hypoxia (Hc) was fitted to a Gaussian curve (A; μ = 0.48, σ = 0.11 with R^2 = 0.88) and the distribution of the contributed SUV uptake by acute hypoxia (Ha) fitted to a Poisson curve (B; λ = 3.20, with R^2 = 0.82); [Maftei et al. 2011(c)].

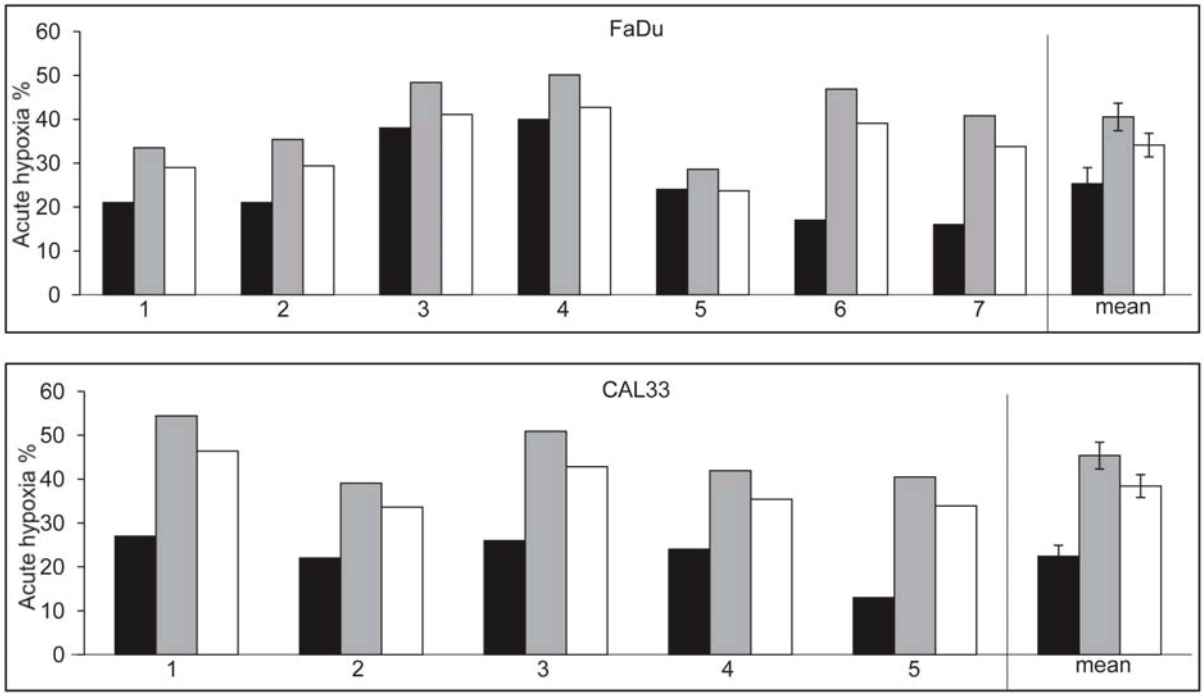

Fig. 16. Fractions of acute hypoxia assessed by the MCSU-based method (black bars), the original Wang model (gray bars) and the modified Wang model (Wang model; white bars) for individual FaDu (upper panel) and CAL33 tumors (lower panel). On the right-hand side the respective mean values ± SEM are shown [modified from Maftei et al. 2011(c)]

For the future, new methods are required to better validate the Wang Model. In contrast to the data published by Wang, recent data suggest that mathematical evaluations to distinguish between chronic and acute hypoxia may not be valid [Mönnich et al. 2012].

3.5 Intra- and intertumor heterogeneity (Publication # 4)

In order to determine whether analysis of one central section is representative for the whole tumor and whether different volumes have an impact on tumor oxygenation, the distribution of the total, chronic and acute hypoxia fractions throughout individual tumors was analyzed and compared between tumors of different volumes. For this, 5 FaDu xenografted tumors of different volumes (FaDu1, V=477 mm^3; FaDu2, V=442 mm^3; FaDu3, V=263 mm^3; FaDu4, V=175 mm^3; FaDu5, V=163 mm^3) were sliced at 3 distinct positions (Fig. 6) situated at the apical, central and basal layer of the tumor. Each block consisted of 4 serial sections. Total hypoxia and hypoxia subtypes were assessed by (immuno-)fluorescence techniques as described previously.

3.5.1 Fractions of vital tumor tissue

First, the effect of increasing tumor volume on the development of necrosis in FaDu tumors was determined by quantitatively assessing the fraction of vital tumor tissue (Fig. 17). In the apical block, there was a gradual increase in vital tissue from larger to smaller tumors. In the largest tumors (FaDu1, FaDu2), the fraction of vital tumor tissue was significantly higher in the basal block (closest to the muscle layer). The mid-sized tumor (FaDu3) behaves similarly, but the difference between the basal and apical block is less pronounced than in the large tumors. Small tumors (FaDu4 and FaDu5) exhibited a significantly lower fraction of vital tumor tissue in the basal (closest to the muscle) compared to the apical block. The fractions of vital tissue pooled over all tumors were comparable in the 3 tissue blocks, suggesting that pooling data from tumors of different volumes leads to a loss of information on distinct intra- and inter-tumor heterogeneity.

3.5.2 Fractions of total, chronic and acute hypoxia

The fractions of total, chronic and acute hypoxia in vital tumor tissue were fairly similar in the 4 serial sections of the individual tissue blocks (Figs. 18 - 20). Additionally, the fractions of chronic hypoxia (38.2 ± 1.3) were consistently higher than those of acute hypoxia (7.1 ± 0.4). The fraction of total hypoxia decreased in large tumors (FaDu1 and FaDu2) from the apical to the basal block (closest to the muscle layer). The mid-sized tumor (FaDu3) exhibited a similar tendency. In the small tumors (FaDu4 and FaDu5), there was an increase in the fraction of total hypoxia in the basal, compared to the apical or central block. The overall mean shows a relatively constant distribution in the overall hypoxic MCSU fraction over all

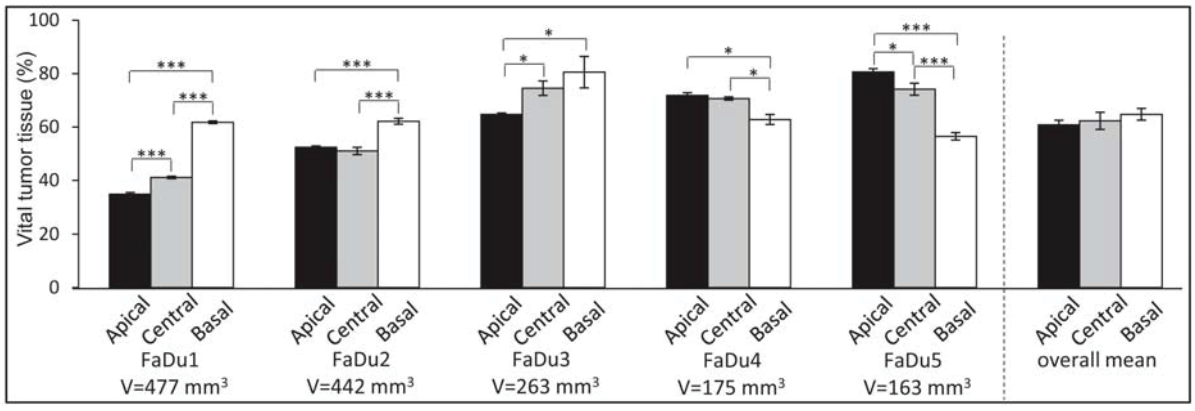

Fig. 17. Mean fractions of vital tumor tissue (± SEM). Apical, central and basal indicate the location of the three different tissue blocks within each tumor. * = p ≤ 0.05, *** = p ≤ 0.001; V = tumor volume [Maftei et al. 2012].

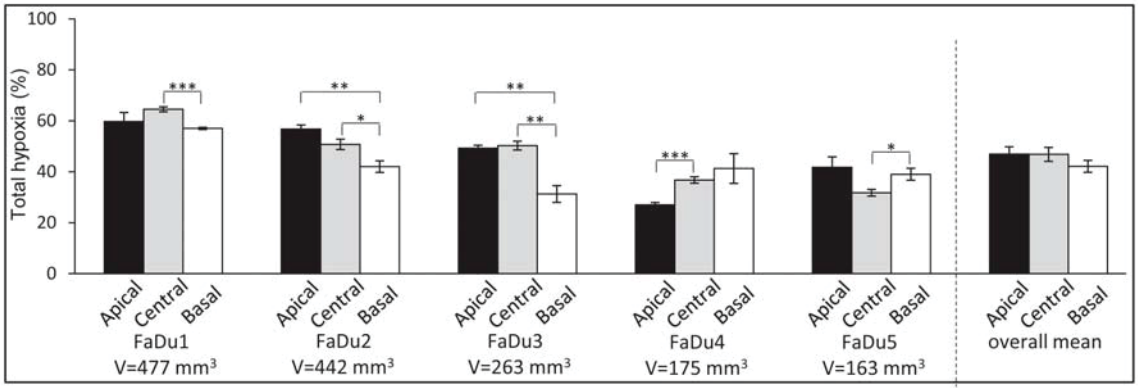

Fig. 18. Mean fractions of total hypoxia (± SEM) in vital tumor tissue. Apical, central and basal indicate the location of the three different tissue blocks within each tumor. * = p ≤ 0.05, ** = p ≤ 0.01, *** = p ≤ 0.001; V = tumor volume [Maftei et al. 2012].

three blocks suggesting again that pooling data from tumors of different volumes leads to a loss of information on distinct intra- and inter-tumor heterogeneity.

The same trend as for total hypoxia was observed for chronic hypoxia (Fig. 19). In large and mid-sizeed tumors, there was a decrease in the chronic hypoxic fraction from the apical to the basal part of the tumor (FaDu2, FaDu3), except FaDu1 where it stayed almost constant over the 3 tissue blocks. One of the small tumors (FaDu4) exhibited a significant increase in the fraction of chronic hypoxia from the apical to the basal part of the tumor. However, the distribution of chronic hypoxia in the other small tumors (FaDu5) was relatively homogeneous. Pooled data from tumors of different volumes leads to a loss of information on distinct intra- and inter-tumor heterogeneity regarding chronic hypoxia.

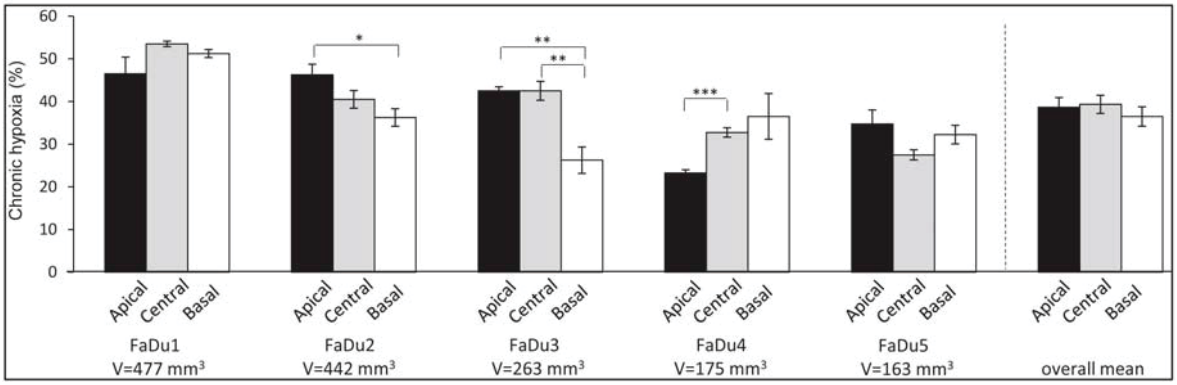

Fig. 19. Mean fractions of chronic hypoxia (± SEM) in vital tumor tissue. Apical, central and basal indicate the location of the three different tissue blocks within each tumor. * = p ≤ 0.05, ** = p ≤ 0.01, *** = p ≤ 0.001; V = tumor volume [Maftei et al. 2012].

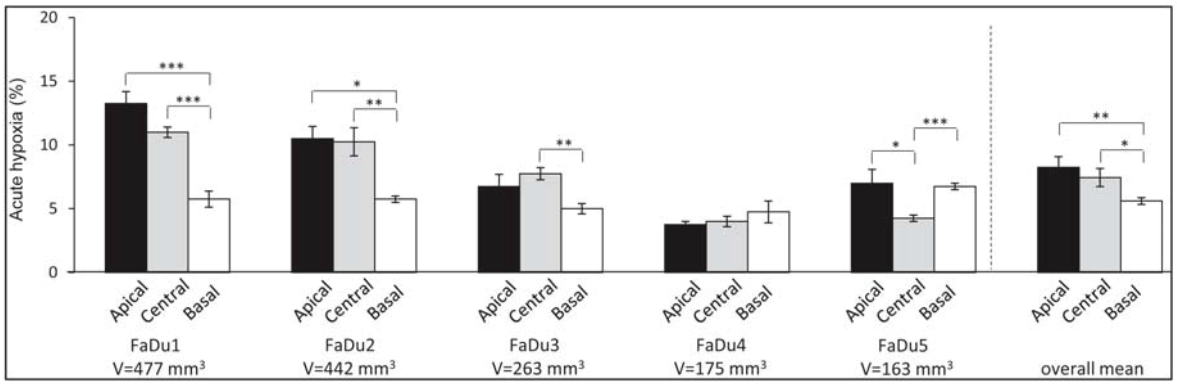

Fig. 20. Mean fractions of acute hypoxia (± SEM) in vital tumor tissue. Apical, central and basal indicate the location of the three different tissue blocks within each tumor. * = $p \leq 0.05$, ** = $p \leq 0.01$, *** = $p \leq 0.001$; V = tumor volume [Maftei et al. 2012].

The fractions of acute hypoxia were also similar to total hypoxia (Fig. 20). Here, in the large tumors (FaDu1, FaDu2) and the mid-sized tumor (FaDu3), the acute hypoxia fraction decreased significantly from the apical to the basal part. In the small tumors, there was a significant increase from the central to the basal tissue block of FaDu5, but no heterogeneous distribution between the blocks was noticed for FaDu4. The pooled data from all blocks of the tumors revealed a decrease in acute hypoxia from the apical to the basal part of the tumor.

4 DISCUSSION

4.1 Vital tumor tissue

Upon fractionated irradiation, xenograft tumors from the 5 cell lines (UT-SCC-5, UT-SCC-14, UT-SCC-15, FaDu, SAS) developed so much necrosis that only tumors irradiated with up to 20 Gy could be analyzed (Fig. 10). Thus, tumors irradiated with a greater total dose (30 to 60 Gy), which would be similar to doses used in the clinic, could not be evaluated. The gradual reduction in vital tumor tissue upon fractionated irradiation was noticed in all 5 tumor lines, but interestingly the higher the fraction of vital tumor tissue before irradiation, the larger the increase in necrotic fraction after treatment (Fig.11). Since FaDu tumors had the largest VTF before irradiation, and are moderately radioresistent (TCD_{50} = 61.5 Gy), this tumor line was chosen for the *in vivo* non-invasive investigation of acute hypoxia distribution. In order to observe the impact of more radioresistant tumors, acute hypoxia distribution was also performed on the tumor line CAL-33 (TCD_{50} = 105 Gy).

4.2 MCSU as a new tool for classification and quantification of tumor hypoxia

Here, a new method was established for the assessment of chronic, acute and hypoxemic hypoxia subtypes [Maftei et al. 2011(a)], which may facilitate current methods to (clinically) identify and eliminate hypoxia. Various endogeneous and exogeneous hypoxia markers are available, and some of them have been used in combination with other microenvironmental parameters such as blood perfusion, vascular architecture, cell proliferation, and apoptosis in order to predict total hypoxia in experimental tumors [Bussink et al. 2003]. The differentiation between hypoxia subtypes could be a useful addition to other technologies, which are only valid for the detection of total hypoxia [Bley et al. 2009, Kotas et al. 2009] or when oxygen measurements in necrotic tissue areas need to be excluded. Plasma flow is a cause of hypoxemic hypoxia and has previously been visualized using window chambers [Dewhirst et al. 1996] and was calculated to represent a very low fraction of vessels (about 9%). This is in line with the fraction of hypoxemic hypoxia identified via the MCSU method. Nevertheless, this later hypoxia subtype still remains difficult to be classified since it can be acute and/or chronic [Bayer et al. 2011]. For this reason, the focus here was mostly on assessing the amount of chronic and acute hypoxia subtypes.

Yaromina et al. [Yaromina et al. 2010, 2011] investigated the same tumor lines mentioned above after staining for perfusion (Hoechst 33342), hypoxia (Pimo) and microvessels

(CD31). They applied quantitative digital analysis to calculate the pimonidazole hypoxic fraction (pHF) and the fraction of perfused vessels (PF). After comparing the pHF values observed by Yaromina et al. with our total hypoxia data for the individual tumors analyzed, a significant positive correlation was found ($p \leq 0.001$).

Quantification of hypoxic fractions using MCSUs takes into account the spatial distribution of perfusion, microvessels and hypoxia in vital tumor tissue. There are several advantages of this technique, such as very good resolution, possibility to distinguish between necrotic and vital tumor tissue, and the ability to differentiate between the three hypoxia subtypes. Nevertheless, there are some limitations that should be noted. For example, the fraction of acute hypoxia is most likely underestimated due to the fact that it takes at least 15 min for pimonidazole to be distributed, reduced and bound (for a review of the time frame of acute hypoxia see Bayer et al. 2011). On the other hand, a single cycle of acute hypoxia can be shorter than 15 min and in this way might escape the detection procedure. Additionally, only two-dimensional hypoxia distribution at a single time point can be evaluated although hypoxia is a very dynamic phenomenon. Another important limitation of this technique is that it would be necessary to surgically remove or biopsy the tumors in the clinic.

4.3 Importance of differentiating between chronic and acute hypoxia

Many authors have focused on distinguishing between chronic and acute hypoxia in experimental and clinical settings. Based on our MCSU method, the amount of acute hypoxia is distinctly less than chronic hypoxia. This is in line with most of the previous published data [Bayer und Vaupel 2012]. For example, in experimentally xenografted tumors, Tufto et al. [Tufto et al. 1995] compared two perfusion markers injected 20 min apart and could see no significant evidence of transient perfusion. Also Benewith et al. [Bennewith et al. 2004] detected only 8 - 20% transient hypoxia using dual hypoxia injection and FACS analysis on xenografted tumors. Concerning clinical data, Goethals et al. [Goethals et al. 2006], calculated only 3.5 % acute hypoxia in human colorectal adenocarcinoma. Even though the fraction of acute hypoxia detected in this and other studies is low [Rofstad et al. 2010], it could be that this hypoxia subtype may still have a great impact on cancer development. For example, exposing tumor-bearing animals to acute cyclic hypoxic stress, enhanced metastatic dissemination [Cairns et al. 2001]. Another aspect is the planning of radiation treatment schedule and the outcome of tumors, which seems to be influenced by the fraction of acute and chronic hypoxia. Ruggieri calculated in a modeling study the dose per fraction, the number of fractions and their relation to the curative dose T_{50} [Ruggieri 2004]. The results from this study suggested a better outcome for chronically hypoxic tumors after a short

hypofractionated irradiation treatment and for acutely hypoxic tumors after a multi-fractionated treatment. Therefore non-invasive detection and quantification of acute and chronic hypoxia might be very promising for clinical application.

4.4 [^{18}F]Fmiso PET/CT and the Wang model, a promising non-invasive method for the quantification of chronic and acute hypoxia

Serial [^{18}F]Fmiso PET/CT imaging was applied for the detection and quantification of chronic and acute hypoxia, and compared to (immuno-)fluorescence staining and assessment of MCSUs on a single cryosection located in the center of each tumor. [^{18}F]Fmiso PET/CT imaging was analyzed using the mathematical model proposed by Wang et al. [Wang et al. 2009]. The original Wang Model estimated larger fractions of acute hypoxia than the MCSU-based method (Fig. 16). This difference could be explained by the fact that the MCSU method calculates the number of microvessels surrounded by acute or chronic hypoxia, while the Wang model estimates [^{18}F]Fmiso uptake, which has no spatial linking. The modified Wang model in turn estimated lower values of acute hypoxia than the original Wang model and improved the correlation with the MCSU-based method. However, there was no significant correlation between values from the MCSU-based method and either the original or modified Wang model. This is probably due to the fact that weighting in the Wang model, is dependent on the tracer uptake in each voxel, which is much larger than a single MCSU can. Therefore, each PET voxel is composed of a mixture of acute, chronic and normoxic MCSUs.

The spatial resolution of micro-PET is quite poor compared to (immuno-)fluorescence microscopy of tumor sections. This inhibits comparison of the same magnification scale in both methods. This is important because extremely heterogeneous distribution of hypoxia has been shown to be found not only across the whole tumor but also within a single voxel [Petit et al. 2009]. Still, some studies have verified [^{18}F]Fmiso as a reliable non-invasive hypoxia marker after finding a significant correlation with pimonidazole staining [Dubois et al. 2004]. In addition, other hypoxia tracers such as FAZA have been reported to accurately represent the microscopic reality [Busk et al. 2009].

One limitation of the Wang model is the necessity of accurate co-registration between the 2 serial PET/CT images (time 0 and time 24 h). In order to overcome this problem, a fixation system was developed and implemented in this project. This fixation system contains a numbered grid and fiducial markers to accurately reproduce the positioning of the tumor bearing mice (Fig. 9). Although the registration errors might be slightly higher than other

internal markers and immobilization methods [Cho et al. 2009, Zhang et al. 2008], our results are acceptable after the intrinsic resolution (about 1.5 mm) of PET is taken into consideration [Disselhorst et al. 2010]. Since the Wang model is based on measurements of tracer uptake at 24 h apart, tumor growth, morphological changes and organ motion [Langen et al. 2001] could represent factors that diminish co-registration precision. Also fitting of the histogram for the calculation of acute and chronic hypoxia depends on the number of bins and their frequency, however for large human tumors, this would not be a problem. Moreover, recent data underline the fact that acute and chronic hypoxia cannot easily be separated using serial PET images, this bringing inconsistency in this field [Mönnich et al. 2012].

In conclusion, neither the original nor the modified Wang model delivered acute hypoxia values that correlate significantly with the MCSU method. This lack of correlation is probably due to non-linear uptake of [^{18}F]Fmiso and the spatial assessment of MCSUs. Nevertheless, the modified Wang model has potential to be used for prediction of radiation response, but still needs preclinical and clinical improvements and validation experiments.

4.5 Heterogenic distribution of tumor hypoxia

A heterogeneous distribution of oxygenation occurring throughout the entire tumor volume as shown in this study is a characteristic of experimental tumors [Vaupel 1977, Vaupel et al. 1981, 1989, 1991] as well as advanced cancer in the clinical setting [Mueller-Klieser et al. 1981, Wendling et al. 1984, Vaupel et al. 1988, 1991, Höckel et al. 1991]. In human tumors, this heterogeneity is underlined by the fact that hypoxic areas are not preferentially located in the center of the tumor, but are randomly distributed without any topological tendency [Höckel et al. 1991, Vaupel et al. 1991, Grosu et al. 2007].

Another aspect of tumor heterogeneity is related to the tumor volume as can be seen in the 5 tumors of different sizes (Fig. 18). Here, it is reported that larger experimental tumors above a certain size are preferentially more hypoxic/necrotic in the region farthest from the muscle, while smaller tumors are more hypoxic/necrotic closest to the skin. Interestingly, the average volume of the evaluated tumors from Publications # 1 and # 2 ($V \approx 284$ mm^3, data not shown), was comparable to the volume of FaDu3 ($V=263$ mm^3), FaDu4 ($V=175$ mm^3) and FaDu5 ($V=163$ mm^3) tumors analyzed in Publication # 4, which were also predominantly normoxic and approximately the same size. It should be noted that the larger tumors, FaDu1 and FaDu2 (Publication # 4) were predominantly hypoxic (over 50% of the total vital tissue). Based on this data and on an earlier oxygenation study [Vaupel et al. 2004, Vaupel 2008], it can be concluded that small xenografted tumors that grow subcutaneously on the leg may

still receive their oxygen and nutrients mostly from the subcutis, allowing them to be more normoxic. In contrary, large tumors, become increasingly independent of subcutaneous vessels, build their own abnormal microvessel system [Vaupel et al. 1989, Vaupel 2004, Margaritescu et al. 2008] and thereby become predominantly hypoxic. Previous studies [Yaromina et al. 2005] claim that the fraction of hypoxia in a single section is similar to pooled data over several serial slices from the center of the tumor, which is in line with our data. However, it is shown here that the amount of hypoxia measured in the central area was not representative for the other regions (apical and basal) but was very similar to the average on the whole tumor (data not shown). Therefore, the amount of tumor hypoxia should be assessed throughout the whole tumor volume to accurately account for heterogeneities in oxygenation.

4.6 Clinical relevance of [^{18}F]Fmiso as a hypoxia marker

Busk et al., [Busk et al. 2009] were among the first to address the question whether PET-hypoxia imaging could be able to generate reliable maps representative of the microscopic reality in a tumor model. They determined that PET-hypoxia imaging has the potential to be used in clinical studies but its prognostic value and its usefulness in image-guided radiotherapy needs to be proven. The potential use of [^{18}F]Fmiso as a hypoxia tracer was tested in spheroids [Rasey et al. 1987]. The authors demonstrated in a comparative study that [^{18}F]Fmiso binds stably in the same population of hypoxic cells as misonidazole does, and can be used as a hypoxia imaging agent *in vivo*. In this study, [^{18}F]Fmiso was chosen as a hypoxia tracer for *in vivo* experiments presented here. Due to its high cellular uptake in hypoxic regions, [^{18}F]Fmiso has been tested in the *in vivo* preclinical [Bentzen et al. 2002] as well as in the clinical [Gagel et al. 2006] setting and was even described to be a valuable tool for therapy response evaluation. Nevertheless, the diffusion of [^{18}F]Fmiso into tumor tissue might not be optimal due to the hydrophilicity of the compound [Dubois et al. 2009]. Other tracers have been developed in the past two decades for detection of hypoxia *in vivo*, such as ^{18}F-FAZA, [^{18}F]EF3 and Cu-ATSM. All of them undergo reduction and bind to macromolecules within the tumor cells [Chitneni et al. 2011]. A perfect hypoxia tracer should fulfill several criteria such as: uptake at clinical relevant pO_2 values (0-10 mm Hg), lipophilic enough to have uniform tissue distribution but hydrophilic enough to have fast clearance and high accumulation only in tumor tissue in order to minimize patient radiation dose. Although none of the tracers have all these properties, [^{18}F]Fmiso remains the most studied agent. In a comparison study of [^{18}F]Fmiso versus [^{18}F]EF3, both tracers showed no difference regarding

intra-tumor distribution and extra-tumor tissue retention, but a faster accumulation of [^{18}F]Fmiso [Dubois et al. 2009].

5 ACKNOWLEDGEMENTS

I would like to thank

First of all, my doctor mother **Univ.-Prof. Dr. Gabriele Multhoff** for giving me the chance to graduate in her laboratory and for her scientific supervision during the three and half years.
Special thanks goes to my mentor **Univ.-Prof. Dr. Peter Vaupel** for his contribution to my scientific development through fruitful discussions, critical judgments and thorough proof-reading of my publications and doctoral thesis.
To **Univ.-Prof. Dr. Bernhard Küster** I would like to thank for conducting the examination process.

The three most important persons in the experimental part of my thesis, **Dr. Christine Bayer, Dr. Sabrina Astner, and Dr. Shi Kuangyu.** I appreciate your help in guiding my experiments, but also in your scientific assistance in my publications and thesis.
Dr. Daniela Shilling and **Dr. Mathias German** as well as all the doctoral students for your help in solving daily problems in the laboratory and for your scientific consultancy during my PhD.
The nuclear medicine group, especially **Dr. Florian Gärtner** and **Sabine Räder** for assisting and helping me by conducting the animal PET/CT experiments.

A great thank goes also to **Univ.-Prof. Dr. Rüdiger Schmitt** and **Dr. Patrick Babinger** from university of Regensburg who made possible continuation of my study in Germany.

My parents **Constantin and Maria.** I just say I love you even if I can not show it to you as often as you would like. I hope this way you are a little bit proud of me and hopefully you can understand and accept more and more my way. Again I love you!
My **brothers and sisters**, for being on my side as long as I can remember, for helping me when I needed anything and for believing in me. Now it is my turn to thank you.

My friends **Adrian and Alina Marinescu, Emöke Toth**, as well as **Stefan Lochbruner** and **Marco Hubert.** I would like to tell you one secret: you gave me more power then you think, especially in the hardest moments, which you all know. I thank you this way.

Unbelievable, but now when I look back I see more and more clearly that you all played a decisive role in my life. That’s why you will stay forever in my heart.

6 CURRICULUM VITAE

First name	Constantin Alin
Surname	Maftei
Date of birth	26/10/1979
Place of birth	Falticeni (Romania)
Address	Veit-Stoß-Str.15, 80687Munich (Germany)
E-Mail	alinmaftei@yahoo.com
Education	
12/2008- 02/2012	Doctoral thesis *„Determination of the Dynamics of Tumor Hypoxia during Radiation Therapy using Biological Imaging on Mouse Xenograft Tumors“* (Dr. rer. nat.) in radiation biology at the “Klinikum rechts der Isar der TU München”
04/2005-08/2008	Chemistry/biology teacher training at the University of Regensburg, Germany. Certificate: intermediate examination (average grade 2.0).
10/1998-03/2005	Masters in biology at the Al. I. Cuza university of Iasi, Romania. Major: molecular genetics (average grade of 9.53*). Master’s thesis: *„Analysis of the DNA Methyltransferase Gene met1 of Volvox carteri“ (*average grade of 10*)
09/1994-08/1998	Agricultural high school in Falticeni, Romania. Major: veterinary medicine, with final examination as veterinary technical assistant and school leaving examination (average grade of 9.07*)
International Experience	
05/2003-09/2004	Exchange student at the University of Regensburg, Germany
10/2002-03/2003	Exchange student at the University of Groningen, the Netherlands
Languages	
	- Romanian - mother tongue - German - business fluent (DSH examination) - English - business fluent - French – basic
*The Romanian grading system: Grades are given from 10 to 1. The minimum grade for passing is 5, the best grade is 10.	

Constantin Alin Maftei

7 REFERENCES

Arabi M, Piert M. Hypoxia PET/CT imaging: implications for radiation oncology. QJ Nucl Med Biol Imaging 2010;54:500–9.

Arteel GE, Thurman RG, Yates JM, et al. Evidence that hypoxia markers detect oxygen gradients in liver: pimonidazole and retrograde perfusion of rat liver. Br J Cancer 1995;72:889-895.

Astner ST, Shi K, Vaupel P, et al. Imaging of tumor physiology: impacts on clinical radiation oncology. Exp Oncol 2010;32:149-52.

Bache M, Kappler M, Said HM, et al. Detection and specific targeting of hypoxic regions within solid tumors: current preclinical and clinical strategies. Curr Med Chem 2008;15:322-38.

Barendsen GW, Koot CJ, van Kersen GR, et al. The effect of oxygen on impairment of the proliferative capacity of human cells in culture by ionizing radiations of different LET. Int J Radiat Biol Relat Stud Phys Chem Med 1966;10:317-27.

Bayer C, Shi K, Astner ST, et al. Acute versus chronic hypoxia: why a simplified classification is simply not enough. Int J Radiat Oncol Biol Phys 2011;80:965-8.

Bayer C, Vaupel P. Acute versus chronic hypoxia in tumors : Controversial data concerning time frames and biological consequences. Strahlenther Onkol 2012;188:616-627.

Bennewith KL, Durand RE. Quantifying transient hypoxia in human tumor xenografts by flow cytometry. Cancer Res 2004;64:6183-6189.

Bentzen L, Keiding S, Horsman MR, et al. Assessment of hypoxia in experimental mice tumours by [18F]fluoromisonidazole PET and pO_2 electrode measurements. Influence of tumour volume and carbogen breathing. Acta Oncol 2002;41:304-12.

Bley CR, Laluhova D, Roos M, et al. Correlation of pretreatment polarographically measured oxygen pressures with quantified contrast-enhanced power Doppler ultrasonography in spontaneous canine tumors and their impact on outcome after radiation therapy. Strahlenther Onkol 2009;185:756-762.

Broerse JJ, Barendsen GW, van Kersen GR. Survival of cultured human cells after irradiation

with fast neutrons of different energies in hypoxic and oxygenated conditions. Int J Radiat Biol Relat Stud Phys Chem Med 1968;13:559-72.

Brown JM. Evidence for acutely hypoxic cells in mouse tumours, and a possible mechanism of reoxygenation. Br J Radiol 1979;52:650–6.

Busk M, Horsman MR, Jakobsen S, et al. Can hypoxia-PET map hypoxic cell density heterogeneity accurately in an animal tumor model at a clinically obtainable image contrast? Radiother Oncol 2009;92:429–36.

Bussink J, Kaanders JH, van der Kogel AJ. Tumor hypoxia at the micro-regional level: clinical relevance and predictive value of exogenous and endogenous hypoxic cell markers. Radiother Oncol 2003;67:3-15.

Cairns RA, Kalliomaki T, Hill RP. Acute (cyclic) hypoxia enhances spontaneous metastasis of KHT murine tumors. Cancer Res 2001;61:8903-8.

Chaplin DJ, Durand RE, Olive PL. Acute hypoxia in tumors: implications for modifiers of radiation effects. Int J Radiat Oncol Biol Phys 1986;12:1279–82.

Chitneni SK, Palmer GM, Zalutsky MR, et al. Molecular imaging of hypoxia. J Nucl Med 2011;52:165-8.

Cho H, Ackerstaff E, Carlin S, et al. Noninvasive multimodality imaging of the tumor microenvironment: registered dynamic magnetic resonance imaging and positron emission tomography studies of a preclinical tumor model of tumor hypoxia. Neoplasia 2009;11:247-59.

Croce CM. Oncogenes and cancer. N Engl J Med 2008;358:502-11.

Dewhirst MW, Kimura H, Rehmus SW, et al. Microvascular studies on the origins of perfusion-limited hypoxia. Br J Cancer (Suppl) 1996;27:S247-S251.

Dewhirst MW, Ong ET, Braun RD, et al. Quantification of longitudinal tissue pO_2 gradients in window chamber tumours: impact on tumour hypoxia. Br J Cancer 1999;79:1717-22.

Disselhorst JA, Brom M, Laverman P, et al. Image-quality assessment for several positron emitters using the NEMA NU 4–2008 standards in the Siemens Inveon small-animal PET scanner. J Nucl Med 2010;51:610–7.

Dubois L, Landuyt W, Haustermans K, et al. Evaluation of hypoxia in an experimental rat tumour model by [^{18}F]fluoromisonidazole PET and immunohistochemistry. Br J Cancer 2004;91:1947–54.

Dubois L, Landuyt W, Cloetens L, et al. [^{18}F]EF3 is not superior to [^{18}F]FMISO for PET-based hypoxia evaluation as measured in a rat rhabdomyosarcoma tumour model. Eur J Nucl Med Mol Imaging 2009;36:209-18.

Erickson K, Braun RD, Yu D, et al. Effect of longitudinal oxygen gradients on effectiveness of manipulation of tumor oxygenation. Cancer Res 2003;63:4705-12.

Folkman J. The vascularization of tumors. Sci Am 1976;234:58-64, 70-3.

Gagel B, Reinartz P, Demirel C, et al. [^{18}F] fluoromisonidazole and [^{18}F] fluorodeoxyglucose positron emission tomography in response evaluation after chemo-/radiotherapy of non-small-cell lung cancer: a feasibility study. BMC Cancer 2006;6:51.

Goethals L, Debucquoy A, Perneel C, et al. Hypoxia in human colorectal adenocarcinoma: comparison between extrinsic and potential intrinsic hypoxia markers. Int J Radiat Oncol Biol Phys 2006;65:246-254.

Grénman R, Carey TE, McClatchey KD, et al. In vitro radiation resistance among cell lines established from patients with squamous cell carcinoma of the head and neck. Cancer 1991;67:2741-7.

Gross MW, Karbach U, Groebe K, et al. Calibration of misonidazole labeling by simultaneous measurement of oxygen tension and labeling density in multicellular spheroids. Int J Cancer 1995;61:567-73.

Grosu AL, Souvatzoglou M, Röper B, et al. Hypoxia imaging with FAZA-PET and theoretical considerations with regard to dose painting for individualization of radiotherapy in patients with head and neck cancer. Int J Radiat Oncol Biol Phys 2007;69:541-51.

Hall EJ, Giaccia AJ. Radiobiology for the Radiologist. Lippincott Williams & Wilkins, Philadelphia USA, Sixth edition 2006.

Hessel F, Krause M, Helm A, et al. Differentiation status of human squamous cell carcinoma xenografts does not appear to correlate with the repopulation capacity of clonogenic tumour cells during fractionated irradiation. Int J Radiat Biol 2004;80:719-27.

Hirst DG, and Flitney FW (1997). The physiological importance and therapeutic potential of nitric oxide in the tumor-associated vasculature. In: Bicknell R, Lewis CE, Ferrara N (eds) Tumor angiogenesis. Oxford: Oxford University Press, 153-167.

Horsman MR. Measurement of tumor oxygenation. Int J Radiat Oncol Biol Phys 1998;42: 701-4.

Höckel M, Schlenger K, Knoop C, et al. Oxygenation of carcinomas of the uterine cervix: evaluation by computerized O_2 tension measurements. Cancer Res 1991;51:6098-102.

Höckel M, Vaupel P. Tumor hypoxia: definitions and current clinical, biologic, and molecular aspects. J Natl Cancer Inst 2001;93:266-76.

Kotas M, Schmitt P, Jakob PM et al. Monitoring of tumor oxygenation changes in head-and-neck carcinoma patients breathing a hyperoxic hypercapnic gas mixture with a non-invasive MRI technique. Strahlenther Onkol 2009;185:19-26.

Krause M, Schmitz M, Noessner E, et al. Adoptive transfer of cytotoxic T-cells for treatment of residual disease after irradiation. Int J Radiat Biol 2007;83:827-36.

Langen KM, Jones DT. Organ motion and its management. Int J Radiat Oncol Biol Phys 2001;50:265–78.

Ljungkvist AS, Bussink J, Rijken PF, et al. Vascular architecture, hypoxia, and proliferation in first-generation xenografts of human head-and-neck squamous cell carcinomas. Int J Radiat Oncol Biol Phys 2002;54:215-228.

López-Lázaro M. A new view of carcinogenesis and an alternative approach to cancer therapy. Mol Med 2010;16:144-53.

Maftei CA, Bayer C, Shi K, et al. Quantitative assessment of hypoxia subtypes in microcirculatory supply units of malignant tumors using (immuno-)fluorescence techniques. Strahlenther Onkol 2011;187:260-6. (a)

Maftei CA, Bayer C, Shi K, et al. Changes in the fraction of total hypoxia and hypoxia subtypes in human squamous cell carcinomas upon fractionated irradiation: Evaluation using pattern recognition in microcirculatory supply units. Radiother Oncol 2011;101:209-16. (b)

Maftei CA, Shi K, Bayer C, et al. Comparison of (immuno-)fluorescence data with serial [^{18}F]Fmiso PET/CT imaging for assessment of chronic and acute hypoxia in head and neck

cancers. Radiother Oncol 2011;99:412-7. (c)

Maftei CA, Bayer C, Shi K, et al. Intra- and intertumor heterogeneities in total, chronic, and acute hypoxia in xenografted squamous cell carcinomas : Detection and quantification using (immuno-)fluorescence techniques. Strahlenther Onkol 2012;188:606-615.

Magat J, Jordan BF, Cron GO, et al. Noninvasive mapping of spontaneous fluctuations in tumor oxygenation using ^{19}F MRI. Med Phys 2010;37:5434-41.

Mărgăritescu C, Simionescu C, Pirici D, et al. Immunohistochemical characterization of tumoral vessels in oral squamous cell carcinoma. Rom J Morphol Embryol 2008;49:447-58.

Mönnich D, Troost EG, Kaanders JH, et al. Modelling and simulation of the influence of acute and chronic hypoxia on [^{18}F]fluoromisonidazole PET imaging. Phys Med Biol 2012;57:1675-84.

Mueller-Klieser W, Vaupel P, Manz R, et al. Intracapillary oxyhemoglobin saturation of malignant tumors in humans. Int J Radiat Oncol Biol Phys 1981;7:1397-404.

Nordsmark M, Bentzen SM, Rudat V, et al. Prognostic value of tumor oxygenation in 397 head and neck tumors after primary radiation therapy. An international multi-center study. Radiother Oncol 2005;77:18-24.

Osinsky S, Friess H, Vaupel P (eds) Tumor hypoxia in the clinical settings. Kyiv, Akademperiodyka 2011.

Pekkola-Heino K, Joensuu H, Klemi P, et al. Relation of DNA ploidy and proliferation rate to radiation sensitivity in squamous carcinoma cell lines. Arch Otolaryngol Head Neck Surg 1994;120:750-4.

Petit SF, Dekker ALAJ, Seigneuric R, et al. Intra-voxel heterogeneity influences the dose prescription for dose-painting with radiotherapy: a modelling study. Phys Med Biol 2009;54:2179–96.

Pires IM, Bencokova Z, Milani M, et al. Effects of acute versus chronic hypoxia on DNA damage responses and genomic instability. Cancer Res 2010;70:925-935.

Raleigh JA, Chou SC, Arteel GE, et al. Comparisons among pimonidazole binding, oxygen electrode measurements, and radiation response in C3H mouse tumors. Radiat Res

1999;151:580-9.

Rasey JS, Grunbaum Z, Magee S, et al. Characterization of radiolabeled fluoromisonidazole as a probe for hypoxic cells. Radiat Res 1987;111:292-304.

Reinhold HS, Blachiwiecz B, Blok A. Oxygenation and reoxygenation in „sandwich" tumours. Bibl Anat 1977;15:270-2.

Rofstad EK, Maseide K. Radiobiological and immunohistochemical assessment of hypoxia in human melanoma xenografts: acute and chronic hypoxia in individual tumors. Int J Radiat Biol 1999;75:1377-93.

Rofstad EK, Gaustad JV, Egeland TA, et al. Tumors exposed to acute cyclic hypoxic stress show enhanced angiogenesis, perfusion and metastatic dissemination. Int J Cancer 2010;127:1535-1546.

Ruggieri P. Hypofractionation in non-small cell lung cancer (NSCLC): suggestions from modelling both acute and chronic hypoxia. Phys Med Biol 2004;49:4811–23.

Schor AM, Pazouki S, Morris J, et al. Heterogeneity in microvascular density in lung tumours: comparison with normal bronchus. Br J Cancer 1998;77:946-51.

Skinner SA, Tutton PJ, O'Brien PE. Microvascular architecture of experimental colon tumors in the rat. Cancer Res 1990;50:2411-7.

Stadler P, Becker A, Feldmann HJ, et al. Influence of the hypoxic subvolume on the survival of patients with head and neck cancer. Int J Radiat Oncol Biol Phys 1999;44:749-54.

Stainsby WN, Snyder B, Welch HG. A pictographic essay on blood and tissue oxygen transport. Med Sci Sports Exerc 1988;20:213-21.

Stewart GD, Ross JA, McLaren DB, et al. The relevance of a hypoxic tumour microenvironment in prostate cancer. BJU Int 2010;105:8-13.

Tatum J, Kelloff GJ, Gillies RJ, et al. Hypoxia: Importance in tumor biology, noninvasive measurement by imaging, and value of its measurement in the management of cancer therapy. Int J Radiat Biol 2006;82:699–757.

Thomlinson RH, Gray l. The histological structure of some human lung cancers and the possible implications for radiotherapy. Br J Cancer 1955;9:539–49.

Tufto I, Rofstad EK. Transient perfusion in human melanoma xenografts. Br J Cancer 1995;71:789-793.

Varia MA, Calkins-Adams DP, Rinker LH, et al. Pimonidazole: a novel hypoxia marker for complementary study of tumor hypoxia and cell proliferation in cervical carcinoma. Gynecol Oncol 1998;71:270-7.

Vaupel P. Hypoxia in neoplastic tissue. Microvasc Res 1977;13:399-408.

Vaupel P. Oxygenation of human tumors. Strahlenther Onkol 1990;166:377-86.

Vaupel P. The role of hypoxia-induced factors in tumor progression. Oncologist 2004;9 (Suppl 5):10-17.

Vaupel P. Hypoxia and aggressive tumor phenotype: implications for therapy and prognosis. Oncologist 2008;13 (Suppl 3):21-26.

Vaupel P, Kluge M, Ambroz MC. Laser Doppler flowmetry in subepidermal tumours and in normal skin of rats during localized ultrasound hyperthermia. Int J Hyperthermia 1988;4:307-21.

Vaupel P, Kallinowski F, Okunieff P. Blood flow, oxygen and nutrient supply, and metabolic microenvironment of human tumors: a review. Cancer Res 1989;49:6449-65.

Vaupel P, Schlenger K, Knoop C, et al. Oxygenation of human tumors: evaluation of tissue oxygen distribution in breast cancers by computerized O_2 tension measurements. Cancer Res 1991;51:3316-22.

Vaupel P, Thews O, Hoeckel M. Treatment resistance of solid tumors: role of hypoxia and anemia. Med Oncol 2001;18:243-59.

Vaupel P, Harrison L. Tumor hypoxia: causative factors, compensatory mechanisms, and cellular response. Oncologist 2004;9(Suppl 5):4–9.

Vaupel P, Höckel M, Mayer A. Detection and characterization of tumor hypoxia using pO_2 histography. Antioxid Redox Signal 2007;9:1221–35.

Vaupel PW, Frinak S, Bicher HI. Heterogeneous oxygen partial pressure and pH distribution in C3H mouse mammary adenocarcinoma. Cancer Res 1981;41:2008-13.

Wendling P, Manz R, Thews G, et al. Heterogeneous oxygenation of rectal carcinomas in

humans: a critical parameter for preoperative irradiation? Adv Exp Med Biol 1984;180:293-300.

Weidner N, Semple JP, Welch WR, et al. Tumor angiogenesis and metastasis-correlation in invasive breast carcinoma. N Engl J Med 1991;324:1-8.

Wyss MT, Hofer S, Hefti M, et al. Spatial heterogeneity of low-grade gliomas at the capillary level: a PET study on tumor blood flow and amino acid uptake. J Nucl Med 2007;48:1047-52.

Yaromina A, Hölscher T, Eicheler W, et al. Does heterogeneity of pimonidazole labelling correspond to the heterogeneity of radiation-response of FaDu human squamous cell carcinoma? Radiother Oncol 2005;76:206-12.

Yaromina A, Zips D, Thames HD, et al. Pimonidazole labelling and response to fractionated irradiation of five human squamous cell carcinoma (hSCC) lines in nude mice: The need for a multivariate approach in biomarker studies. Radiother Oncol 2006;81:122-29.

Yaromina A, Thames H, Zhou X, et al. Radiobiological hypoxia, histological parameters of tumour microenvironment and local tumour control after fractionated irradiation. Radiother Oncol 2010;96:116-22.

Yaromina A, Kroeber T, Meinzer A, et al. Exploratory study of the prognostic value of microenvironmental parameters during fractionated irradiation in human squamous cell carcinoma xenografts. Int J Radiat Oncol Biol Phys 2011;80:1205-13.

Yasui H, Matsumoto S, Devasahayam N, et al. Low-field magnetic resonance imaging to visualize chronic and cycling hypoxia in tumor-bearing mice. Cancer Res 2010;70:6427-36.

Wang K, Yorke E, Nehmeh SA, et al. Modeling acute and chronic hypoxia using serial images of ^{18}F-FMISO PET. Med Phys 2009;36:4400-8.

Zhang M, Huang M, Le C, et al. Accuracy and reproducibility of tumor positioning during prolonged and multi-modality animal imaging studies. Phys Med Biol 2008;53:5867–82.

Appendix

1. Maftei CA, Bayer C, Shi K, Astner ST, Vaupel P. Quantitative assessment of hypoxia subtypes in microcirculatory supply units of malignant tumors using (immuno-)fluorescence techniques. Strahlenther Onkol 2011;187:260-6.

Strahlentherapie
und Onkologie

Original Article

Quantitative Assessment of Hypoxia Subtypes in Microcirculatory Supply Units of Malignant Tumors Using (Immuno-)Fluorescence Techniques*

Constantin-Alin Maftei, Christine Bayer, Kuangyu Shi, Sabrina T. Astner, Peter Vaupel[1]

Background and Purpose: Hypoxia is a characteristic of tumors, is known to increase aggressiveness, and causes treatment resistance. Traditional classification suggests two types of hypoxia: chronic and acute. Acute hypoxia is mostly caused by transient disruptions in perfusion, while chronic hypoxia is caused by diffusion limitations. This classification may be insufficient in terms of pathogenetic and pathophysiological mechanisms. Therefore, we quantified hypoxia subtypes in tumors based on (immuno-) fluorescent marker distribution patterns in microcirculatory supply units (MCSUs).
Material and Methods: Cryosections from hSCC lines (SAS, FaDu, UT-SCC-5, UT-SCC-14, UT-SCC-15) were analyzed. Hypoxia was identified by pimonidazole, perfusion by Hoechst 33342, and endothelial cells by CD31. The following patterns were identified in vital tumor tissue: (1) normoxia: Hoechst 33342 fluorescence around microvessels, no pimonidazole, (2) chronic hypoxia: Hoechst 33342 fluorescence around microvessels, pimonidazole distant from microvessels, (3) acute hypoxia: no Hoechst 33342 fluorescence around microvessels, pimonidazole in immediate vicinity of microvessels, and (4) hypoxemic hypoxia: Hoechst 33342 fluorescence and pimonidazole directly around microvessels.
Results: Quantitative assessment of MCSUs show predominance for normoxia in 4 out of 5 tumor lines (50.1–72.8%). Total hypoxia slightly prevails in UT-SCC-15 (56.9%). Chronic hypoxia is the dominant subtype (65.4–85.9% of total hypoxia). Acute hypoxia only accounts for 12.9–29.8% and hypoxemic hypoxia for 1.2–6.4% of total hypoxia. The fraction of perfused microvessels ranged from 82.5–96.6%.
Conclusion: Chronic hypoxia is the prevailing subtype in MCSUs. Acute hypoxia and hypoxemic hypoxia account for only a small fraction. This approach enables assessment and recognition of different hypoxia subtypes including hypoxemic hypoxia and may facilitate methods to (clinically) identify and eliminate hypoxia.

Key words: Tumor hypoxia · Acute hypoxia · Chronic hypoxia · Hypoxia subtypes · Perfusion-limited hypoxia · Diffusion-limited hypoxia · Microcirculatory supply unit

Strahlenther Onkol 2011
DOI 10.1007/s00066-010-2216-0

Quantitative Erfassung verschiedener Hypoxieformen in mikrozirkulatorischen Versorgungseinheiten maligner Tumoren mit Hilfe von (Immun-)Fluoreszenztechniken

Hintergrund und Ziel: Hypoxie ist ein Charakteristikum solider Tumoren, führt zur Tumorprogression und Therapieresistenz. Traditionell werden chronische und akute Hypoxie unterschieden. Erstere beruht vor allem auf Diffusionslimitierungen, letztere bevorzugt auf Perfusionsstörungen. Diese Klassifizierung reicht nicht aus, um pathogenetische und pathophysiologische Mechanismen weiter aufzuklären. Deshalb werden Hypoxiesubtypen in mikrozirkulatorischen Versorgungseinheiten (MCSUs) mit Hilfe von (Immun-)Fluoreszenztechniken identifiziert.
Material und Methoden: Gefrierschnitte von xenotransplantierten menschlichen Plattenepithelkarzinomen (SAS, FaDu, UT-SCC-5, UT-SCC-14, UT-SCC-15) werden nach Pimonidazol-Färbung zur Hypoxiemarkierung, Hoechst-33342-Fluoreszenz zum Perfusionsnachweis und CD31-Gefäßdarstellung untersucht. Folgende Muster können in vitalem Gewebe nachgewiesen werden: (1) Normoxie: Hoechst-33342-Fluoreszenz um Gefäße, keine Pimonidazol-Anfärbung; (2) chronische Hypoxie: Hoechst-33342-Fluoreszenz in direkter Gefäßnähe, Pimonidazol in einer gewissen Distanz zu den Gefäßen; (3) akute Hypoxie: Hoechst-33342-Fluoreszenz fehlt, Pimonidazol in unmittelbarer Gefäßnachbarschaft und (4) hypoxämische Hypoxie: Hoechst-33342-Fluoreszenz und Pimonidazol in direkter Gefäßnachbarschaft.

*Presented in part at the 16th Jahreskongress der Deutschen Gesellschaft für Radioonkologie (DEGRO), Magdeburg, Germany, 2010.

[1]Department of Radiotherapy and Radiation Oncology, Klinikum rechts der Isar, Technical University of Munich, Munich, Germany.

Received: August 26, 2010; accepted: October 13, 2010
Published Online: March 24, 2011

Ergebnisse: Die Verteilungsmuster von Hoechst, Pimonidazol und CD31 in den MCSUs weisen darauf hin, dass in 4 der 5 Tumorlinien normoxische Areale überwiegen (50,1–72,8%). Lediglich UT-SCC-15-Tumoren sind überwiegend (56,9%) hypoxisch. Die Analyse der Hypoxiesubtypen zeigt, dass chronische Hypoxie eindeutig überwiegt (65,4–85,9% der Gesamthypoxie). Auf die akute Hypoxie entfallen lediglich 12,9–29,8% der Gesamthypoxie. Der Anteil der hypoxämischen Hypoxie ist am kleinsten (1,2–6,4% der Gesamthypoxie). Die Fraktion der perfundierten Gefäße beträgt 82,5–96,6%.
Schlussfolgerung: Chronische Hypoxie herrscht in mikrozirkulatorischen Versorgungseinheiten der untersuchten Plattenepithelkarzinome vor. Akute und hypoxämische Hypoxie spielen nur eine untergeordnete Rolle. Der experimentelle Ansatz erlaubt erstmalig die Erfassung der hypoxämische Hypoxie im Tumorgewebe und ermöglicht eine Differenzierung verschiedener Hypoxiesubtypen. Die beschriebene Methode könnte die (quantitative) Detektion hypoxischer Areale und klinisch relevante Maßnahmen zur Verbesserung des Oxygenierungsstatus erleichtern.

Schlüsselwörter: Tumorhypoxie · Akute Hypoxie · Chronische Hypoxie · Hypoxieformen · Diffusionslimitierte Hypoxie · Perfusionslimitierte Hypoxie · Mikrozirkulatorische Versorgungseinheit

Introduction

Hypoxia is a characteristic feature of malignant solid tumors and is known to increase aggressiveness and acquired treatment resistance under certain pathophysiological conditions [25, 26, 29, 31]. Considering treatment resistance, oxygen concentrations below 1–2% can lead to substantial limitations in the efficacy of oxygen-dependent treatment modalities, such as standard radiotherapy, some chemotherapy (and combinations thereof), photodynamic therapy, and immunotherapy [28].

According to the traditional classification used in experimental and clinical oncology, a distinction is made between two types of hypoxia: chronic and acute. Thomlinson and Gray [23] set the basis for the description of chronic hypoxia (diffusion-limited hypoxia). It has been assumed to be mainly caused by critical limitations in oxygen diffusion from tumor microvessels into the surrounding respiring tissue. In the case of a central microvessel, the supplied tumor volume resembles a truncated cone with continuously decreasing diffusion distances from the arterial to the venous end [12]. In addition to this type of hypoxia, Brown [6] has initiated awareness of the existence and possible importance of acute hypoxia for tumor biology and cancer therapy. Chaplin et al. [7] thereafter verified acute hypoxia in experimental tumors. According to these reports, acute hypoxia is mainly caused by temporary, local disturbances in perfusion or strong variations in red blood cell fluxes and, thus, in fluctuations of the microvascular oxygen supply (perfusion-limited hypoxia).

In general, *chronic hypoxia* (i.e., hypoxia lasting longer than 2 hours) leads to anti-proliferative effects, induces G_1 arrest in the cell cycle and, in the additional absence of key nutrients, leads to death of normal and most tumor cells. Chronic hypoxia can, thus, limit tumor growth and tumor progression [19, 25, 26]. In contrast, acute, fluctuating or cyclic hypoxia (shorter than approximately 2 hours) can promote tumor aggressiveness. These opposing hypoxia-related responses and biological pathways are called the "Janus face" of tumor hypoxia [26, 27, 30].

Upon *acute hypoxia*, a small fraction of tumor cells can escape hypoxia-induced cell damage by triggering (transient) changes in transcription, gene and protein expression favoring tumor progression (via hypoxia-responsive processes at oxygen concentrations below 1%). At oxygen concentrations below 0.1%, malignant cells can undergo (permanent) genomic and epigenomic modifications for development of survival strategies of aggressive phenotypes [10, 14].

The pathophysiology and consequences of chronic and acute hypoxia and their various subtypes have been discussed in detail recently [2, 3]. The fraction of these (mostly coexisting) subtypes of hypoxia in solid tumors at a given time has been discussed controversially so far. In a series of experimental tumors, acute hypoxia has been described as the dominating type of oxygen depletion [13, 20, 22], whereas in others, only low levels of acute hypoxia were detected [4, 8, 9, 15, 24].

In this study, quantitative assessment of hypoxia subtypes using (immuno-)fluorescence techniques are described. The evaluation of different hypoxia subtypes is based on the categorization of the oxygenation and perfusion status of individual microcirculatory supply units (MCSUs) in vital tissue of xenografted human squamous cell carcinomas (hSCC) of the head and neck region. Here, MCSUs are defined as vital tumor tissue areas supplied by a microvessel.

Material and Methods

Tumor Lines

In this study, we have examined five xenografted human squamous cell carcinoma (hSCC) lines of varying radiation resistance as assessed by TCD_{50} (radiation dose in Gy necessary to locally control 50% of tumors). Information concerning the cell lines used (UT-SCC-15, UT-SCC-14, FaDu, SAS, and UT-SCC-5), the mouse tumor model, local tumor control assays, and pimonidazole and Hoechst 33342 injection has been described in detail previously [18, 32, 34, 35]. Cryosections from the middle of the tumors were kindly provided by Prof. Dr. M. Baumann (OncoRay, Dresden, Germany).

Histology

For hypoxia detection, pimonidazole (Hypoxyprobe, Burlington, MA, USA) was injected i.p. at 100 mg/kg body weight in a volume of 0.1 ml saline 1 hour before tumor excision, and the perfusion marker Hoechst 33342 (Sigma, Deisenhofen, Germany) was given i.v. at 15 mg/kg body weight in a volume of 0.1 ml saline 1 minute before tumor-bearing mice were sac-

rificed [33]. Tumor excision followed immediately upon animal sacrifice. Tumors were then shock frozen in liquid nitrogen and stored at –80 °C. Thereafter, 10 µm cryosections were processed in Dresden and sent to Munich on dry ice. Before staining, cryosections were fixed in cold (4 °C) acetone, air dried, and rehydrated in PBS.

Pimonidazole was stained with the Mab FITC-labeled anti-pimonidazole antibody (Hypoxyprobe, Burlington, MA, USA) diluted 1:50 in primary antibody diluent (PAD, Serotec, Oxford, U.K.) by incubating for 1 hour at 37 °C in the dark [1, 17].

Microvessels were stained using the purified rat anti-mouse CD31 antibody (MEC 13.3, BD PharMingen, Heidelberg, Germany) diluted 1:100 in PAD. Anti-CD31 was detected using the secondary antibody, AlexaFluor 594 (Invitrogen, Eugene, OR, USA) diluted 1:200 in PBS for 1 hour at 37 °C in the dark. The cryosections were then embedded in fluorescent mounting medium (DAKO, Glostrup, Denmark) and stored at 4 °C.

Necrotic areas were detected by staining serial slices with hematoxylin and eosin and excluded from subsequent analyses.

Microcirculatory Supply Units

For quantification of (immuno-)fluorescence staining, we counted the total number of microcirculatory supply units (MCSUs) in individual whole tumor cross-sections. A MCSU is defined as vital tumor tissue area supplied by a microvessel. The individual whole tumor cross-sections were scanned and photographed using the AxioVision 4.7 and the multidimensional and mosaix modules (Zeiss, Jena, Germany). The pictures obtained were visually evaluated by two independent researchers (CB, CM) by categorizing MCSUs according to their perfusion and oxygenation status (see Figure 1).

On average, 207 MCSUs were analyzed per whole tumor cross-section for UT-SCC-15 tumors, 404 for UT-SCC-14 tumors, 529 for FaDu tumors, 300 for SAS tumors, and 411 for UT-SCC-5 tumors. The number of tumors investigated was as follows: n = 5 for UT-SCC-15, n = 8 for UT-SCC-14, n = 7 for FaDu, n = 7 for SAS, and n = 8 for UT-SCC-5.

Analysis of whole tumor cryosections revealed the following four immanent MCSU patterns: (1) tumor normoxia: Hoechst 33342 fluorescence around a microvessel and no pimonidazole staining (Figure 1a); (2) diffusion-limited hypoxia: Hoechst 33342 fluorescence around a microvessel, pimonidazole staining in areas distant from a microvessel (≥ 100 µm; Figure 1b); (3) acute perfusion stop: no Hoechst 33342 fluorescence around a microvessel and pimonidazole staining in immediate vicinity of a microvessel (Figure 1c), and (4) acute/chronic hypoxemic hypoxia: Hoechst 33342 fluorescence and pimonidazole staining directly surrounding a microvessel (Figure 1d).

Statistical Analyses

Statistical analyses were performed using the statistical package for social sciences (SPSS, Chicago, IL). Data are presented as mean values ± SEM. The Pearson's coefficient of correlation (r) and linear regression analysis were used to determine the relationships between variables. p values < 0.05 were considered to be statistically significant.

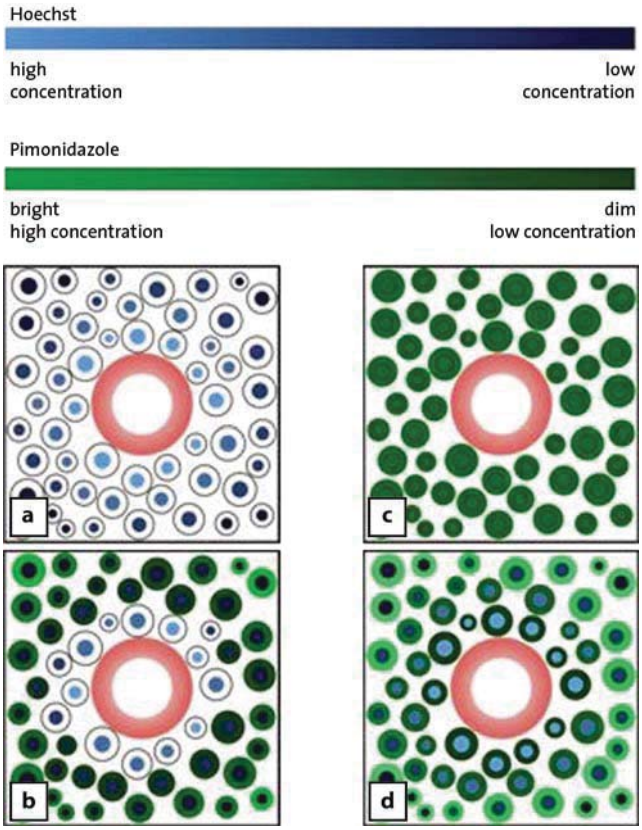

Figure 1. Sketches representing the four microcirculatory supply units (MCSUs): tumor normoxia (**a**); (chronic) diffusion-limited hypoxia (**b**); (acute) perfusion-limited hypoxia (**c**); (acute/chronic) hypoxemic hypoxia (**d**). The *red* circle in the center represents a microvessel. The color bar indicates fluorescence intensities for Hoechst 33342 (*blue*) and pimonidazole (*green*).

Abbildung 1. Schematische Darstellung der 4 mikrozirkulatorischen Versorgungseinheiten (MCSUs): Tumor-Normoxie (**a**): chronische, diffusionslimitierte Hypoxie (**b**); akute, perfusionslimitierte Hypoxie (**c**); (akute/chronische) hypoxämische Hypoxie (**d**). Der *rote* Ring im Zentrum stellt jeweils die Tumorkapillare dar. Die beiden Farbskalen am oberen Rand der Abbildung geben die Fluoreszenz-Intensitäten bzw. Konzentrationen für Hoechst 33342 (*blau*) und Pimonidazole (*grün*) wieder.

Results

According to the previously described categorization, representative stainings are shown in Figure 2 for the four different oxygenation status in xenografted squamous cell carcinomas (SCCs). These experimental patterns, thus, confirm our assumption predicted in Figure 1.

The quantitative analysis of the MCSUs in the different tumor lines is depicted in Figure 3. In this figure, the fraction of normoxic and overall hypoxic MCSUs is shown in the left column. As can be seen, normoxia is dominant in 4 out of the

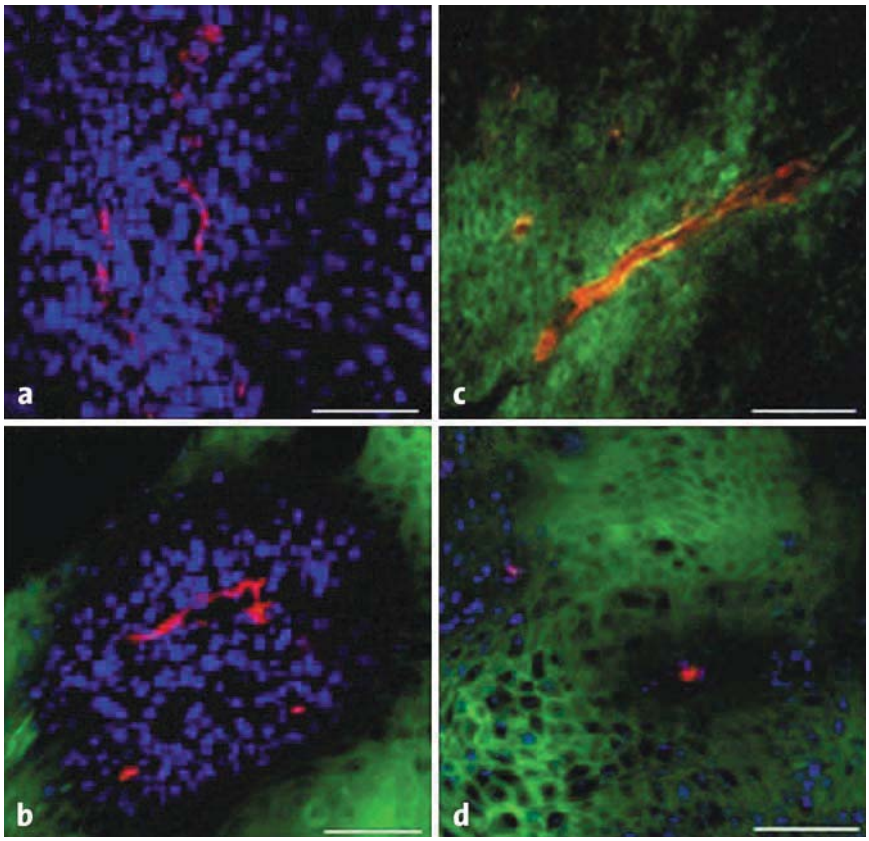

Figure 2. Representative tissue sections showing examples of the four MCSUs as suggested in Figure 1: tumor normoxia (**a**); (chronic) diffusion-limited hypoxia (**b**); (acute) perfusion-limited hypoxia (**c**); (acute/chronic) hypoxemic hypoxia (**d**). Hoechst 33342 fluorescence of perfused areas is shown in *blue*, pimonidazole staining of hypoxia in *green*, and CD31 staining for microvessels in *red*. *White scale bars* indicate 100 µm.

Abbildung 2. Repräsentative Gewebeschnitte mit 4 unterschiedlichen mikrozirkulatorischen Versorgungseinheiten (vgl. Schemata in Abbildung 1.): Normoxisches Tumorgewebe (**a**); chronische, diffusionslimitierte Hypoxie (**b**); akute, perfusionslimitierte Hypoxie (**c**); (akute/chronische) hypoxämische Hypoxie (**d**). *Blau*: Hoechst-33342-Fluoreszenz in perfundierten Arealen; *grün*: Pimonidazol-Färbung hypoxischer Gewebeabschnitte; *rot*: CD31-Färbung von Endothelzellen. Die Länge der *weißen Balken* entspricht jeweils 100 µm.

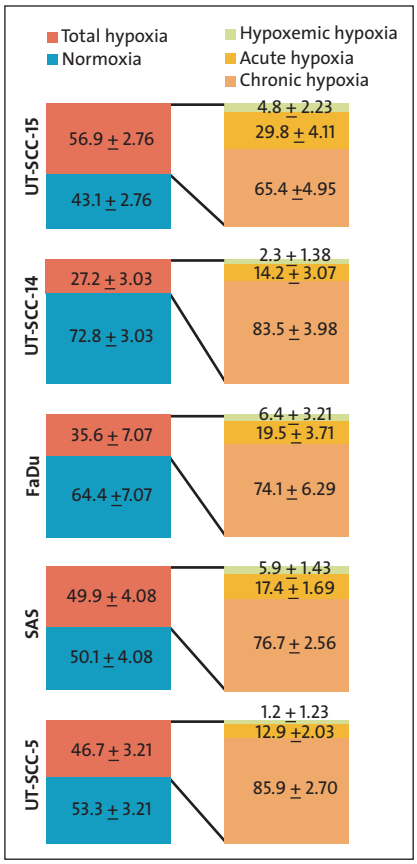

Figure 3. Quantitative analysis of microcirculatory supply units (MCSUs) in five different hSCC tumor lines. The left column shows the fraction of normoxic and overall hypoxic MCSUs, the right column exhibits the fraction of different subtypes of hypoxia relative to total hypoxia. Data are shown as mean ± SEM.

Abbildung 3. Quantitative Analyse mikrozirkulatorischer Versorgungseinheiten (MCSUs) in 5 verschiedenen Xenotransplantaten menschlicher Plattenepithelkarzinome. Linke Säule: Normoxie- und Gesamt-Hypoxieanteile in den verschiedenen Tumorlinien. Rechte Säule: Anteile der Hypoxiesubtypen an der ermittelten Gesamthypoxie der jeweiligen Tumorlinie. Dargestellt sind Mittelwerte ± SEM.

5 tumor lines (UT-SCC-14, FaDu, SAS, and UT-SCC-5). Total hypoxia slightly predominates only in the MCSUs of the UT-SCC-15 tumors (56.9 ± 2.76).

Hypoxia subtypes in the different hSCC tumor lines are presented in the right column of Figure 3. In this presentation, hypoxia subtypes are quantified relative to total hypoxia (the latter normalized to 100% for each tumor line). As can be seen, diffusion-limited (chronic) hypoxia consistently is the prevailing subtype (range from 65.4 ± 4.95% to 85.9 ± 2.70% of total hypoxia). Acute hypoxia only accounts for 12.9 ± 2.03% to 29.8 ± 4.11% of total hypoxia and, thus, clearly is not the predominant hypoxia subtype in the tumor lines investigated. It can, however, consistently be detected in our study. Hypoxemic hypoxia (acute or chronic) represents the smallest fraction of total hypoxia in all tumor lines (ranging from 1.20 ± 1.23% to 6.40 ± 3.21%).

In this study, we additionally evaluated the fraction of perfused microvessels (positive CD31 staining surrounded by Hoechst fluorescence) relative to the total number of CD31-positive microvessels in vital tumor tissue. Perfused microvessels encompass microvessels in MCSUs exhibiting normoxia, chronic hypoxia, and hypoxemic hypoxia. The fraction of perfused microvessels in the cryosections investigated ranged from 82.5 ± 3.20% to 96.6 ± 0.56% (Table 1).

Table 1. List of selected parameters used for correlation studies (data not included in Figure 3). Displayed are the mean values of histological parameters ± SEM and TCD_{50} values with 95% confidence interval (in parentheses). PF_{MCSU}: fraction of perfused vessels assessed in microcirculatory supply units (this study); PF: fraction of perfused vessels as assessed by quantitative digital analysis [33]; pHF: fraction of hypoxia based on pimonidazole staining [33]; TCD_{50}: radiation dose in Gy necessary to locally control 50% of all tumors [33].

Tabelle 1. Zusammenstellung von verwendeten Korrelationsanalysen-Parametern, die nicht in Abb. 3 aufgelistet sind. Dargestellt sind Mittelwerte der histologischen Parameter ± SEM und TCD_{50}-Werte mit 95% Konfidenzintervallen (in Klammern). PF_{MCSU}: Anteil perfundierter Gefäße in mikrozirkulatorischen Versorgungseinheiten (diese Studie); PF: errechneter Anteil perfundierter Gefäße auf der Grundlage von quantitativen digitalen Analysen [33]; pHF: ermittelter Hypoxieanteil anhand von Pimonidazol-Färbungen [33]; TCD_{50}: Strahlendosis in Gy, die benötigt wird, um 50% aller Tumoren lokal zu kontrollieren [33].

Tumor line	PF_{MCSU} (%)	PF (%)	pHF (%)	TCD_{50} (Gy)
UT-SCC-15	82.5 ± 3.20	63.4 ± 8.78	35.2 ± 4.96	37.7 (14; 49)
UT-SCC-14	96.6 ± 0.56	82.7 ± 2.94	20.5 ± 1.93	44.2 (35; 49)
FaDu	94.0 ± 0.87	90.4 ± 1.93	12.7 ± 0.84	61.5 (30; 53)
SAS	91.6 ± 1.35	76.8 ± 3.90	22.3 ± 2.57	99.1 (91; 108)
UT-SCC-5	94.0 ± 0.94	70.7 ± 7.60	23.9 ± 1.71	101.8 (88; 117)

Discussion

Data presented in this study clearly show that with one exception (UT-SCC-15), normoxia prevails in the xenografted hSCC tumor lines investigated. In all tumor cell lines, chronic hypoxia is the predominant hypoxia subtype. Acute and hypoxemic hypoxia are relatively rare based on evaluation of MCSUs. The fact that chronic hypoxia prevails is in line with data presented earlier for other tumor lines. For example, in human tumor xenografts, Bennewith et al. [4] calculated between 8% and 20% transient hypoxia using dual hypoxia marker injection and FACS analysis, and Tufto et al. [24] found no significant evidence of transient perfusion after comparison of two perfusion markers injected 20 minutes apart. In human colorectal adenocarcinoma, the fraction of acute hypoxia was reported to be 3.5% [11]. In contrast to our data, Rofstad et al. [20, 22] have shown in human melanoma xenografts that acute hypoxia prevails and leads to a higher metastatic potential than chronically hypoxic cells. Considering pathophysiological consequences, we assume that even if the fraction of acute hypoxia is very low in our study, it still can be of great biological importance. Rofstad et al. [21] recently demonstrated direct relevance for the impact of acute hypoxia. The authors exposed animals carrying human xenograft tumors to acute cyclic hypoxic stress and detected enhanced angiogenesis, perfusion, and metastatic dissemination. The existence of plasma flow (causative of hypoxemic hypoxia) was previously visualized in mammary tumors transplanted into window chambers and calculated to be present in a low fraction of vessels (≈ 9%), which is similar to our data [9].

Yaromina et al. [34] investigated the same tumor lines using Hoechst 33342 fluorescence, pimonidazole, and CD31 staining, and quantitative digital analysis to calculate the fraction of perfused vessels (PF) and pimonidazole hypoxic fraction (pHF). We compared the fraction of hypoxia subtypes obtained in our study with recent pHF values communicated by these authors [33]. We found a significant positive correlation between the fraction of total hypoxia calculated in our experiments with published pHF values for the same tumor lines ($p = 0.017$). In addition, there was a positive correlation between the fraction of acute hypoxia assessed in our experiments and pHF data ($p = 0.035$) and a trend for a correlation between the fraction of chronic hypoxia in our study and pHF values. Considering the fact that pimonidazole detects chronic hypoxia more efficiently than acute hypoxia, it is surprising that acute hypoxia contributes most to the correlation between total hypoxia and pHF. One reason for this may be that our determination of chronic hypoxia is based on the indirect quantification of microvessels in the vicinity of pimonidazole stained regions, whereas acutely hypoxic microvessels are directly surrounded by pimonidazole staining. Furthermore, there is a trend for correlation between the PF data extracted from MCSUs in our study and the PF values calculated by Yaromina et al. [33] using identical tumor lines ($p = 0.05$). Taken together, our results show that using quite different methods to quantify hypoxia, comparable results can be obtained. Therefore, the MCSU approach is a valuable tool to estimate not only the total hypoxic fraction, but also allows the identification of hypoxia subtypes.

Comparison of our data (fraction of normoxia, total hypoxia, subtypes of hypoxia, and PF) with TCD_{50} data published by Yaromina et al. [33] did not reveal any significant correlation. Previous analysis of the hSCC xenograft tumors used in our study revealed no relationship between pimonidazole binding and TCD_{50} [36]. Surprisingly, in our experiments, the tumor line with the lowest TCD_{50} value (UT-SCC-15) is the most hypoxic and the tumor line with the highest TCD_{50} value (UT-SCC-5) is only moderately hypoxic (total hypoxia).

Of all the hypoxic subtypes, only chronic hypoxia showed a weak correlation with TCD_{50}. The lack of significance was due to the tumor line with the highest fraction of total hypoxia (UT-SCC-15). Removal of this tumor line from statistical analysis revealed a highly significant correlation between TCD_{50} and chronic hypoxia ($r = 0.999$, $p < 0.001$). A similar correlation was not found for acute or hypoxemic hypoxia.

In order to quantify individual MCSUs, it is necessary to study the spatial distribution of perfusion, microvessels and hypoxia in tumor tissue. This was achieved by analyzing (immuno-)fluorescence staining patterns. The advantage of this technique is that there is very good resolution and necrotic tissue can be excluded. However, certain limitations in this method should be noted. For example, acute hypoxia may be underestimated due to the fact that hypoxia needs to last long enough

to allow distribution and reduction of the hypoxia marker. Therefore, chronic (diffusional) hypoxia and chronic hypoxemic hypoxia may be more accurately detected than acute hypoxia and acute hypoxemic hypoxia. In addition, only a two-dimensional aspect of a small tissue volume at a certain point in time is evaluated, despite the fact that pronounced spatial and temporal heterogeneity of the parameters assessed is a characteristic feature of malignant tumors, both on a microscopic and macroscopic scale. A further important limitation of this technique in the clinical setting is the requirement for invasive removal of a tumor biopsy.

Conclusions

Overall, the data of this study show that chronic hypoxia is the prevailing subtype of tumor hypoxia. Acute and hypoxemic hypoxia account for only a small fraction in xenografts of human squamous cell carcinomas of the head and neck region. Analysis of microcirculatory supply units (MCSUs) enables the assessment of hypoxemic hypoxia, may assist in recognition of different hypoxia subtypes and may facilitate the application of methods to (clinically) identify and eliminate hypoxia. Furthermore, quantification of hypoxia subtypes in MCSUs could be a useful addition to other technologies, which are only valid for the detection of total hypoxia [e.g., 5, 16] and when oxygen measurements in necrotic tissue areas need to be excluded.

Acknowledgments

This study has been supported in part by grants of the Deutsche Forschungsgemeinschaft (DFG: Ba 3514/1-1), the Bundesministerium für Bildung und Forschung (BMBF: 01EZ0826), and the Deutsche Krebshilfe (106758). The authors would like to thank Prof. Dr. M. Baumann for providing tumor cryosections.

References

1. Arteel GE, Thurman RG, Yates JM, et al. Evidence that hypoxia markers detect oxygen gradients in liver: pimonidazole and retrograde perfusion of rat liver. Br J Cancer 1995;72:889–95.
2. Bayer C, Maftei C-A, Astner ST, et al. Subtypes of chronic and acute hypoxia in tumors according to different causative mechanisms. Strahlenther Onkol 2010;186 (Suppl 1):66.
3. Bayer C, Shi K, Astner ST, et al. Acute versus chronic hypoxia: why a simplified classification is simply not enough. Int J Radiat Oncol Biol Phys 2011; in press.
4. Bennewith KL, Durand RE. Quantifying transient hypoxia in human tumor xenografts by flow cytometry. Cancer Res 2004;64:6183–9.
5. Bley CR, Laluhova D, Roos M, et al. Correlation of pretreatment polarographically measured oxygen pressures with quantified contrast-enhanced power Doppler ultrasonography in spontaneous canine tumors and their impact on outcome after radiation therapy. Strahlenther Onkol 2009;185:756–62.
6. Brown JM. Evidence for acutely hypoxic cells in mouse tumours, and a possible mechanism of reoxygenation. Br J Radiol 1979;52:650–6.
7. Chaplin DJ, Durand RE, Olive PL. Acute hypoxia in tumors: implications for modifiers of radiation effects. Int J Radiat Oncol Biol Phys 1986;12:1279–82.
8. Chaplin DJ, Olive PL, Durand RE. Intermittent blood flow in a murine tumor: radiobiological effects. Cancer Res 1987;47:597–601.
9. Dewhirst MW, Kimura H, Rehmus SW, et al. Microvascular studies on the origins of perfusion-limited hypoxia. Br J Cancer 1996;27(Suppl):S247–51.
10. Giaccia AJ. Hypoxic stress proteins: survival of the fittest. Semin Radiat Oncol 1996;6:46–58.
11. Goethals L, Debucquoy A, Perneel C, et al. Hypoxia in human colorectal adenocarcinoma: comparison between extrinsic and potential intrinsic hypoxia markers. Int J Radiat Oncol Biol Phys 2006;65:246–54.
12. Groebe K, Vaupel P. Evaluation of oxygen diffusion distances in human breast cancer xenografts using tumor-specific in vivo data: role of various mechanisms in the development of tumor hypoxia. Int J Radiat Oncol Biol Phys 1988;15:691–7.
13. Gulliksrud K, Vestvik IK, Galappathi K, et al. Detection of different hypoxic cell subpopulations in human melanoma xenografts by pimonidazole immunohistochemistry. Radiat Res 2008;170:638–50.
14. Hoeckel M, Vaupel P. Tumor hypoxia: definitions and current clinical, biologic, and molecular aspects. J Natl Cancer Inst 2001;93:266–76.
15. Kimura H, Braun RD, Ong ET, et al. Fluctuations in red cell flux in tumor microvessels can lead to transient hypoxia and reoxygenation in tumor parenchyma. Cancer Res 1996;56:5522–8.
16. Kotas M, Schmitt P, Jakob PM. et al. Monitoring of tumor oxygenation changes in head-and-neck carcinoma patients breathing a hyperoxic hypercapnic gas mixture with a non-invasive MRI technique. Strahlenther Onkol 2009;185:19–26.
17. Ljungkvist AS, Bussink J, Rijken PF, et al. Vascular architecture, hypoxia, and proliferation in first-generation xenografts of human head-and-neck squamous cell carcinomas. Int J Radiat Oncol Biol Phys 2002;54:215–28.
18. Maftei C-A, Bayer C, Astner ST, et al. Quantitative assessment of hypoxia subtypes in xenografted human tumors. Strahlenther Onkol 2010;186(Suppl 1):69.
19. Pires IM, Bencokova Z, Milani M, et al. Effects of acute versus chronic hypoxia on DNA damage responses and genomic instability. Cancer Res 2010;70: 925–35.
20. Rofstad EK, Galappathi K, Mathiesen B, et al. Fluctuating and diffusion-limited hypoxia in hypoxia-induced metastasis. Clin Cancer Res 2007;13:1971–8.
21. Rofstad EK, Gaustad JV, Egeland TA, et al. Tumors exposed to acute cyclic hypoxic stress show enhanced angiogenesis, perfusion and metastatic dissemination. Int J Cancer 2010;127:1535–46.
22. Rofstad EK, Maseide K. Radiobiological and immunohistochemical assessment of hypoxia in human melanoma xenografts: acute and chronic hypoxia in individual tumours. Int J Radiat Biol 1999;75:1377–93.
23. Thomlinson RH, Gray l. The histological structure of some human lung cancers and the possible implications for radiotherapy. Br J Cancer 1955;9:539–49.
24. Tufto I, Rofstad EK. Transient perfusion in human melanoma xenografts. Br J Cancer 1995;71:789–93.
25. Vaupel P. The role of hypoxia-induced factors in tumor progression. Oncologist 2004;9(Suppl 5):10–7.
26. Vaupel P. Hypoxia and aggressive tumor phenotype: implications for therapy and prognosis. Oncologist 2008;13(Suppl 3):21–6.
27. Vaupel P. Pathophysiology of tumors. In: Molls M, Vaupel P, Nieder C, et al. (eds) The impact of tumor biology on cancer treatment and multidisciplinary strategies. Berlin-Heidelberg: Springer, 2009:51–92.
28. Vaupel P. Physiological mechanisms of treatment resistance. In: Molls M, Vaupel P, Nieder C, et al. (eds) The impact of tumor biology on cancer treatment and multidisciplinary strategies. Berlin-Heidelberg: Springer, 2009:273–90.
29. Vaupel P, Harrison L. Tumor hypoxia: causative factors, compensatory mechanisms, and cellular response. Oncologist 2004;9(Suppl 5):4–9.
30. Vaupel P, Mayer A. Effects of anaemia and hypoxia on tumor biology. In: Bokemeyer C, Ludwig H (eds) Anaemia in cancer. European school of oncology scientific updates. 2nd edn. Edinburgh-London: Elsevier, 2005:47–66.
31. Vaupel P, Mayer A. Hypoxia in cancer: significance and impact on clinical outcome. Cancer Metastasis Rev 2007;26:225–39.
32. Yaromina A, Krause M, Thames H, et al. Pre-treatment number of clonogenic cells and their radiosensitivity are major determinants of local tumour control after fractionated irradiation. Radiother Oncol 2007;83:304–10.
33. Yaromina A, Kroeber T, Meinzer A, et al. Exploratory study of the prognostic value of microenvironmental parameters during fractionared irradiation in

human squamuous cell carcinoma xenografts. Int J Radiat Oncol Biol Phys 2011; in press.
34. Yaromina A, Thames H, Zhou X, et al. Radiobiological hypoxia, histological parameters of tumour microenvironment and local tumour control after fractionated irradiation. Radiother Oncol 2010;96:116–22.
35. Yaromina A, Zips D, Thames HD, et al. Pimonidazole labelling and response to fractionated irradiation of five human squamous cell carcinoma (hSCC) lines in nude mice: The need for a multivariate approach in biomarker studies. Radiother Oncol 2006;81:122–9.
36. Zips D, Yaromina A, Schutze C, et al. Experimental evaluation of functional imaging for radiotherapy. Strahlenther Onkol 2007;183(Suppl 2):41–2.

Address for Correspondence
Christine Bayer, Ph.D.
Department of Radiotherapy and Radiation Oncology,
Klinikum rechts der Isar
Technical University of Munich
Ismaninger Str. 22
81675 München
Germany
Phone (+49/89) 4140-4302, Fax -4296
e-mail: christine.bayer@lrz.tum.de

2. Maftei CA, Bayer C, Shi K, Astner ST, Vaupel P. Changes in the fraction of total hypoxia and hypoxia subtypes in human squamous cell carcinomas upon fractionated irradiation: Evaluation using pattern recognition in microcirculatory supply units. Radiother Oncol 2011;101:209-16.

Radiotherapy and Oncology 101 (2011) 209–216

Contents lists available at ScienceDirect

Radiotherapy and Oncology

journal homepage: www.thegreenjournal.com

Hypoxia

Changes in the fraction of total hypoxia and hypoxia subtypes in human squamous cell carcinomas upon fractionated irradiation: Evaluation using pattern recognition in microcirculatory supply units

Constantin-Alin Maftei, Christine Bayer *, Kuangyu Shi, Sabrina T. Astner, Peter Vaupel

Department of Radiotherapy and Radiation Oncology, Technical University of Munich, Germany

ARTICLE INFO

Article history:
Received 8 December 2010
Received in revised form 6 May 2011
Accepted 6 May 2011
Available online 3 June 2011

Keywords:
Tumor hypoxia
Hypoxia subtypes
Chronic hypoxia
Acute hypoxia
Fractionated irradiation
Microcirculatory supply units

ABSTRACT

Background and purpose: Evaluate changes in total hypoxia and hypoxia subtypes in vital tumor tissue of human head and neck squamous cell carcinomas (hHNSCC) upon fractionated irradiation.
Materials and methods: Xenograft tumors were generated from 5 hHNSCC cell lines (UT-SCC-15, FaDu, SAS, UT-SCC-5 and UT-SCC-14). Hypoxia subtypes were quantified in cryosections based on (immuno-)fluorescent marker distribution patterns of Hoechst 33342 (perfusion), pimonidazole (hypoxia) and CD31 (endothelium) in microcirculatory supply units (MCSUs). Tumors were irradiated with 5 or 10 fractions of 2 Gy, 5×/week.
Results: Upon irradiation with 10 fractions, the overall fraction of hypoxic MCSUs decreased in UT-SCC-15, FaDu and SAS, remained the same in UT-SCC-5 and increased in UT-SCC-14. Decreases were observed in the proportion of chronically hypoxic MCSUs in UT-SCC-15, in the fraction of acutely hypoxic MCSUs in UT-SCC-15 and SAS, and in the percentage of hypoxemically hypoxic MCSUs in SAS tumors. After irradiation with 5 fractions, there were no significant changes in hypoxia subtypes. Changes in the overall fraction of hypoxic MCSUs were comparable to corresponding alterations in the proportions of acutely hypoxic MCSUs. There was no correlation between radiation resistance (TCD_{50}) and any of the investigated hypoxic fractions upon fractionated irradiation.
Conclusions: This study shows that there are large alterations in the fractions of hypoxia subtypes upon irradiation that can differ from changes in the overall fraction of hypoxic MCSUs.
 Radiotherapy and Oncology 101 (2011) 209–216

Head and neck tumors often contain hypoxic regions that are known to worsen treatment outcome for these patients [e.g., 1–3]. Acute and chronic are the two most commonly investigated forms of hypoxia in experimental and clinical oncology. The longest known (sub-)type of hypoxia, chronic or diffusion-limited hypoxia, was first described by Thomlinson and Gray in 1955 [4]. Evidence for the existence of acute hypoxia was initially proposed by Brown [5] and was verified some years later by Chaplin et al. [6]. A third less commonly discussed subtype of hypoxia, hypoxemic hypoxia, can be either acute (e.g., due to transient plasma flow) or chronic (e.g., during a long-term reduction in oxygen content in the blood caused by tumor anemia) and can have drastic and far-reaching pathophysiological consequences [7]. Evidence of hypoxemic hypoxia in experimental tumors has been previously detected using the window chamber method [8,9].

All three hypoxia subtypes vary in their perfusion-dependent nutrient supply, waste removal and delivery of anti-cancer agents and can substantially limit the efficiency of radiation therapy, oxygen-dependent chemotherapy, photodynamic therapy and immunotherapy [10–12]. Hypoxia reduces the efficacy of radiation cell kill directly due to a lack in fixation of DNA damage and indirectly through changes in transcription, gene and protein expression, and hypoxic clonogenic cells that survive radiation treatment can cause tumor recurrence [13]. An interesting aspect of acute hypoxia is that this subtype, caused by perfusion fluctuations during treatment, could protect tumor cells, yet be ready to resume proliferation shortly thereafter [14]. Clinically relevant differences between acute and chronic hypoxia have been observed [for a review see 15], however, investigations on the direct effect of radiation treatment on all individual hypoxia subtypes is lacking.

Various methods exist to assess tumor oxygenation in experimental and human tumors [for reviews see: 16–20]. The most commonly used methods include: the pO_2 electrode, nitroimidazole detection in tissue sections and PET-imaging using radioactive tracers (e.g., nitroimidazoles and copper compounds) [for a recent review see: 21]. All these methods have limitations for use in the clinical setting. The pO_2 electrode method is invasive and can only be used on accessible tumors that need to be measured in multiple areas to obtain reliable results. Additionally, pO_2 readings from

* Corresponding author. Address: Department of Radiotherapy and Radiation Oncology, Klinikum rechts der Isar, Technical University of Munich, Ismaninger Strasse 22, 81675 Munich, Germany.
E-mail address: christine.bayer@yahoo.com (C. Bayer).

0167-8140/$ - see front matter © 2011 Elsevier Ireland Ltd. All rights reserved.
doi:10.1016/j.radonc.2011.05.023

necrotic tissue areas should be excluded before oxygen data can be used, e.g., as predictive or prognostic factors [22]. Two of the most commonly used nitroimidazole compounds, pimonidazole and EF5, bind covalently to hypoxic cells at pO_2 levels <10 mm Hg and can either be detected in PET or immunohistochemistry in tumor sections. The limitations are that tumor biopsies need to be made available or in the case of xenograft tumors, the mice need to be sacrificed for tumor excision. Unfortunately, the use of radiolabelled nitrominidazoles in experimental tumors is limited due to the fact that the resolution even in micro-PET is relatively poor. Importantly, only very few studies exist validating the use of nitroimidazole-PET for hypoxia detection in animals [e.g., 23–25] and in humans [e.g., 26–30].

Investigations on the changes in oxygenation during the course of fractionated radiation treatment have revealed inconsistent results. Although many studies report a reduction in hypoxia during radiation treatment, some tumors show an increase or no change in hypoxia. In spontaneous canine tumors, initially hypoxic tumors (median pO_2 values $\leqslant$10 mm Hg) remained hypoxic or became better oxygenated, and initially less hypoxic tumors became more hypoxic during fractionated radiation treatment [31–33].

Brizel et al. observed no significant changes in the hypoxia status in head and neck cancer patients upon fractionated irradiation compared to pretreatment levels [34]. In cervix carcinoma patients, tumor hypoxia (proportion of pO_2 values < 5 mm Hg) decreased in 15 and increased in 4 out of 19 cervix carcinoma patients following fractionated radiation with 40–45 Gy [35]. Interestingly, in head and neck cancer [36], and cervical cancer [37] patients, progressive disease was worse in patients with hypoxic tumors that remained hypoxic during radiation treatment.

Until now, changes in the fraction of hypoxia subtypes upon fractionated irradiation have not yet been taken into consideration. We recently described a technique to quantify hypoxic subtypes in microcirculatory supply units (MCSUs) in tumor cryosections [38]. Therefore, the purpose of this study was to evaluate changes in the overall fraction of hypoxic MCSUs and hypoxia subtypes in vital tumor tissue by means of pattern recognition in MCSUs in five different xenografted human head and neck cancer lines of varying radiation sensitivity.

Material and methods

Tumor lines

Five xenografted human squamous cell carcinoma (hHNSCC) lines of varying radiation resistance were investigated. For detailed information concerning the cell lines used (UT-SCC-15, UT-SCC-14, FaDu, SAS and UT-SCC-5), the mouse tumor model and local tumor control assays (TCD_{50}) see Yaromina et al. [39]. In brief, tumors were transplanted subcutaneously into the right hind leg of nude mice that were whole body irradiated with 4 Gy (200 kV X-rays, 0.5 mm Cu filter) 2–5 days before transplantation. Whole body irradiation was performed to suppress residual immune reactions (e.g., of NK cells) of nude mice.

Local tumor irradiation

Local tumor irradiation has been described previously [39]. Briefly, 200 kV X-rays were applied (0.5 mm Cu filter, $\approx$1 Gy/min) at 2 Gy per fraction 5 times per week to all tumors, except SAS tumors, which received only 1.84 Gy per fraction due to technical reasons [39]. The tumors were excised (for histological examination) 24 h after 5 or 10 fractions of irradiation. All irradiations were performed on non-anesthetized animals. Mice entered the experiment when the tumors reached 7 mm in diameter.

Histology

Pimonidazole and Hoechst 33342 injections, as well as the preparation of cryosections were performed at the OncoRay laboratory (Dresden, Germany) as previously described [39]. Briefly, the hypoxia marker pimonidazole (Hypoxyprobe, Burlington, MA, USA) was injected i.p. at 100 mg/kg body weight in a volume of 0.1 ml saline 1 h before tumor excision, and the perfusion marker Hoechst 33342 (Sigma, Deisenhofen, Germany) was given i.v. at 15 mg/kg body weight in a volume of 0.1 ml saline 1 min before tumor-bearing mice were sacrificed. Tumor excision followed immediately upon animal sacrifice. Thereafter, tumors were shock frozen in liquid nitrogen and stored at −80 °C. Ten micrometer cryosections from the middle of each tumor were processed in Dresden and sent to Munich on dry ice. Before staining, cryosections were fixed in cold (4 °C) acetone, air dried and rehydrated in PBS.

Pimonidazole was stained with the Mab FITC-labeled anti-pimonidazole antibody (Hypoxyprobe, Burlington, MA, USA) diluted 1:50 in primary antibody diluent (PAD, Serotec, Oxford, UK) by incubating for 1 h at 37 °C in the dark [40,41]. Microvascular endothelium was stained using the purified rat anti-mouse CD31 antibody (MEC 13.3, BD PharMingen, Heidelberg, Germany) diluted 1:100 in PAD. Anti-CD31 was detected using the secondary antibody; AlexaFluor 594 (Invitrogen, Eugene, OR, USA) diluted 1:200 in PBS for 1 h at 37 °C in the dark. The cryosections were then embedded in fluorescent mounting medium (DAKO, Glostrup, Denmark) and stored at 4 °C.

Necrotic tissue areas were detected by staining adjacent slices with hematoxylin and eosin and excluded from the analysis.

Microcirculatory supply units

The fractions of normoxia and total hypoxia, as well as hypoxia subtypes (chronic, acute and hypoxemic) were quantified in microcirculatory supply units (MCSUs) as reported recently by Maftei et al. [38]. A MCSU is defined as vital tumor tissue area supplied by a microvessel (see Fig. 1). The individual whole tumor cross-sections were scanned and photographed using an AxioCam MRc5 camera, the AxioVision 4.7 program including the multidimensional and mosaix modules (Zeiss, Jena, Germany) for automatic compilation of individual pictures. Each tumor section was sequentially scanned at 100× using a fluorescence microscope (Axioskop 2, Zeiss, Jena, Germany) with three separate filters for Hoechst 33342 (260 nm excitation and 460 nm emission), FITC (480 nm excitation and 535 nm emission) and Alexa Fluor 594 (540 nm excitation and 605 nm emission). The pictures obtained were visually scored blinded by two independent researchers (C.B., C.M.) with very good inter-observer reproducibility. Individual MCSUs were categorized according to their perfusion and oxygenation status (see Fig. 2). The number of MCSUs in each category (normoxia, acute hypoxia, chronic hypoxia or hypoxemic hypoxia) were then counted and normalized to the total number of MCSUs assessed. In this way, it was possible to calculate the fraction of normoxic MCSUs, acutely hypoxic MCSUs, chronically hypoxic MCSUs and hypoxemically hypoxic MCSUs. The overall fraction of hypoxic MCSUs is the sum of the fractions of acutely, chronically and hypoxemically hypoxic MCSUs.

For calculation of the vital tissue fraction, necrotic regions were first outlined on digital images of whole tumor cross-sections. The amount of pixels in necrotic and total tumor areas were quantified using Adobe Photoshop CS4 extended, version 11.0.1. Vital tissue areas were calculated by subtracting the necrotic area from the total tumor area. The vital tumor fraction was calculated by dividing the vital tumor area by the total tumor area.

On average, between 207 and 529 MCSUs were analyzed per whole tumor cross-section for non-irradiated control tumors, be-

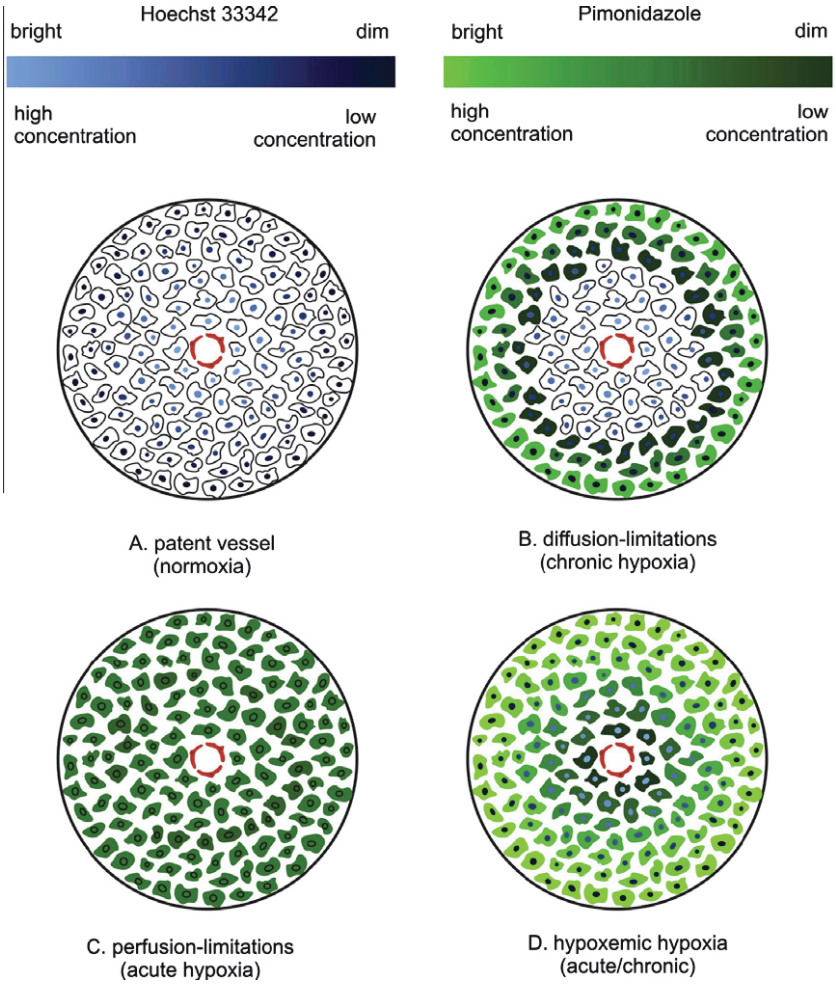

Fig. 1. Schematic diagrams representing microcirculatory supply units (MCSUs) with different oxygenation states: (A) tumor normoxia; (B) (chronic) diffusion-limited hypoxia; (C) (acute) perfusion-limited hypoxia; (D) (acute/chronic) hypoxemic hypoxia. The red circle in the center represents microvascular endothelial lining. The color bars indicate fluorescence intensities for Hoechst 33342 (blue) and pimonidazole (green).

tween 269 and 426 MCSUs for tumors irradiated with 5×2 Gy, and between 283 and 735 MCSUs for tumors irradiated with 10×2 Gy. The total number of tumors investigated per tumor line was 5–8 for control tumors, 7–10 for tumors irradiated with 5×2 Gy and 7–8 for tumors irradiated with 10×2 Gy.

Statistical analyses

Statistical analyses were performed using the statistical package for social sciences (SPSS, Chicago, IL, USA). Data are presented as mean values ± SEM. The student's t-test was used to evaluate the differences between non-irradiated controls and 5×2 Gy and 10×2 Gy fractions of irradiation. The Pearson's coefficient of correlation (R) and linear regression analysis were used to determine the relationships between variables. p-values < 0.05 were considered to be statistically significant.

Results

Fraction of vital tumor tissue before and after fractionated irradiation

Xenografted tumors of various human head and neck squamous cell carcinoma (hHNSCC) lines with comparable volumes and identical transplantation site (but significantly different TCD_{50} values) were investigated. Hematoxylin and eosin sections showed substantially different necrotic or vital tissue fractions before irradiation (see Supplementary material). FaDu tumors had the highest (91.1 ± 3.6%) and UT-SCC-15 the lowest proportion of vital tissue (47.3 ± 5.8%) of the five tumor lines investigated. Other tumor types were grouped in between.

Upon fractioned irradiation using 5×2 Gy, and 10×2 Gy, respectively, the fraction of vital tumor tissue significantly dropped in FaDu ($p < 0.001$) and UT-SCC-5 ($p = 0.006$) tumors following a total dose of 20 Gy (see Supplementary material). There was a trend for a decline in SAS, UT-SCC-14 and UT-SCC-15 tumors. The higher the vital tissue fraction (VTF) before irradiation, the larger the increase in necrotic areas upon irradiation with 10×2 Gy (see Supplementary material). The largest increase in necrotic fraction was thus observed in FaDu tumors (from 9% to 35%, $\Delta = +26\%$), the smallest rise in necrotic fraction was detected in UT-SCC-15 tumors (from 53% to 58%, $\Delta = +5\%$).

Oxygenation status before and after fractionated irradiation

The oxygenation status of the hHNSCC lines was quantified in microcirculatory supply units (MCSUs) of vital tumor tissue before, and following 5×2 Gy and 10×2 Gy. Changes in the normoxic and hypoxic fractions varied considerably between the tumor lines before and during treatment and also showed opposing directions of changes upon irradiation (see Fig. 3). The fraction of normoxic MCSUs significantly increased upon 5×2 Gy and 10×2 Gy for UT-SCC-15 tumors (from 43.1 ± 2.2% to 56.4 ± 2.2%, and to

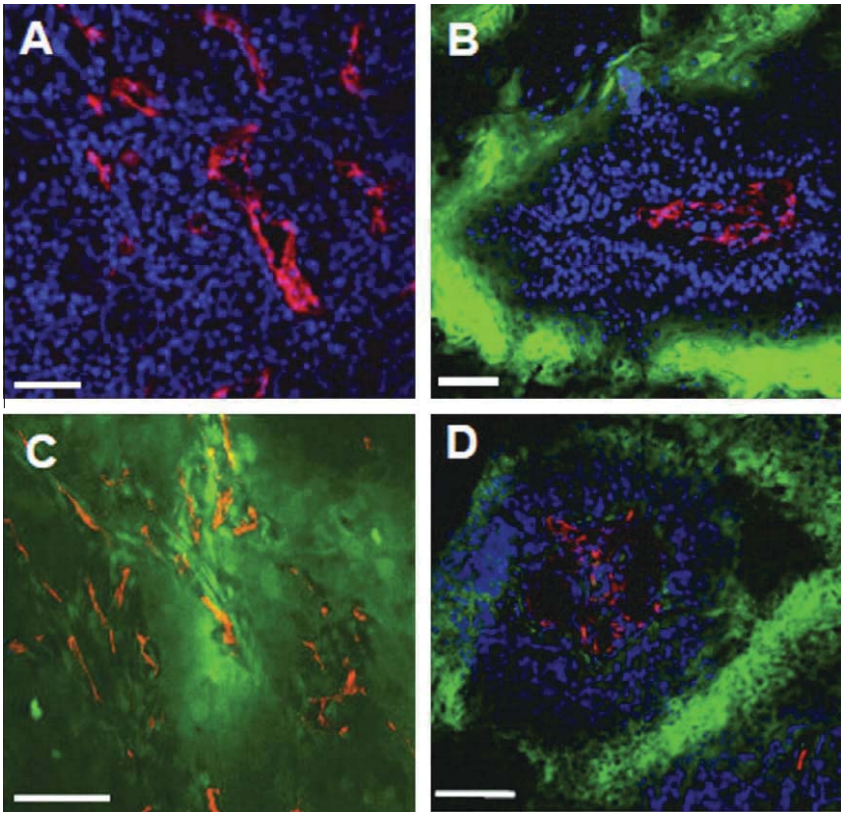

Fig. 2. Representative tissue sections showing examples of different oxygenation states as suggested in Fig. 1: (A) tumor normoxia; (B) (chronic) diffusion-limited hypoxia; (C) (acute) perfusion-limited hypoxia; (D) (acute/chronic) hypoxemic hypoxia. Hoechst 33342 fluorescence of cells in perfused areas is shown in blue, pimonidazole staining of hypoxic cells in green, and CD31 staining for microvascular endothelial cells in red. White scale bars indicate 100 μm.

67.6 ± 2.6% after finishing treatment). In two tumor lines, rises in the proportion of normoxic MCSUs were observed only after 10 × 2 Gy: FaDu (from 64.4 ± 5.6% to 79.6 ± 3.0%) and SAS (from 56.1 ± 3.6% to 69.6 ± 4.8%). Accordingly, there was a corresponding decrease in the overall fraction of hypoxic MCSUs in these tumor lines (see Fig. 3). For UT-SCC-5, there was no significant change in the fraction of normoxic MCSUs and the overall fraction of hypoxic MCSUs. Compared to the UT-SCC-15 and FaDu tumor lines, UT-SCC-14 exhibited an opposing direction in changes upon fractionated irradiation. Here the fraction of normoxic MCSUs significantly decreased upon fractionated irradiation, and the overall fraction of hypoxic MCSUs increased accordingly. The fraction of normoxic MCSUs in UT-SCC-14 tumors decreased from 73 ± 3% to 62 ± 4% (5 × 2 Gy) and to 58 ± 3% (10 × 2 Gy). As a result, a significant increase in the overall fraction of hypoxic MCSUs was observed (see Fig. 3).

Upon finishing the fractionated irradiation up to a total dose of 20 Gy, the largest increase in the fraction of normoxic MCSUs (+24.5%) was observed in the tumor line with the lowest percentage of normoxic MCSUs before start of treatment (43.1%), and the smallest rise in the necrotic fraction (+5%) during treatment (UT-SCC-15). In contrast, in the tumor line with the highest fraction of normoxic MCSUs (72.8%; UT-SCC-14) before treatment, hypoxic tissue regions enlarged following 5 × 2 Gy and 10 × 2 Gy. Interestingly, this divergent behavior upon fractionated irradiation is not reflected by differences in radiosensitivity, since these two tumor lines mentioned above have comparable TCD_{50} values (37.7 Gy, and 44.2 Gy, respectively [39].

The fractions of hypoxia subtypes (chronic, acute and hypoxemic) upon fractionated irradiation are depicted in Fig. 4. Chronic hypoxia is the most abundant subtype in all tumor lines before and after treatment (varying from 23.4% to 40.1% before treatment and from 16.3% to 30.1% upon 10 × 2 Gy). The only significant change in the fraction of chronically hypoxia MCSUs upon irradiation was seen in UT-SCC-15 tumors (−11.4%). The fractions of acutely hypoxic MCSUs ranged from 3.4% to 17.5% before, and from 3.1% to 11.8% after fractionated irradiation. Significant drops in the fraction of acutely hypoxic MCSUs were observed in UT-SCC-15 tumors (−11.5%) and SAS tumors (−4.8%) after completion of treatment (see Fig. 4).

The fraction of hypoxemically hypoxic MCSUs, the smallest subtype of hypoxia ranged from 0.5% to 3.6% before radiation and from 0.6% to 4.0% upon 10 × 2 Gy. A significant decrease in this hypoxia subtype was observed in SAS tumors (−2.5%) after finishing irradiation.

Discussion

In this study, five different tumor lines from a single entity (hHNSCC lines xenografted in nude mice) were analyzed during the course of a fractionated radiation scheme with 5 × 2 and 10 × 2 Gy. Unfortunately, the mouse xenograft tumors used in this study became too necrotic at total doses higher than 20 Gy so that we were not able to investigate tumor cryosections at clinically relevant doses of 60 Gy and higher. In all five tumor lines, there was a gradual reduction in vital tissue fraction during irradiation, which was more prominent in tumors containing a larger pretreatment vital tissue fraction.

In three of five tumors (UT-SCC-15, FaDu and SAS), the **overall** fraction of hypoxic MCSUs decreased, in UT-SCC-5 there was no change and in UT-SCC-14 the overall proportion of hypoxic MCSUs increased upon fractionated irradiation with 5 × 2 and 10 × 2 Gy (Fig. 3). These results are in accordance with data from an earlier

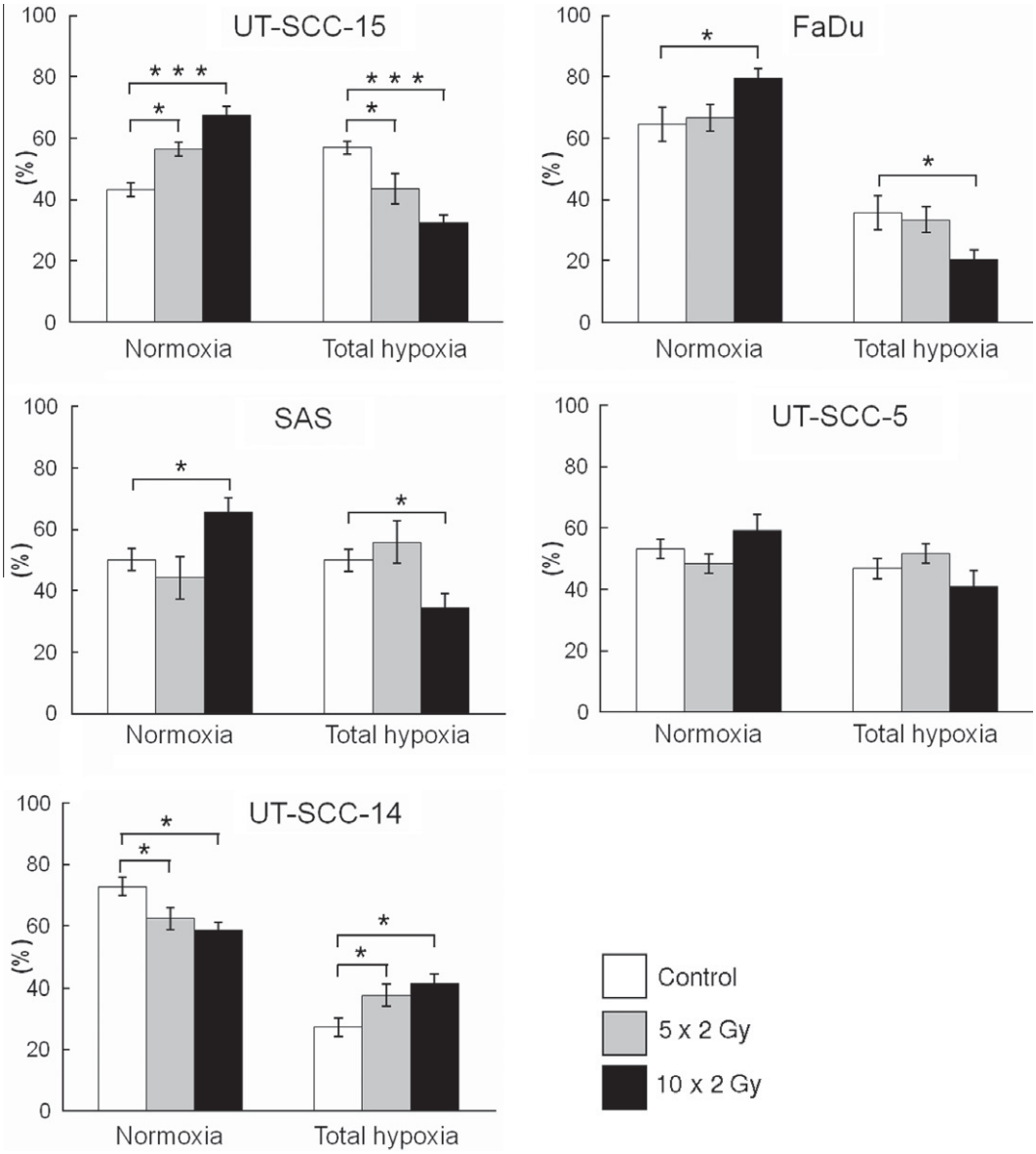

Fig. 3. Fraction of normoxic MCSUs ("normoxia") and overall fraction of hypoxic MCSUs ("total hypoxia") before (control) and upon fractionated irradiation with 5 × 2 Gy and 10 × 2 Gy (SAS tumors: 5 × 1.84 Gy, 10 × 1.84 Gy) in five human xenograft hHNSCC lines. $^{*}p < 0.05$, $^{***}p < 0.001$ as compared to control data. Mean values ± SEM are presented.

study by Yaromina et al. [39] assessing the pimonidazole hypoxic fraction (pHF; no assessment of hypoxia subtypes) in the exact same five tumor lines used in our study. They observed a similar pattern in hypoxic fraction during fractionated irradiation and found a decrease in hypoxic fraction throughout the course of a fractionated irradiation in UT-SCC-15, FaDu, SAS and UT-SCC-5 and a significant increase after 5 × 2 Gy in UT-SCC-14. This confirms that assessment of the hypoxic fraction via pattern recognition in MCSUs (this study, [38]) reveals similar results as previously communicated [39,42]. In the latter studies, the hypoxic tumor area was determined by dividing the number of pimonidazole positive pixels by the vital tumor area.

Whether or not overall hypoxia increases or decreases during radiation in xenograft tumor models could -inter alia- depend on the time of hypoxia assessment and the dose applied. For example, Bussink et al. described a maximal decrease in the hypoxic fraction 7 h after irradiation followed by an increase in hypoxic fraction up to day 11 after a single large dose of 10 Gy in a hHNSCC xenograft line [43]. Similarly, Kim and Brown found a rapid increase in the hypoxic fraction in a hHNSCC line after a 10 Gy single large dose, which returned to approximately baseline after 6 h and stayed the same up to 24 h [44]. In a further study on human melanoma xenografts, the total hypoxic fraction increased rapidly after either 10 Gy single dose or 7 fractions of 2 Gy, then returned to pretreatment values within 24 h and stayed at that level for up to 10 days [45]. In rat rhabdomyosarcomas, a steady increase in the frequency of low pO_2 values (0–5 mm Hg) was not observed until after 3 (45 Gy) and 4 (60 Gy) weeks of fractionated irradiation (3 Gy/fraction, 5×/week) [46,47]. In FaDu head and neck tumor xenografts, the pimonidazole hypoxic fraction first increased after 3 fractions of 3 Gy and continually decreased from 6 to 15 daily fractions of 3 Gy [48,49]. Additional xenograft tumors have shown decreases, increases and no change in the total hypoxic fraction during fractionated irradiation [50,51]. Taken together, these experiments suggest that at 24 h after the final fraction of irradiation (the time used in this study), the hypoxic fraction most likely represents changes in hypoxia upon cumulative doses and not immediate changes in hypoxia due only to the last fraction.

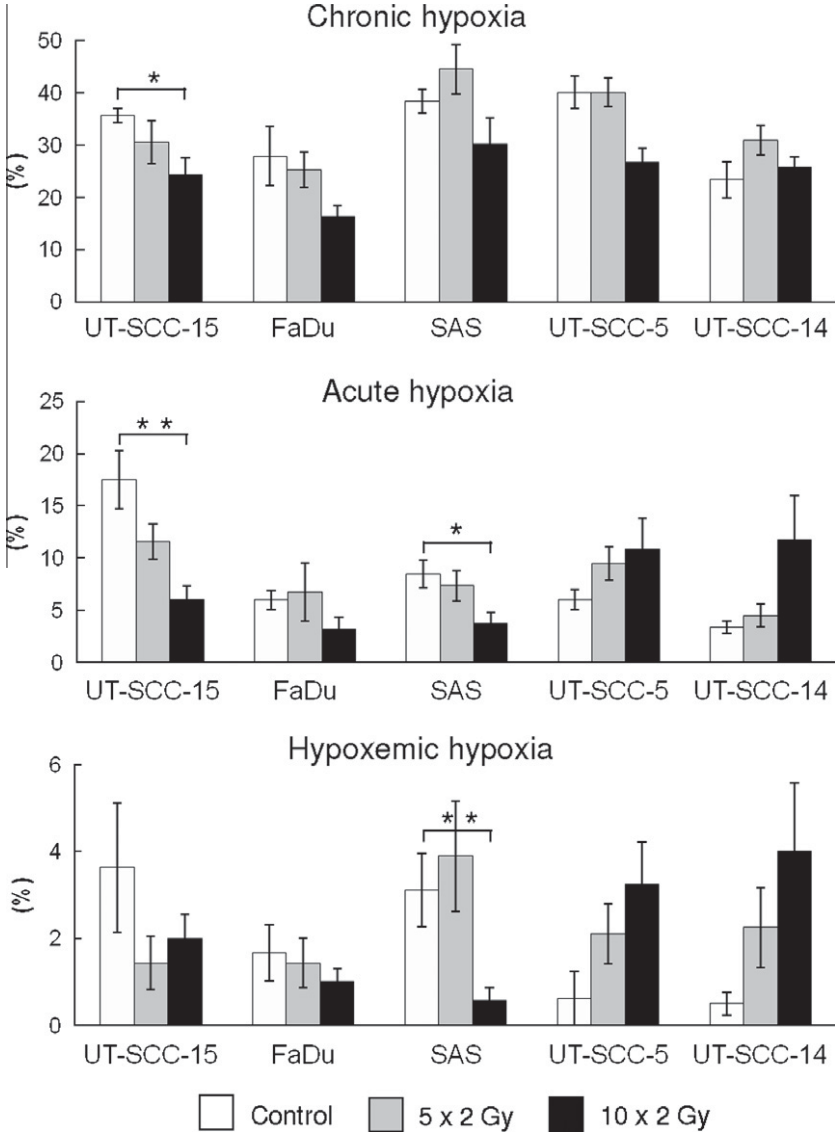

Fig. 4. Changes in the fraction of chronically hypoxic MCSUs ("chronic hypoxia"), acutely hypoxic MCSUs ("acute hypoxia") and hypoxemically hypoxic MCSUs ("hypoxemic hypoxia") before (control) and upon fractionated irradiation with 5 × 2 Gy and 10 × 2 Gy (SAS tumors: 5 × 1.84 Gy, 10 × 1.84 Gy) in five human xenograft hHNSCC lines. $^{*}p < 0.05$, $^{**}p < 0.01$ as compared to control data. Mean values ± SEM are presented.

Until now, different subtypes of hypoxia have not been taken into consideration. To the best of our knowledge, this is the first time that the fractions of hypoxia subtypes (chronic, acute and hypoxemic) in MCSUs have been quantified during fractionated irradiation. **Chronic hypoxia** was the most prominent subtype in all tumor lines before and during fractionated irradiation, followed by acute and hypoxemic hypoxia. In four tumor lines, there was no change in the fraction of chronically hypoxic MCSUs during treatment and in UT-SCC-15 there was a significant decrease in the fraction of chronically hypoxic MCSUs after 10 × 2 Gy (Fig. 4). No significant changes were observed in **acute hypoxia** during treatment in three tumor lines and significant reductions in the proportion of acutely hypoxic MCSUs were seen in UT-SCC-15 and SAS tumor lines after 10 × 2 Gy, and 10 × 1.84 Gy, respectively. The only significant change in **hypoxemic hypoxia** was a large decrease in the SAS tumor line after 10 × 1.84 Gy. Interestingly, the largest increase in the fraction of acutely hypoxic MCSUs was observed in the only tumor line showing an increase in the overall fraction of hypoxic MCSUs during radiation treatment, UT-SCC-14 (Fig. 3). Although, this was not significant due to large inter-tumor variability, it seems that the increase in the overall percentage of hypoxic MCSUs in this tumor line could predominantly be due to an increase in the fraction of acutely hypoxic MCSUs. Since this tumor is very radiosensitive (TCD_{50} = 44.2), it is possible that the proportion of acutely hypoxic MCSUs after fractionated irradiation in the tumor lines investigated does not contribute greatly to local tumor control upon radiation. This is surprising because acute (cycling, intermittent) hypoxia is thought to play a major role in the development of tumor aggressiveness due to changes in the transcriptome, proteome and genome [10,22,52]. On the other hand, the changes in the fraction of acutely hypoxic MCSUs during fractionated irradiation related best to alterations in the overall percentage of hypoxic MCSUs (Figs. 3 and 4).

No correlation was found between the fractions of hypoxia subtypes and TCD_{50} as a parameter of radiation sensitivity. Yaromina et al. [39] reported that the pimonidazole hypoxic tissue volume (pHV; relative to the total tumor area and relative to the tumor volume at time of excision; tumor necrosis was not excluded) and not the pimonidazole hypoxic fraction (pHF; relative to the vital tumor area) correlated with TCD_{50}. This suggests that tumor volume

growth rate in addition to the vital tissue fraction needs to be taken into consideration when considering hypoxia relevant for local tumor control upon fractionated irradiation. In addition, Wouters and Brown [53] have suggested that intermediate pO_2 levels (between fully oxygenated and hypoxic) could be more important than pHF in determining response to fractionated radiotherapy.

In conclusion, using quantification of hypoxia subtypes in MCSUs, it was possible to monitor the amount of acute, chronic and hypoxemic hypoxia during fractionated irradiation. This study shows that there are large variations in the fractions of hypoxia subtypes upon irradiation and that alterations in the fraction of acutely hypoxic MCSUs correlates best with changes in the overall fraction of hypoxic MCSUs. Neither the changes in total hypoxia nor in hypoxia subtypes upon fractionated irradiation were able to reflect radiation resistance in the tumor lines investigated.

Conflict of interest statement

No conflict of interest declared by the authors.

Acknowledgments

This study has been supported in part by grants of the Deutsche Forschungsgemeinschaft (DFG: Ba 3514/1-1) and the Bundesministerium für Bildung und Forschung (BMBF: 01EZ0826). The authors would like to thank Prof. Dr. M. Baumann for providing tumor cryosections.

Appendix A. Supplementary data

Supplementary data associated with this article can be found, in the online version, at doi:10.1016/j.radonc.2011.05.023.

References

[1] Nordsmark M, Overgaard M, Overgaard J. Pretreatment oxygenation predicts radiation response in advanced squamous cell carcinoma of the head and neck. Radiother Oncol 1996;41:31–9.
[2] Nordsmark M, Overgaard J. A confirmatory prognostic study on oxygenation status and loco-regional control in advanced head and neck squamous cell carcinoma treated by radiation therapy. Radiother Oncol 2000;57:39–43.
[3] Nordsmark M, Bentzen SM, Rudat V, et al. Prognostic value of tumor oxygenation in 397 head and neck tumors after primary radiation therapy. An international multi-center study. Radiother Oncol 2005;77:18–24.
[4] Thomlinson RH, Gray l. The histological structure of some human lung cancers and the possible implications for radiotherapy. Br J Cancer 1955;9:539–49.
[5] Brown JM. Evidence for acutely hypoxic cells in mouse tumours, and a possible mechanism of reoxygenation. Br J Radiol 1979;52:650–6.
[6] Chaplin DJ, Durand RE, Olive PL. Acute hypoxia in tumors: implications for modifiers of radiation effects. Int J Radiat Oncol Biol Phys 1986;12:1279–82.
[7] Bayer C, Shi K, Astner ST, Maftei C-A, Vaupel P. Acute versus chronic hypoxia: Why a simplified classification is simply not enough. Int J Radiat Oncol Biol Phys 2011. doi:10.1016/j.ijrobp.2011.02.049.
[8] Dewhirst MW, Ong ET, Braun RD, et al. Quantification of longitundinal tissue pO_2 gradients in window chamber tumours: impact on tumour hypoxia. Br J Cancer 1999;79:1717–22.
[9] Erickson K, Braun RD, Yu D, et al. Effect of longitudinal oxygen gradients on effectiveness of manipulation of tumor oxygenation. Cancer Res 2003;63:4705–12.
[10] Vaupel P. Tumor microenvironmental physiology and its implications for radiation oncology. Semin Radiat Oncol 2004;14:198–206.
[11] Vaupel P. Hypoxia and aggressive tumor phenotype: implications for therapy and prognosis. Oncologist 2008;13:21–6.
[12] Vaupel P. Physiological mechanisms of treatment resistance. In: Molls M, Vaupel P, Nieder C, Anscher MS, editors. The impact of tumor biology on cancer treatment and multidisciplinary strategies. Berlin: Springer; 2009. p. 273–90.
[13] Baumann M, Krause M, Hill R. Exploring the role of cancer stem cells in radioresistance. Nat Rev Cancer 2008;8:545–54.
[14] Durand RE. Intermittent blood flow in solid tumors – an under-appreciated source of drug resistance. Cancer Metastasis Rev 2001;20:57–61.
[15] Bristow RG, Hill RP. Hypoxia, DNA repair and genetic instability. Nat Rev Cancer 2008;8:180–92.
[16] Bache M, Kappler M, Said HM, Staab A, Vordermark D. Detection and specific targeting of hypoxic regions within solid tumors: current preclinical and clinical strategies. Curr Med Chem 2008;15:322–38.
[17] Evans S, Koch C. Prognostic significance of tumor oxygenation in humans. Cancer Lett 2003;195:1–16.
[18] Horsman MR, Nordsmark M, Overgaard J. Techniques to assess the oxygenation of human tumors. State of the art. Strahlenther Onkol 1998;174:2–5.
[19] Tatum J, Kelloff GJ, Gillies RJ, et al. Hypoxia: Importance in tumor biology, noninvasive measurement by imaging, and value of its measurement in the management of cancer therapy. Int J Radiat Biol 2006;82:699–757.
[20] Vaupel P, Höckel M, Mayer A. Detection and characterization of tumor hypoxia using pO_2 histography. Antioxid Redox Signal 2007;9:1221–35.
[21] Arabi M, Piert M. Hypoxia PET/CT imaging: implications for radiation oncology. QJ Nucl Med Biol Imaging 2010;54:500–9.
[22] Vaupel P, Mayer A. Hypoxia in cancer: significance and impact on clinical outcome. Cancer Metastasis Rev 2007;26:225–39.
[23] Busk M, Horsman MR, Jakobsen S, et al. Imaging hypoxia in xenografted and murine tumors with ^{18}F-Fluoroazomycin arabinoside: A comparative study involving microPET, autoradiography, pO_2-polarography, and fluorescence microscopy. Int J Radiat Oncol Biol Phys 2008;70:1202–12.
[24] Busk M, Munk OL, Jakobsen S, et al. Assessing hypoxia in animal tumor models based on pharmacokinetic analysis of dynamic FAZA PET. Acta Oncol 2010;49:922–33.
[25] Troost EGC, Laverman P, Philippens MEP, et al. Correlation of [^{18}F] FMISO autoradiography and pimonidazole immunohistochemistry in human head and neck carcinoma xenografts. Eur J Nucl Med Mol Imaging 2008;35:1803–11.
[26] Grosu A-L, Souvatzoglou M, Röper B, et al. Hypoxia imaging with FAZA-PET and theoretical considerations with regard to dose painting for individualization of radiotherapy in patients with head and neck cancer. Int J Radiat Oncol Biol Phys 2007;69:541–51.
[27] Koh W-J, Bergman KS, Rasey JS, et al. Evaluation of oxygenation status during fractionated radiotherapy in human nonsmall cell lung cancers using [F-18]fluoromisonidazole positron emission tomography. Int J Radiat Oncol Biol Phys 1995;33:391–8.
[28] Lee N, Nehmeh S, Schöder H, et al. Prospective trial incorporating pre-/mid-treatment [^{18}F]-misonidazole positron emission tomography for head-and-neck cancer patients undergoing concurrent chemoradiotherapy. Int J Radiat Oncol Biol Phys 2009;75:101–8.
[29] Nehmeh SA, Lee NY, Schröder H, et al. Reproducibility of intratumor distribution of ^{18}F-fluoromisondizole in head and neck cancer. Int J Radiat Oncol Biol Phys 2008;70:235–42.
[30] Thorwath D, Alber M. Implementation of hypoxia imaging into treatment planning and delivery. Radiother Oncol 2010;97:172–5.
[31] Achermann RE, Ohlerth SM, Bley CR, et al. Oxygenation of spontaneous canine tumors during fractionated radiation therapy. Strahlenther Onkol 2004;180:297–305.
[32] Brurberg KG, Skogmo HK, Graff BA, Olsen DR, Rofstad EK. Fluctuations in pO_2 in poorly and well-oxygenated spontaneous canine tumors before and during fractionated irradiation. Radiother Oncol 2005;77:220–6.
[33] Thrall DE, Larue SM, Pruitt AF, Case B, Dewhirst MW. Changes in tumour oxygenation during fractionated hyperthermia and radiation therapy in spontaneous canine sarcomas. Int J Hyperthermia 2006;22:365–73.
[34] Brizel DM, Dodge RK, Clough RW, Dewhirst MW. Oxygenation of head and neck cancer: changes during radiotherapy and impact on treatment outcome. Radiother Oncol 1999;53:113–7.
[35] Cooper RA, West CML, Logue JP, et al. Changes in oxygenation during radiotherapy in carcinoma of the cervix. Int J Radiat Oncol Biol Phys 1999;45:119–26.
[36] Lyng H, Tanum G, Evensen JF, Rofstad EK. Changes in oxygen tension during radiotherapy of head and neck tumors. Acta Oncol 1999;38:1037–42.
[37] Dunst J, Hänsgen G, Lautenschläger C, Füchsel G, Becker A. Oxygenation of cervical cancers during radiotherapy and radiotherapy + cis-retinoic acid/interferon. Int J Radiat Oncol Biol Phys 1999;43:367–73.
[38] Maftei C-A, Bayer C, Shi K, Astner ST, Vaupel P. Quantitative assessment of hypoxia subtypes in microcirculatory supply units of malignant tumors using (immuno-)fluorescence techniques. Strahlenther Onkol 2011;187:260–6.
[39] Yaromina A, Kroeber T, Meinzer A, et al. Exploratory study of the prognostic value of microenvironmental parameters during fractionated irradiation in human squamous cell carcinoma xenografts. Int J Radiat Oncol Biol Phys 2011. doi:10.1016/j.ijrobp.2011.02.015.
[40] Arteel GE, Thurman RG, Yates JM, Raleigh JA. Evidence that hypoxia markers detect oxygen gradients in liver: pimonidazole and retrograde perfusion of rat liver. Br J Cancer 1995;72:889–95.
[41] Ljungkvist AS, Bussink J, Rijken PF, Kaanders JH, van der Kogel AJ, Denekamp J. Vascular architecture, hypoxia, and proliferation in first-generation xenografts of human head-and-neck squamous cell carcinomas. Int J Radiat Oncol Biol Phys 2002;54:215–28.
[42] Rijken PFJW, Peters JPW, van der Kogel AJ. Quantitative analysis of varying profiles of hypoxia in relation to functional vessels in different human glioma xenograft lines. Radiat Res 2002;157:626–32.
[43] Bussink J, Kaanders JHAM, Rijken PFJW, Raleigh JA, Van der Kogel AJ. Changes in blood perfusion and hypoxia after irradiation of a human squamous cell carcinoma xenograft tumor line. Radiat Res 2000;153:398–404.
[44] Kim IH, Brown JM. Reoxygenation and rehypoxiation in the SCCVII mouse tumor. Int J Radiat Oncol Biol Phys 1994;29:493–7.
[45] Rofstad EK. Hypoxia and reoxygenation in human melanoma xenografts. Int J Radiat Oncol Biol Phys 1989;17:81–9.

[46] Thews O, Zywietz F, Lecher B, Vaupel P. Quantitative changes of metabolic and bioenergetic parameters in experimental tumors during fractionated irradiation. Int J Radiat Oncol Biol Phys 1999;45:1281–8.
[47] Zywietz F, Reeker W, Kochs E. Tumor oxygenation in a transplanted rat rhabdomyosarcoma during fractionated irradiation. Int J Radiat Oncol Biol Phys 1995;32:1391–400.
[48] Petersen C, Zips D, Krause M, et al. Repopulation of FaDu human squamous cell carcinoma during fractionated radiotherapy correlates with reoxygenation. Int J Radiat Oncol Biol Phys 2001;51:483–93.
[49] Petersen C, Eicheler W, Frömmel A, et al. Proliferation and micromilieu during fractionated irradiation of human FaDu squamous cell carcinoma in nude mice. Int J Radiat Biol 2003;79:469–77.
[50] Baumann M, Appold S, Zimmer J, et al. Radiobiological hypoxia, oxygen tension, interstitial fluid pressure and relative viable tumour area in two human squamous cell carcinomas in nude mice during fractionated radiotherapy. Acta Oncol 2001;4:519–28.
[51] Stüben G, Thews O, Pöttgen C, Stuschke M, Sack H. Tumor oxygenation during fractionated radiotherapy. Acta Oncol 1999;2:209–13.
[52] Höckel M, Vaupel P. Tumor hypoxia: definitions and current clinical, biological and molecular aspects. J Natl Cancer Inst 2001;93:266–76.
[53] Wouters BG, Brown JM. Cells at intermediate oxygen levels can be more important than the "hypoxic fraction" in determining tumor response to fractionated radiotherapy. Radiat Res 1997;147:541–50.

3. Maftei CA, Shi K, Bayer C, Astner ST, Vaupel P. Comparison of (immuno-)fluorescence data with serial [^{18}F]Fmiso PET/CT imaging for assessment of chronic and acute hypoxia in head and neck cancers. Radiother Oncol 2011;99:412-7.

Radiotherapy and Oncology 99 (2011) 412–417

Contents lists available at ScienceDirect

Radiotherapy and Oncology

journal homepage: www.thegreenjournal.com

Experimental radiobiology

Comparison of (immuno-)fluorescence data with serial [^{18}F]Fmiso PET/CT imaging for assessment of chronic and acute hypoxia in head and neck cancers

Constantin-Alin Maftei, Kuangyu Shi, Christine Bayer *, Sabrina T. Astner, Peter Vaupel

Department of Radiotherapy and Radiation Oncology, Technical University of Munich, Germany

ARTICLE INFO

Article history:
Received 30 April 2011
Received in revised form 24 May 2011
Accepted 28 May 2011
Available online 28 June 2011

Keywords:
Tumor hypoxia
Chronic hypoxia
Acute hypoxia
Microcirculatory supply units
[^{18}F]Fmiso PET/CT
Wang model

ABSTRACT

Purpose: Both, acute and chronic hypoxia can have unfavorable impacts on tumor progression and therapy response. The aim of this study was to optimize a macroscopic technique for the quantification of acute and chronic hypoxia (Wang model assessment of serial [^{18}F]Fmiso PET/CT imaging) by comparing with a microscopic technique [(immuno-)fluorescence staining in tumor cryosections].

Materials and methods: Tumor pieces from the human squamous cell carcinoma lines from the head and neck FaDu and CAL33 were xenografted into the hind leg of NMRI nu/nu mice. Tumor-bearing mice were placed on an in-house developed multi-point fixation system and subjected to two consecutive dynamic [^{18}F]Fmiso PET/CTs within a 24 h interval. The Wang model was applied to SUV (standard uptake values) to quantify the fractions of acute and chronic hypoxia. Hypoxia subtypes were also assessed in vital tumor tissue of cryosections from the same tumors for (immuno-)fluorescence distributions of Hoechst 33342 (perfusion), pimonidazole (hypoxia), and CD31 (endothelium) using pattern recognition in microcirculatory supply units (defined as vital tumor tissue area supplied by a single microvessel).

Results: Using our multi-point fixation system, acceptable co-registration (registration errors ε ranged from 0.34 to 1.37) between serial PET/CT images within individual voxels was achieved. The Wang model consistently yielded higher fractions of acute hypoxia than the MCSU method. Through specific modification of the Wang model ($Wang_{mod}$), it was possible to reduce the fraction of acute hypoxia. However, there was no significant correlation between the fractions of acute hypoxia in individual tumors assessed by the $Wang_{mod}$ model and the MCSU method for either tumor line (FaDu: $r = 0.68$, $p = 0.21$ and CAL33: $r = 0.71$, $p = 0.18$). This lack of correlation is most-likely due to the difference between the non-linear uptake of [^{18}F]Fmiso and the spatial assessment of MCSUs.

Conclusions: Whether the Wang model can be used to predict radiation response after serial [^{18}F]Fmiso PET imaging, needs to be confirmed in experimental and clinical studies.

Two subtypes of hypoxia exist that are relevant in clinical and experimental radiation oncology, namely chronic and acute hypoxia [1]. Chronic (diffusion-limited) hypoxia is generally accepted to be caused by critical limitations in oxygen diffusion from microvessels to tumor cells [2]. Acute (perfusion-limited) hypoxia results from temporary, local disturbances in perfusion or strong variations in red blood cell fluxes and thus in fluctuations of the microvascular oxygen supply [3–5].

Acute hypoxia may play a major role in tumor progression and metastasis. Cairns et al. [6] randomly assigned tumor-bearing mice to either, control, chronic hypoxia or acute hypoxia by breathing different inspiratory gas mixtures and found an increase in metastasis formation upon exposure to acute hypoxia. Previous studies in a mouse tumor model using murine melanoma cells demonstrated that experimental acute hypoxia in solid tumors has the potential to trigger lung metastases [7,8]. In this experiment, nicotinamide was administered to reduce acute hypoxia and had a promising effect on the reduction of lung metastases. After irradiation with 10 Gy, it was shown that acute exposure of tumor-bearing mice to hypoxic gas mixtures significantly increased tumor growth as compared to irradiation alone [9]. Finally, the planning of radiation treatment schedules and outcome seems to be influenced by the fraction of acute and chronic hypoxia in solid tumors. Ruggieri [10] calculated the dose per fraction, the number of fractions and their relation to the curative dose D_{50}. The results from this modeling study suggest a better outcome for chronically hypoxic tumors after a short hypofractionated irradiation treatment and for acutely hypoxic tumors after a multi-fractionated treatment. Therefore, non-invasive prediction of the fraction of acute hypoxia in solid tumors might be a valuable tool for estimating the aggressiveness of tumors, their progression and metastatic potential.

* Corresponding author. Address: Department of Radiotherapy and Radiation Oncology, Klinikum rechts der Isar, Technical University of Munich, Ismaninger Strasse 22, 81675 Munich, Germany.
E-mail address: christine.bayer@yahoo.com (C. Bayer).

0167-8140/$ - see front matter © 2011 Elsevier Ireland Ltd. All rights reserved.
doi:10.1016/j.radonc.2011.05.079

A method to assess the levels of chronic and acute hypoxia in cryosections of xenografted head and neck tumors has recently been described by Maftei et al. [11,12]. This evaluation has shown that chronic hypoxia is present in a much higher extent than acute hypoxia. The Wang model has recently been proposed to quantify chronic and acute hypoxia after serial [^{18}F]Fmiso PET/CT scanning in human head and neck cancers [13]. In the present study, the original Wang model was optimized for the (macroscopic) quantification of hypoxia subtypes after serial [^{18}F]Fmiso PET scanning and compared to the levels of chronic and acute hypoxia assessed (microscopically) in tumor cryosections.

Materials and methods

Tumor lines and mice

Xenografted tumors were derived from two established human squamous cell carcinoma cell lines of the head and neck: FaDu (a hypopharyngeal tumor; American Type Culture Collection, Rockville, MD, USA) and CAL-33 (a tumor of the tongue; Deutsche Sammlung von Mikroorganismen und Zellkulturen, Braunschweig, Germany). The mouse experiments described here have been approved according to German animal welfare regulations (approval # 55.2-1-54-2531-52-07; District government of Upper Bavaria).

The experiments were performed using 7–10-week-old female NMRI (nu/nu) mice (Charles River, Sulzfeld, Germany). First, the mice were whole-body irradiated to suppress residual immune reactions (e.g., of NK cells) with 4 Gy (200 kV X-rays, 0.5 mm Cu filter, 1 Gy/min) using the Gulmay RS225A device (Gulmay Medical, Camberley, UK). Two–3 days later, source tumor pieces of approx. 1 mm^3 were transplanted into the right hind leg of anaesthetized mice [Medetomidin (0.50 mg/kg) + Midazolam (5.0 mg/kg) + Fentanyl (0.05 mg/kg); i.m.]. Immediately after transplantation, the mice were injected with the respective antagonists (2.5 mg/kg atipamezol, 0.50 mg/kg flumazenil and 1.2 mg/kg naloxon; i.m.). Tumor diameters (in three-dimensions) were measured twice per week by ultrasound (Logiq-5; GE Healthcare, Solingen, Germany). Tumor volumes were determined by the formula of a rotational ellipsoid: $(\pi/6)abc$.

[^{18}F]Fmiso PET/CT imaging and assessment of hypoxia subtypes using the Wang model

All animals underwent two dynamic [^{18}F]Fmiso PET/CT scans on consecutive days at an interval of 24 h using the Siemens Inveon microPET/CT (Knoxville, TN, USA). During image acquisition, each animal was immobilized on an in-house developed coordinated multi-point fixation system, which ensures the investigated area to be positioned in a reproducible way. In addition, two external CT contrast lines (Imeron 300; Bracco Imaging, Konstanz, Germany) were painted onto the tumor skin at the exact same locations for the two scans.

After a CT scan, 10–15 MBq [^{18}F]Fmiso (IASON, Graz, Austria) were injected intravenously into the tumor-bearing mice anaesthetized with isoflurane, and dynamic PET data were acquired for 2 hr. Two venous blood samples (2–7 μl each) were taken directly after scanning, weighed, and the activity concentration of ^{18}F in the blood measured in a gamma-counter (1480 Wizard, PerkinElmer, Turku, Finland). The images were reconstructed using the filtered back-projection (FBP) algorithm (Ramp filter, cutoff frequency 0.5 cycles/pixel, 46 frames of varying durations from 1–900 s). Attenuation correction was applied based on the acquired CT data. Additionally, all measurements were corrected for physical decay, dead time and non-uniformity of microPET response. A measured system calibration factor was used to convert voxel count rates to activity concentrations. The voxel size of the reconstructed image data was $0.78 \times 0.78 \times 0.80$ mm^3.

The images from two consecutive scans were co-registered based on the CT-visible fixation pins on the immobilization system. The registration error was computed as the average Euclidean distance between selected points from the CT contrast lines on the skin overlying the tumor. Contours of the tumors were outlined manually based on CT images using PMOD software (version 3.1; PMOD Technologies, Zurich, Switzerland). Imaging data from the last frame were then converted into SUV values and the total activity within the tumor area of the two scans was normalized by rescaling them to be the same.

To analyze the serial PET scans and estimate the fraction of acute hypoxia, the original model described by Wang et al. [12] was applied. This model assumes that both chronic and acute hypoxia contribute to the [^{18}F]Fmiso images and the total uptake H in a voxel is the sum of the contributions

$$H = H_a + H_c$$

where H_a is the contribution of acute, and H_c is the contribution of chronic hypoxia. Then, the total uptake H_1 and H_2 from the two PET scans of the same voxel can be written as

$$H_1 = H_{a1} + H_c$$
$$H_2 = H_{a2} + H_c$$

which assumes that the "chronic" contribution, H_c, is unchanged in the two scans and due to PET noise resembles a Gaussian distribution. Therefore, a part of the uptake was extracted, which fits best to a Gaussian distribution. To do so, the uptakes H_1 and H_2 were sorted into high H_h and small H_s readings in the same voxel. The fraction of H_h is denoted $\omega = H_{ah}/H_h$ as due to acute hypoxia and defined as $x = \Delta H/H_h$, where ΔH is H_h–H_s. Finally, a relation between ω and x was assumed:

$$\omega = \rho x^\beta = \rho \frac{\Delta H^\beta}{H_h^\beta}$$

For voxels with H_h, the chronic hypoxia was then calculated as

$$H_c = (1 - \rho x^\beta) H_h$$

Here, $\beta = 0.6$ was derived from a Monte-Carlo simulation. To model the "chronic" contribution, the model iteratively adapted ρ until it achieved a best fit with the maximized R-square (R^2). The model was re-implemented in MATLAB (Version R2010a, The Mathworks, Natick, MA, USA).

In addition to the expression of acute hypoxia $\omega = H_{ah}/H_h$ as described by Wang et al. [13], we also fitted the data to the fraction of the average contribution $(H_{ah} + H_{as})/(H_h + H_s)$ for the assessment of the fraction of acute hypoxia (modified Wang model).

Histology and (immuno-)fluorescence techniques

Pimonidazole (Hypoxyprobe, Burlington, MA, USA) dissolved in saline was administrated i.v. immediately before the second PET scanning at a concentration of 80 mg/kg body weight. Hoechst 33342 (Sigma, Deisenhofen, Germany) was dissolved in saline and administrated i.v. at a concentration of 15 mg/kg body weight 1 min before sacrificing the animal. Tumor excision followed immediately upon animal sacrifice. Thereafter, tumors were embedded in O.C.T. Compound (Sakura, Alphen aan den Rijn, Netherlands), frozen on dry ice, and stored at −80 °C. Ten micrometers cryosections from the middle of each tumor were fixed in cold (4 °C) acetone, air dried and rehydrated in PBS.

Pimonidazole was stained with the Mab FITC-labeled anti-pimonidazole antibody (Hypoxyprobe, Burlington, MA, USA)

diluted 1:50 in primary antibody diluent (PAD, Serotec, Oxford, UK) by incubating for 1 h at 37 °C in the dark [14,15]. Microvascular endothelium was stained using the purified rat anti-mouse CD31 antibody (MEC 13.3, BD PharMingen, Heidelberg, Germany) diluted 1:100 in PAD. Anti-CD31 was detected using an AlexaFluor 594- or Cy5-labeled goat anti-rat secondary antibody (Invitrogen, Eugene, OR, USA) diluted 1:200 or 1:50, respectively, in PBS for 1 h at 37 °C in the dark. The cryosections were then embedded in fluorescent mounting medium (DAKO, Glostrup, Denmark) and stored at 4 °C. Necrotic tissue areas were detected in the same slices by staining with hematoxylin and eosin.

Microcirculatory supply units

The fractions of chronic hypoxia and acute hypoxia (relative to total hypoxia) were quantified in microcirculatory supply units (MCSUs) as reported recently by Maftei et al. [11]. A MCSU is defined as vital tumor tissue area supplied by a microvessel. The individual whole tumor cross-sections were scanned and photographed using the AxioVision 4.7 and the multi-dimensional and mosaix modules (Zeiss, Jena, Germany). The pictures obtained were visually evaluated by two independent researchers (C.B., C.M.) by categorizing MCSUs according to their oxygenation status. Seven FaDu tumors and five CAL33 tumors were analyzed according to the protocol described. On average, 629 and 305 MCSUs per whole tumor cross-section were counted for FaDu and Cal-33, respectively.

Statistical analyses

Statistical analyses were performed using the statistical package for social sciences (SPSS, Chicago, IL, USA). Data are presented as mean values ± SEM. Linear regression analysis and Pearson's correlation coefficient, r, were used to test correlations between variables.

Results

Fig. 1 shows an example of the co-registration between 0 and 24 h of the CT (A) and PET (B) images of FaDu tumor # 7. The tumors were fixed between three pins on a coordinated multi-point fixation system and painted with CT contrast solution. These external markers (pins and tumor painting) could then be seen in the CT analysis and allowed for the precise co-registration between serial PET data. The maximum error (ε) of the co-registration of PET/CT from 0 to 24 h varied from 0.34 to 1.37. Only two tumors were excluded from the data analysis due to bad co-registration ($\varepsilon > 1.0$).

Data from standard uptake values (SUV; % injection dose/g) of [^{18}F]Fmiso at 0 and 24 h were analyzed using the original Wang model to calculate the fraction of chronic (Fig. 2A) and acute hypoxia (Fig. 2B). The quality of fitting to a Gaussian distribution for the contribution of chronic hypoxia in this example is 0.88, while the fitting of a Poisson distribution for the contribution of acute hypoxia is 0.82. The quality of primary fitting (R^2 of the Gaussian distribution) for the computation ranged from 0.62 to 0.97. The animals with bad fitting quality ($R^2 < 0.70$) were excluded from further analysis. Table 1 summarizes the co-registration errors of serial PET/CT data and the fitting quality of the Wang model data, as well as the volumes of the tumors investigated.

For comparison, tumor cryosections from the same mice were stained and analyzed for distribution patterns of hypoxia (pimonidazole), microvessel endothelium (CD31) and perfusion (Hoechst 33342) to calculate the fraction of chronic and acute hypoxia (Fig. 3). The fraction of acute hypoxia (aHF) based on MCSUs was similar for both tumor lines at 25.3 ± 3.69% for FaDu and 22.4 ± 2.50% for CAL 33. The estimated mean aHF using the Wang model analysis of serial [^{18}F]Fmiso PET/CT was significantly higher than data based on the MCSU method: 40.5 ± 3.13% for FaDu ($p = 0.008$) and 45.4 ± 3.06% for CAL33 ($p < 0.001$). In order to correct for these higher values, the original Wang model was modified for estimation based on the fraction of average contribution (Wang_{mod}). After modification, the mean aHF was reduced to 34.1 ± 2.69% for FaDu ($p = 0.077$ compared to the MCSU-based method) and to 38.4 ± 2.60% for CAL33 ($p = 0.002$ compared to the MCSU-based method).

Fig. 4 shows the comparison between the aHF based on the MCSU method and estimation using the original Wang model and the modified Wang model for each individual tumor. The differences in the aHF determined by the MCSU-based method did not correlate with the differences in the aHF assessed by either the original Wang model (FaDu: $r = 0.52$, $p = 0.23$ and CAL33: $r = 0.56$, $p = 0.19$) or the modified Wang model (FaDu: $r = 0.68$, $p = 0.21$ and CAL33: $r = 0.71$, $p = 0.18$).

Discussion

In this study, the fractions of acute and chronic hypoxia were assessed using serial [^{18}F]Fmiso PET/CT imaging data and (immuno-)fluorescence staining of cryosections. Here, the original Wang model consistently estimated larger fractions of acute hypoxia than the MCSU-based method (Fig. 4). Modification of the Wang model for the fraction of average contribution reduced the aHF values, but did not reach the values obtained using the MCSU-based method. This can be explained by the fact that the MCSU method is based on the number of microvessels surrounded by either acute or chronic hypoxia (Fig. 3), while the Wang model estimates the fraction of the contribution of [^{18}F]Fmiso uptake, which has no spatial linking. Both acutely and chronically hypoxic MCSUs are similar in size and influence. For the Wang model, the weighting is dependent on the contribution of the uptake in all voxels and the "acute" MCSU has larger areas for tracer uptake than the "chronic" MCSU, leading to higher contribution of acute hypoxia to the total uptake. Thus, the estimated fraction of acute hypoxia using the Wang model will be higher than the MCSU-based method.

Additionally, only weak correlations were observed between the results of the MCSU-based method and the Wang model for both cell lines. This could again be due to the fact that the MCSU method is based on the spatial classification of vessels, while the Wang model depends on the signal contribution of the tracer uptake. The spatial heterogeneity and the non-linear uptake of the [^{18}F]Fmiso tracer make it difficult to observe a linear correlation between the results.

The poor spatial resolution of micro-PET limits its value to accurately detect tumor hypoxia, which is extremely heterogeneous. However, this heterogeneity has been shown to not only exist across the tissue, but also inside a small scale imaging voxel [16]. Additionally, similar comparisons between PET-hypoxia imaging and total hypoxia assessed after pimonidazole staining have been investigated by others and indicate that hypoxia PET can reliably quantify hypoxia in animal models. For example, significant correlations have been found between the mean [^{18}F]Fmiso PET and pimonidazole signal intensity in five human head and neck cancer xenografts [17,18]. According to Dubois et al. [19], a significant relationship between [^{18}F]Fmiso PET and pimonidazole staining qualifies this tracer as reliable for non-invasive hypoxia detection in tumors. Busk et al. [20] reported that FAZA PET-based hypoxia imaging can accurately reflect the underlying microscopic reality.

One disadvantage of the quantification of subtypes of hypoxia based on the Wang model is that an exact overlap of serial PET images and precise and reproducible positioning of the tumor is required. In order to tackle this problem with minimal invasiveness,

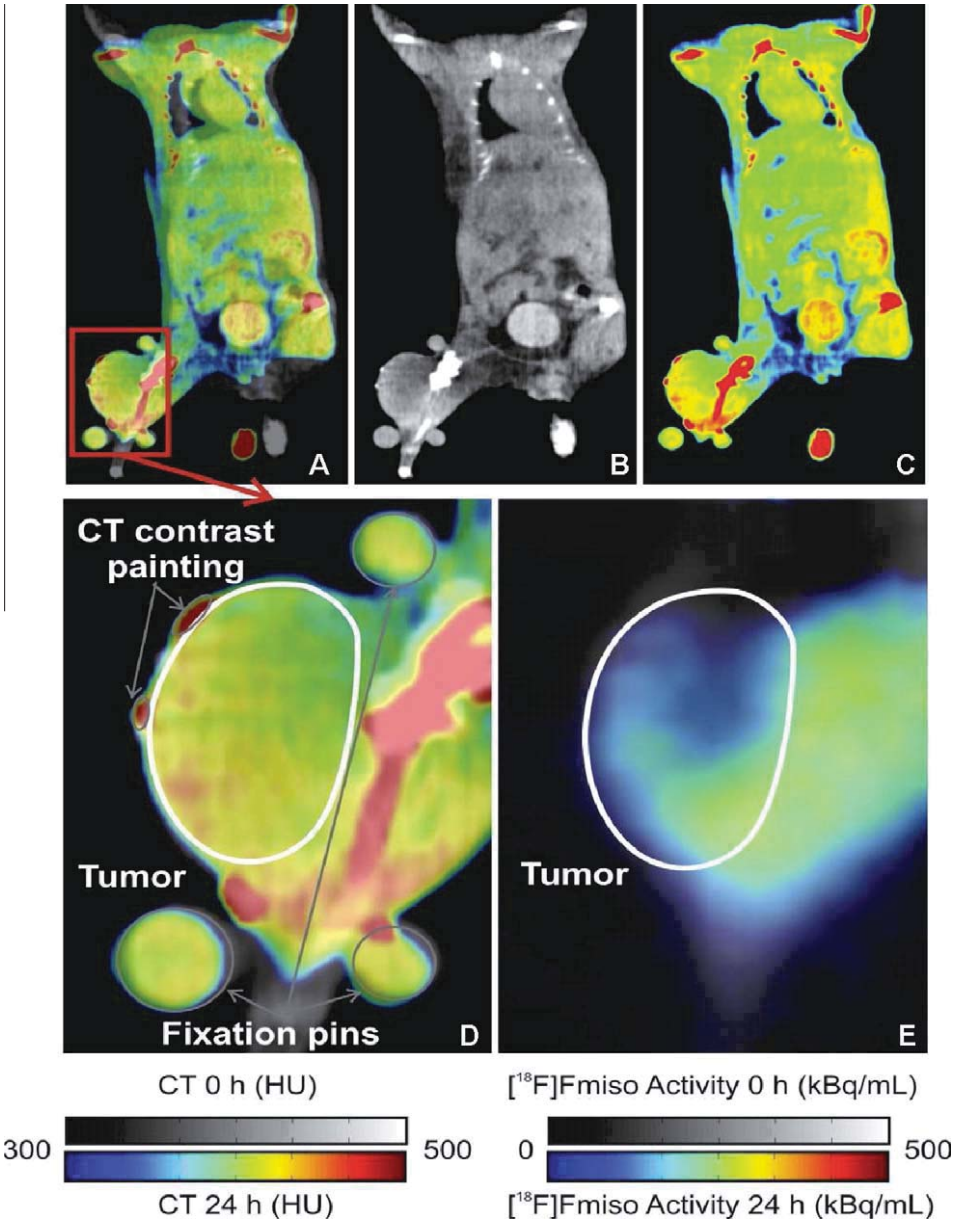

Fig. 1. Example of a co-registration between 0 and 24 h for FaDu tumor # 7. (A) Shows the fusion of the two serial CT images (0 and 24 h), (B) is the CT image at 0 h (gray scale) and (C) is the CT image at 24 h (color scale). Detailed views of the acquired over-lapped CT (D) and PET (E) images of the investigated tumor area are represented in the bottom panels. The gray contours indicate the external fixation pins and tumor skin painted with CT contrast solution, the white contour denotes the investigated tumor area.

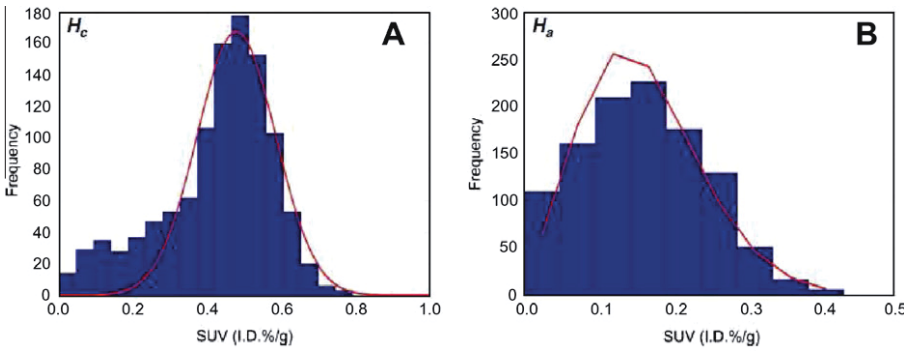

Fig. 2. Example of the Wang model fitting for FaDu tumor # 5. The distribution of the contributed SUV uptake by chronic hypoxia (H_c) was fitted to a Gaussian curve (A; $\mu = 0.48$, $\sigma = 0.11$ with $R^2 = 0.88$) and the distribution of the contributed SUV uptake by acute hypoxia (H_a) fitted to a Poisson curve (B; $\lambda = 3.20$, with $R^2 = 0.82$).

Table 1
Co-registration error values, curve fitting values (R^2), and volumes of all tumors analyzed after serial [^{18}F]Fmiso PET/CT.

Tumor line	Co-registration error (ε)	R^2 Gaussian distribution	R^2 Poisson distribution	Tumor volume (mm^3)
FaDu (1)	0.65	0.97	0.82	1255
FaDu (2)	0.50	0.73	0.76	1626
FaDu (3)	0.34	0.86	0.90	776
FaDu (4)	0.39	0.91	0.90	849
FaDu (5)	0.71	0.88	0.82	522
FaDu (6)	0.41	0.90	0.80	431
FaDu (7)	0.54	0.95	0.87	418
CAL33 (1)	0.91	0.94	0.70	140
CAL33 (2)	0.50	0.87	0.88	300
CAL33 (3)	0.84	0.97	0.95	122
CAL33 (4)	0.85	0.97	0.95	189
CAL33 (5)	0.51	0.93	0.71	99.3

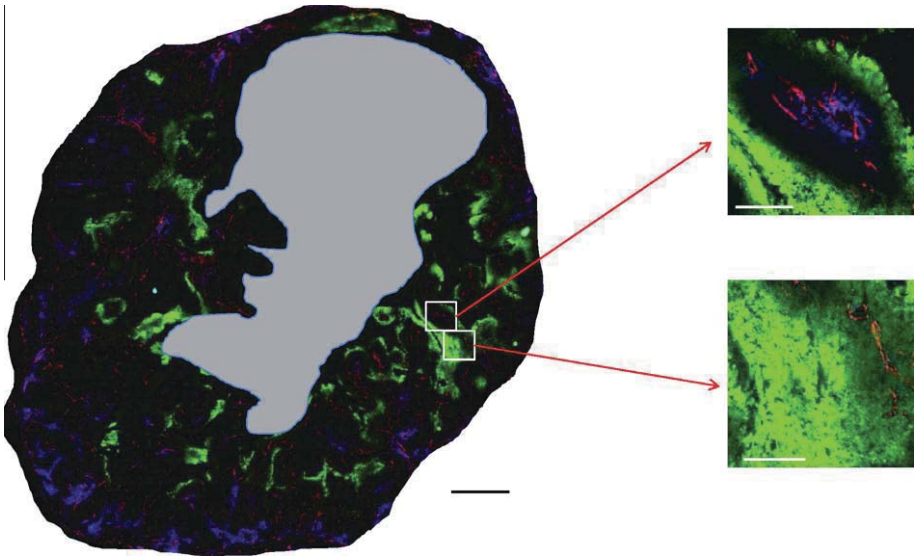

Fig. 3. (Immuno-)fluorescence staining for pimonidazole (green), CD31 (red) and Hoechst 33342 (blue) of FaDu tumor # 5. The boxes denote representative examples of chronic and acute hypoxia. The gray area represents necrosis, white bars = 200 μm, black bar = 1000 μm.

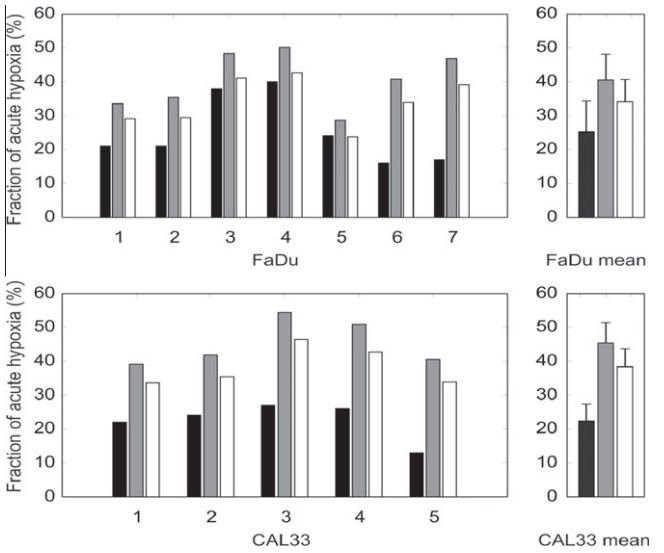

Fig. 4. Fractions of acute hypoxia assessed by the MCSU-based method (black bars), the original Wang model (gray bars) and the modified Wang model (Wang$_{mod}$; white bars) for individual FaDu (upper panel) and CAL33 tumors (lower panel). The panels on the right-hand side show the respective mean values ± SEM.

we have constructed a special fixation system containing a numbered grid to accurately position the tumor-bearing mice. Although our registration error might be increased compared to other immobilization and internal marker methods [21,22], the results are within the acceptable range concerning the intrinsic resolution (around 1.5 mm) of microPET [23].

Another disadvantage of the Wang model is that co-registration precision is hard to guarantee due to tumor growth, morphological changes or organ motions [24]. Additionally, the fitting of a histogram for the calculation of hypoxia subtypes is dependent on the number of bins and the bin frequency. Thus, this method is tumor size-dependent and should lead to better results if used on larger human tumors.

In conclusion, there was no correlation between the microscopic MCSU-based method and either the original or modified macroscopic Wang model. This lack of correlation is most-likely due to the difference between the non-linear uptake of [^{18}F]Fmiso and the spatial assessment of MCSUs. Although patient-specific adaptation of radiotherapy based on [^{18}F]Fmiso PET imaging seems to be promising, hypoxia levels change over time and with treatment (for reviews see [25,26]). Whether the Wang model can help to improve the prediction of radiation response after serial [^{18}F]Fmiso PET imaging, needs to be confirmed in experimental and clinical studies.

Conflict of interest

No conflict of interest declared by the authors.

Acknowledgments

This study has been supported in part by a Grant from the Bundesministerium für Bildung und Forschung (BMBF: 01EZ0826). The authors would like to thank Dr. K. Wang for help with interpretation and implementation of the Wang model.

References

[1] Bayer C, Shi K, Astner ST, Maftei C-A, Vaupel P. Acute versus chronic hypoxia: why a simplified classification is simply not enough. Int J Radiat Oncol Biol Phys 2011. doi:10.1016/j.ijrobp.2011.02.049.
[2] Thomlinson RH, Gray I. The histological structure of some human lung cancers and the possible implications for radiotherapy. Br J Cancer 1955;9:539–49.
[3] Brown JM. Evidence for acutely hypoxic cells in mouse tumours, and a possible mechanism of reoxygenation. Br J Radiol 1979;52:650–6.
[4] Chaplin DJ, Durand RE, Olive PL. Acute hypoxia in tumors: implications for modifiers of radiation effects. Int J Radiat Oncol Biol Phys 1986;12:1279–82.
[5] Dewhirst MW, Kimura H, Rehmus SWE, et al. Microvascular studies on the origins of perfusion-limited hypoxia. Br J Cancer 1996;74:S247–51.
[6] Cairns RA, Kalliomaki T, Hill RP. Acute (cyclic) hypoxia enhances spontaneous metastasis of KHT murine tumors. Cancer Res 2001;61:8903–8.
[7] Masunaga S, Matsumoto Y, Hirayama R, et al. Significance of manipulating intratumor hypoxia in the effect on lung metastases in radiotherapy, with reference to its effect on the sensitivity of intratumor quiescent cells. Clin Exp Metastasis 2009;26:693–700.
[8] Masunaga S, Matsumoto Y, Kashino G, et al. Significance of manipulating tumour hypoxia and radiation dose rate in terms of local tumour response and lung metastatic potential, referring to the response of quiescent cell populations. Br J Radiol 2010;83:776–84.
[9] Martinive P, Defresne F, Bouzin C, et al. Preconditioning of the tumor vasculature and tumor cells by intermittent hypoxia: implications for anticancer therapies. Cancer Res 2006;66:11736–44.
[10] Ruggieri P. Hypofractionation in non-small cell lung cancer (NSCLC): suggestions from modelling both acute and chronic hypoxia. Phys Med Biol 2004;49:4811–23.
[11] Maftei CA, Bayer C, Shi K, Astner ST, Vaupel P. Quantitative assessment of hypoxia subtypes in microcirculatory supply units of malignant tumors using (immuno-)fluorescence techniques. Strahlenther Onkol 2011;187:260–6.
[12] Maftei CA, Bayer C, Shi K, Astner ST, Vaupel P. Changes in the fraction of total hypoxia and hypoxia subtypes in human squamous cell carcinomas upon fractionated irradiation: Evaluation using pattern recognition in microcirculatory supply units. Radiother Oncol 2011. doi:10.1016/j.radonc.2011.05.023.
[13] Wang K, Yorke E, Nehmeh SA, Humm JL, Ling CC. Modeling acute and chronic hypoxia using serial images of ^{18}F-FMISO PET. Med Phys 2009;36:4400–8.
[14] Arteel GE, Thurman RG, Yates JM, Raleigh JA. Evidence that hypoxia markers detect oxygen gradients in liver: pimonidazole and retrograde perfusion of rat liver. Br J Cancer 1995;72:889–95.
[15] Ljungkvist AS, Bussink J, Rijken PF, et al. Vascular architecture, hypoxia, and proliferation in first-generation xenografts of human head-and-neck squamous cell carcinomas. Int J Radiat Oncol Biol Phys 2002;54:215–28.
[16] Petit SF, Dekker ALAJ, Seigneuric R, et al. Intra-voxel heterogeneity influences the dose prescription for dose-painting with radiotherapy: a modelling study. Phys Med Biol 2009;54:2179–96.
[17] Troost EG, Laverman P, Philippens ME, et al. Correlation of [^{18}F]FMISO autoradiography and pimonidazole [corrected] immunohistochemistry in human head and neck carcinoma xenografts. Eur J Nucl Med Mol Imaging 2008;35:1803–11.
[18] Troost EG, Laverman P, Kaanders JHAM, et al. Imaging hypoxia after oxygenation-modification: Comparing [^{18}F]FMISO autoradiography with pimonidazole immunohistochemistry in human xenograft tumors. Radiother Oncol 2006;80:157–64.
[19] Dubois L, Landuyt W, Haustermans K, et al. Evaluation of hypoxia in an experimental rat tumour model by [(18)F]fluoromisonidazole PET and immunohistochemistry. Br J Cancer 2004;91:1947–54.
[20] Busk M, Horsman MR, Jakobsen S, et al. Can hypoxia-PET map hypoxic cell density heterogeneity accurately in an animal tumor model at a clinically obtainable image contrast? Radiother Oncol 2009;92:429–36.
[21] Zhang M, Huang M, Le C, et al. Accuracy and reproducibility of tumor positioning during prolonged and multi-modality animal imaging studies. Phys Med Biol 2008;53:5867–82.
[22] Cho H, Ackerstaff E, Carlin S, et al. Noninvasive multimodality imaging of the tumor microenvironment: registered dynamic magnetic resonance imaging and positron emission tomography studies of a preclinical tumor model of tumor hypoxia. Neoplasia 2009;11:247–59.
[23] Disselhorst JA, Brom M, Laverman P, et al. Image-quality assessment for several positron emitters using the NEMA NU 4–2008 standards in the Siemens Inveon small-animal PET scanner. J Nucl Med 2010;51:610–7.
[24] Langen KM, Jones DT. Organ motion and its management. Int J Radiat Oncol Biol Phys 2001;50:265–78.
[25] Thorwarth D, Alber M. Implementation of hypoxia imaging into treatment planning and delivery. Radiother Oncol 2010;97:172–5.
[26] Troost EGC, Schinagl DAX, Bussink J, Oyen WJG, Kaanders JHAM. Clinical evidence on PET-CT for radiation therapy planning in head and neck tumours. Radiother Oncol 2010;96:328–34.

4. Maftei CA, Bayer C, Shi K, Vaupel P. Intra- and intertumor heterogeneities in total, chronic, and acute hypoxia in xenografted squamous cell carcinomas: Detection and quantification using (immuno-)fluorescence techniques. Strahlenther Onkol 2012;188:606-615.

Strahlenther Onkol 2012 · 188:606–615
DOI 10.1007/s00066-012-0105-4
Received: 24. January 2012
Accepted: 8. March 2012
Published online: 14. Juni 2012

C.-A. Maftei[1] · C. Bayer[1] · K. Shi[2] · P. Vaupel[1]
[1] Department of Radiotherapy and Radiation Oncology, Klinikum rechts der Isar, Technische Universität München, Munich
[2] Department of Nuclear Medicine, Klinikum rechts der Isar, Technische Universität München, Munich

Intra- and intertumor heterogeneities in total, chronic, and acute hypoxia in xenografted squamous cell carcinomas

Detection and quantification using (immuno-)fluorescence techniques

Head and neck cancers often contain hypoxic regions, which are unevenly distributed throughout the tumor mass [12, 22, 25, 38]. Oxygen concentrations below 1%, in turn, can lead to the development of an aggressive phenotype and to limitations in the efficacy of oxygen-dependent treatment modalities, such as standard radiotherapy, some chemotherapy, immunotherapy, and photodynamic therapy through direct and indirect mechanisms [29, 30, 33, 34].

Hypoxia in tumors is traditionally classified into two subtypes: chronic and acute. *Chronic hypoxia*, also known as diffusion-limited hypoxia, was first described by Thomlinson and Gray [27]. It has been assumed to be principally caused by limitations in oxygen diffusion from microvessels into the surrounding tumor area. The existence of *acute hypoxia* or perfusion-limited hypoxia was first discussed by Brown [8] and experimentally verified by Chaplin et al. [10]. According to Chaplin et al., acute hypoxia is mainly caused by temporary, local disturbances in perfusion or strong variations in red blood cell flux. There are great differences in the pathophysiology and biological/clinical consequences of chronic and acute hypoxia [5, 6, 31]. Therefore, it is paramount to distinguish between the two hypoxia subtypes in experimental and clinical oncology.

Detection of tumor hypoxia in experimental settings and in human tumors can be achieved using various techniques [1, 3, 4, 11, 26, 38] such as the use of O_2-sensitive microsensors, detection of nitroimidazole adducts in tissue sections, and PET-imaging using radioactive tracers (e.g., nitroimidazoles and copper compounds). Some of the methods that can distinguish between acute (fluctuating) and chronic (stable) hypoxia include the window chamber preparation [23], FACS analysis after dual perfusion marker injection [10], laser Doppler flowmetry [36], paired survival curve analysis [24], electron paramagnetic resonance imaging (EPRI) [43], ^{19}F MRI (magnetic resonance imaging) [19], serial [^{18}F]Fmiso PET/CT imaging combined with mathematical modeling [7, 18, 44], and (immuno-)fluorescence techniques [15, 16].

The experimental approach used in the present study utilizes staining patterns of hypoxia (pimonidazole), perfusion (Hoechst 33342), and microvascular endothelium (CD31) in tumor cryosections to assess total, chronic, and acute hypoxia. Using this method, each microcirculatory supply unit (MCSU = vital tumor tissue area supplied by a microvessel) in a tumor cross-section is first categorized into either normoxic, chronically hypoxic, or acutely hypoxic and thereafter quantitatively assessed [16]. Ex vivo staining of nitroimidazole adducts in experimental tumors is often analyzed in a single central slice of the tumor only [9, 15, 16, 17, 18, 41, 45]. However, the microenvironment in the center of a tumor may not be necessarily representative of the whole tumor. Therefore, we investigated whether analysis of one central section is representative for the whole tumor and whether different volumes have an impact on the tumor oxygenation status. For this, the fractions of total, chronic, and acute hypoxia were assessed in cryosections throughout different layers of tumors of varying volumes.

Using these (immuno-)fluorescence techniques, significant intra- and intertumor heterogeneities were found. Thus, data obtained from single central sections are not necessarily representative for the entire tumor, especially when considering tumors of substantially different volumes.

Material and methods

Tumor lines

The established FaDu human hypopharyngeal squamous cell carcinoma line (American Type Culture Collection, Rockville, MD, USA) was used for xe-

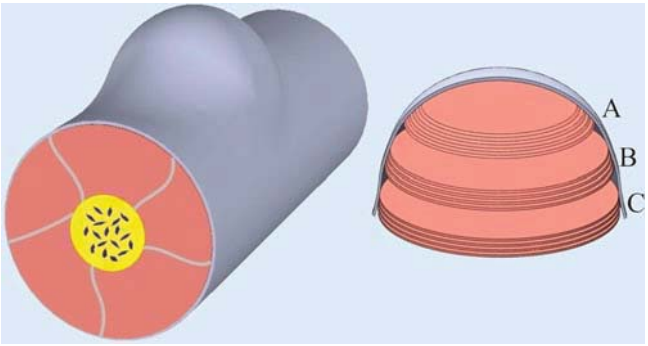

Fig. 1 ▲ Sketch representing the subcutaneous tumor location on the hind leg (*left*) and tumor tissue slicing (*right*). *A* represents the apical tissue block, *B* the central tissue block, and *C* the basal tissue block (closest to the muscle layer). From each tissue block, 4 serial, 10 µm cryosections were processed

nografting in nude mice. For detailed information concerning the mouse model see [18, 41]. In brief, 1 mm^3 tumor pieces were transplanted subcutaneously into the hind leg of anesthetized NMRI nu/nu mice (Charles River, Sulzfeld, Germany). In order to completely suppress the residual immune system (NK cells), mice were whole-body irradiated with 4 Gy (200 kV X-rays, 0.5 mm Cu filter, 1 Gy/min), 2–3 days before tumor transplantation using the Gulmay RS 225 A (Gulmay Medical Ltd, Camberley, UK) device. To prevent any bacterial infection, mice received 40 mg/l ciprofloxacin (Fresenius Kabi, Bad Homburg, Germany) in their drinking water for 10 days, starting on the day of whole-body irradiation. Measurements of tumor volume were performed (in three dimensions) twice per week by ultrasound using a Logiq-5 device (GE Healthcare, Solingen, Germany). Tumor volumes were determined by the formula of a rotational ellipsoid: ($V = \pi/6 \bullet abc$). The mouse experiments described here have been approved according to German animal welfare regulations (approval no. 55.2–1-54-2531-52-07; District Government of Upper Bavaria).

Histology

The hypoxia marker pimonidazole (Hypoxyprobe, Burlington, MA, USA) was injected into the tail vein at a concentration of 100 mg/kg body weight in 50 µl saline 2 h before animal sacrifice, and the perfusion marker Hoechst 33342 (Sigma, Deisenhofen, Germany) was given i.v. at a concentration of 15 mg/kg body weight in a volume of 50 µl saline 1 min before tumor-bearing mice were sacrificed. Immediately thereafter, the tumors were excised, embedded in O.C.T. compound (Sakura, Alphen aan den Rijn, Netherlands), frozen on dry ice, and stored at −80 °C until cryosections were processed [18, 42].

Each tumor was sliced into three tissue blocks A–C (**Fig. 1**, right). Within these tissue blocks, four 10 µm thick serial sections were processed. The apical tissue block is farthest from the muscle layer, the central tissue block is from the middle, and the basal tissue block is next to the muscle layer. Before staining, cryosections were fixed in cold acetone (4 °C), air dried, and rehydrated in PBS. Pimonidazole was stained with the Mab FITC-labeled anti-pimonidazole antibody (Hypoxyprobe, Burlington, MA, USA) diluted 1:50 in primary antibody diluent (PAD, Serotec, Oxford, U.K.) by incubating for 1 h at 37 °C in the dark [2, 14]. Microvascular endothelium was stained using the purified rat anti-mouse CD31 antibody (MEC 13.3, BD PharMingen, Heidelberg, Germany) diluted 1:100 in PAD. Anti-CD31 was detected using the secondary antibody AlexaFluor 594 (Invitrogen, Eugene, OR, USA) diluted 1:200 in PBS for 1 h at 37 °C in the dark. The cryosections were then embedded in fluorescent mounting medium (DAKO, Glostrup, Denmark) and stored at 4 °C [16, 17, 18].

Necrotic tissue areas were detected by removing the cover slip of the slices previously used for (immuno-)fluorescence staining, followed by staining with hematoxylin and eosin, and exclusion of necrotic tissue area from the analysis [18].

Microcirculatory supply units

The fractions of normoxia (normoxic MCSUs), chronic hypoxia (chronically hypoxic MCSUs), and acute hypoxia (acutely hypoxic MCSUs) were quantified in microcirculatory supply units (MCSUs) as reported earlier [15, 16, 17, 18]. A MCSU is defined as the vital tumor tissue area supplied by a microvessel. MCSUs were quantified in whole tumor cross-sections, which were scanned and photographed using the AxioVision 4.7 and the multidimensional and mosaix modules (Zeiss, Jena, Germany). The pictures obtained were visually evaluated by two independent researchers (C.B., C.M.) by categorizing MCSUs according to their perfusion and oxygenation status. On average, 451 MCSUs were analyzed per serial section in tissue block A, 579 MCSUs in tissue block B, and 609 MCSUs in tissue block C. The rising numbers reflect increasing areas from top to bottom, due to the shape of the tumors.

For calculation of the vital tissue fraction, necrotic regions were first outlined on digital images of whole tumor cross-sections. The number of pixels in necrotic and total tumor areas were quantified using Adobe Photoshop CS4 extended, version 11.0.1. Vital tissue areas were assessed by subtracting the necrotic area from the total tumor area. The vital tumor fraction was calculated by dividing the vital tumor area by the total tumor area.

Statistical analyses

Statistical analyses were performed using the statistical package for social sciences (SPSS, Chicago, IL, USA). Data are presented as mean values ± SEM. The student's t-test was used to evaluate differences between serial sections, between tissue blocks within a single tumor and between tumors of increasing volumes.

Results

In this study, we assessed intra- and intertumor heterogeneities of total, chronic and acute hypoxia in vital tumor tissue of xenografted FaDu tumors of different volumes (FaDu1, V = 477 mm^3; FaDu2, V = 442 mm^3; FaDu3, V = 263 mm^3; Fa-

Abstract · Zusammenfassung

Strahlenther Onkol 2012 · 188:606–615 DOI 10.1007/s00066-012-0105-4

C.-A. Maftei · C. Bayer · K. Shi · P. Vaupel

Intra- and intertumor heterogeneities in total, chronic, and acute hypoxia in xenografted squamous cell carcinomas. Detection and quantification using (immuno-)fluorescence techniques

Abstract

Background. Heterogeneously distributed hypoxia is a major characteristic of solid tumors. (Immuno-)fluorescence detection of hypoxia in experimental tumors is frequently assessed in a single central section; however, this may not necessarily be representative of the whole tumor. In order to determine whether analysis of one central section is exemplary of the whole tumor and whether different volumes have an impact on tumor oxygenation, we assessed the fractions of total (TH), chronic (CH), and acute hypoxia (AH) throughout different layers of tumors of varying volumes.

Materials and methods. Xenografted FaDu human squamous cell carcinomas of different volumes were investigated for intra- and intertumor heterogeneities. Tissue blocks located at the apical, central, and basal layer were sliced from individual tumors. Four serial cryosections were analyzed from each tissue block. Vital tumor tissue was explored for the distribution of Hoechst 33342 (perfusion), pimonidazole (hypoxia), and CD31 (endothelium) to assess TH, CH, and AH.

Results. Fractions of TH, CH, and AH were consistently similar in the serial sections of individual tissue blocks. However, significant differences were found between the apical, central, and basal blocks that were even opposite depending on the tumor volume. Pooled data from all three tissue blocks revealed significantly higher fractions of hypoxia in the large tumors than in the small tumors.

Conclusion. FaDu tumors exhibit a heterogeneous and volume-dependent oxygenation status. Assessing the average fractions of TH, CH, and AH from central blocks corresponds best to the average of the entire tumor. However, information on intratumor heterogeneities is lost, especially when considering tumors of substantially different volumes.

Keywords

Neoplasms · Hypoxia · Hypoxia subtypes · Oxygenation heterogeneities · Microcirculatory supply unit

Intra- und intertumorale Heterogenitäten totaler, chronischer und akuter Hypoxie in xenotransplantierten Plattenepithelkarzinomen. Nachweis und Quantifizierung mittels (Immun-)fluoreszenz

Zusammenfassung

Hintergrund. Heterogen verteilte Hypoxieareale sind ein Charakteristikum solider Tumoren. Der Sauerstoffmangel im Gewebe kann mit (Immun-)Fluoreszenz erfasst und Subtypen analysiert werden, wobei in der Regel Schnitte aus dem Tumorzentrum Verwendung finden. Diese Querschnitte sind möglicherweise nicht repräsentativ für den Gesamttumor. Um dies zu überprüfen, wurden die Anteile der totalen (TH), chronischen (CH) und akuten Hypoxie (AH) in verschiedenen Schichten unterschiedlich großer Tumoren untersucht.

Material und Methoden. Intra- und intertumorale Heterogenitäten der Oxygenierung wurden in xenotransplantierten FaDu-Plattenepithelkarzinomen ermittelt. Hierzu wurde aus den jeweiligen Tumoren zunächst ein apikaler, zentraler und basal gelegener Gewebeblock entnommen, aus dem wiederum jeweils vier serielle Kryoschnitte für eine weitergehende Analyse aufgearbeitet wurden. Anhand der Perfusionsverteilung (Hoechst-33342-Fluoreszenz), einer Hypoxiedetektion (mit Pimonidazol) und Gefäßnachweisen (mit CD 31) erfolgte in diesen Kryoschnitten eine Quantifzierung der TH-, CH- und AH-Fraktionen.

Ergebnisse. Die TH-, CH- und AH-Anteile waren in den Serienschnitten der individuellen Gewebeblöcke durchaus vergleichbar. Ein Vergleich der apikalen, zentralen und basalen Blöcke zeigte dagegen signifikante (z. T. gegenläufige, volumenabhängige) Unterschiede. Gepoolte Daten aller untersuchten Gewebeblöcke weisen daraufhin, dass die Hypoxie mit ansteigendem Tumorvolumen zunimmt.

Schlussfolgerung. FaDu-Tumoren zeigen eine heterogene Gewebeoxygenierung, so dass die TH-, CH- und AH-Anteile, die anhand von Einzelschnitten ermittelt wurden, nicht zwangsläufig repräsentativ für den Gesamttumor sind, vor allem bei der Beurteilung von Tumoren unterschiedlicher Größe. Die mittleren Fraktionen der Hypoxiesubtypen aus dem Zentralblock entsprechen weitgehend den jeweiligen Fraktionen des gesamten Tumors, jedoch gehen bei der Mittelung Informationen zur intratumoralen Heterogenität verloren.

Schlüsselwörter

Neoplasien · Hypoxie · Hypoxiesubtypen · Heterogene Oxygenierung · Mikrozirkulatorische Versorgungseinheit

Du4, V = 175 mm^3; FaDu5, V = 163 mm^3). For this, frozen tumors were sliced into three tissue blocks situated at the apical, central, and basal area of the tumor (**Fig. 1**, *right*). From each of these three tissue blocks, four serial sections were analyzed. Total hypoxia and hypoxia subtypes were assessed by (immuno-)fluorescence techniques and categorization of the oxygenation and perfusion status of individual MCSUs in vital tissue of xenografted tumors [15, 16, 17, 18].

Fractions of vital tumor tissue

In order to determine what effect increasing tumor volumes have on the development of necrosis within this tumor line, the fraction of vital tissue was quantitatively assessed. The amount of vital tissue was quite similar in the four serial sections of individual tissue blocks (**Fig. 2**). However, there were significant differences in vital tumor tissue between the apical, central, and basal blocks, and the smaller tumors contained a higher fraction of vital tumor tissue than the larger tumors (**Fig. 3**). The fraction of vital tumor tissue was highest in the basal tissue block (closest to the muscle layer) in the larger tumors (FaDu1 and FaDu2) and the mid-sized tumor (FaDu3), and highest in the apical tissue block

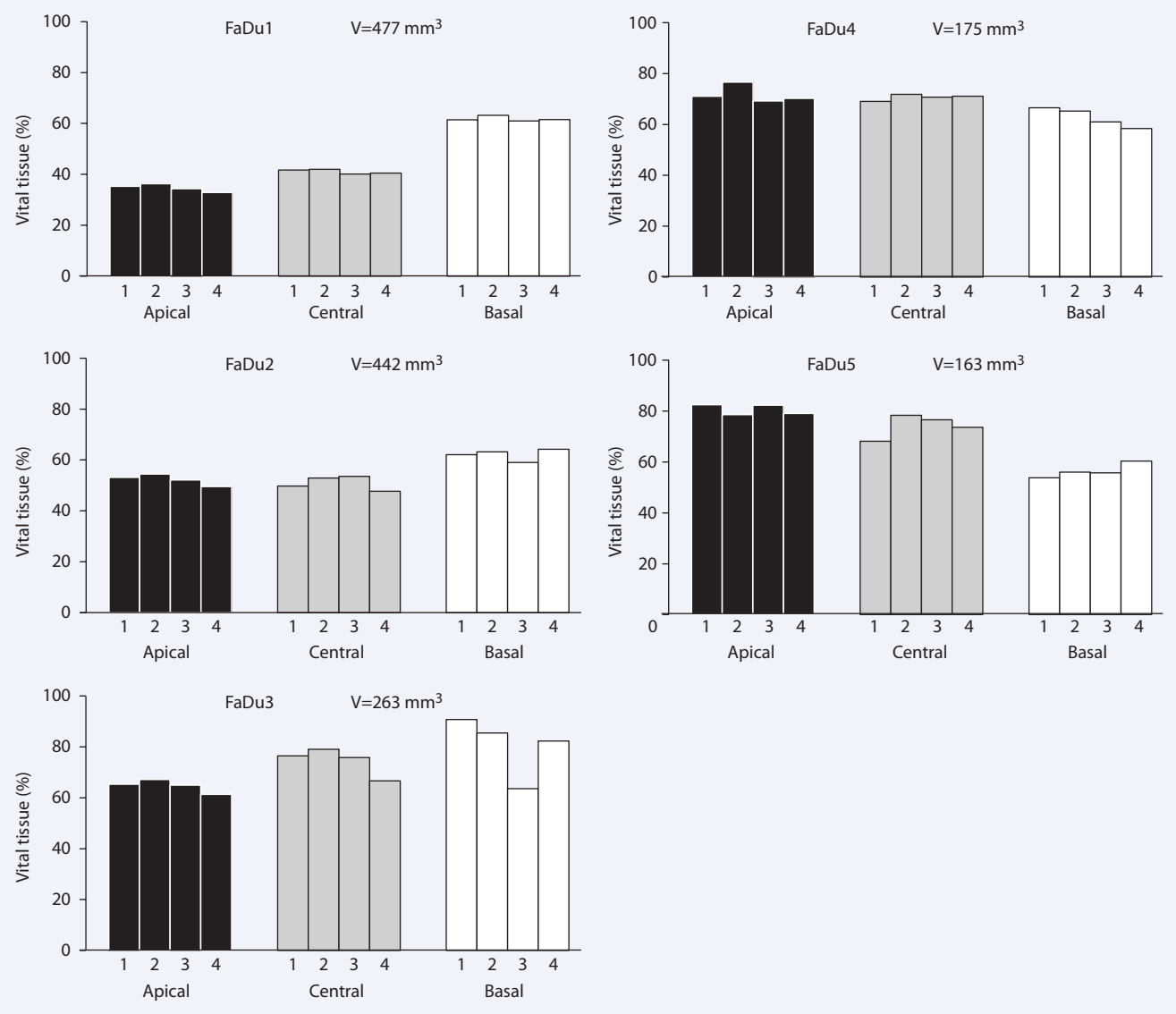

Fig. 2 ▲ Fractions of vital tumor tissue in serial cryosections of various tissue blocks. *Apical*, *central*, and *basal* indicate the location of the three different tissue blocks within the tumor. Numbers *1–4* represent the serial slices within one tissue block; *V* tumor volume

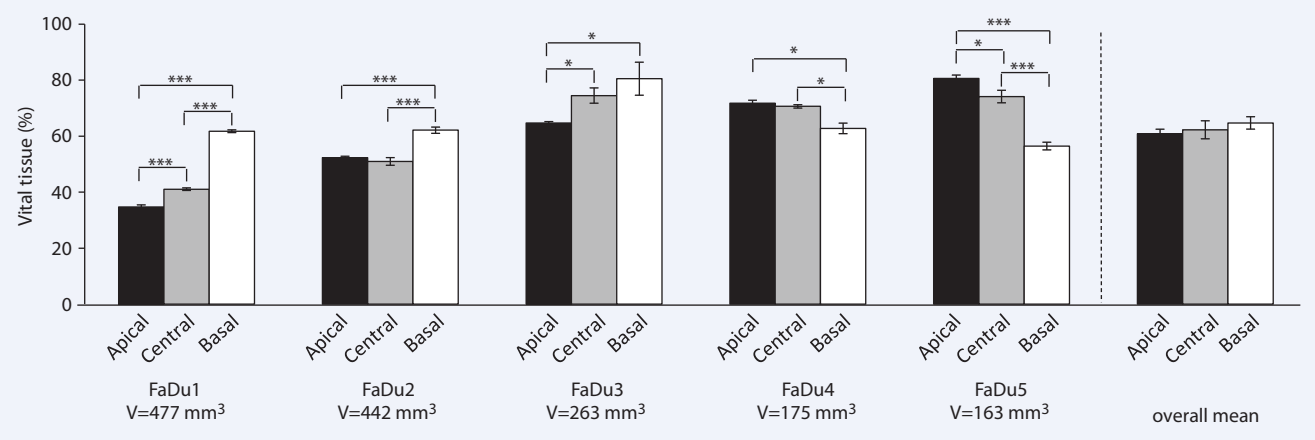

Fig. 3 ▲ Mean fractions (± SEM) of vital tumor tissue. *Apical*, *central*, and *basal* indicate the location of the three different tissue blocks within each tumor. *V* tumor volume. * $p \leq 0.05$, *** $p \leq 0.001$

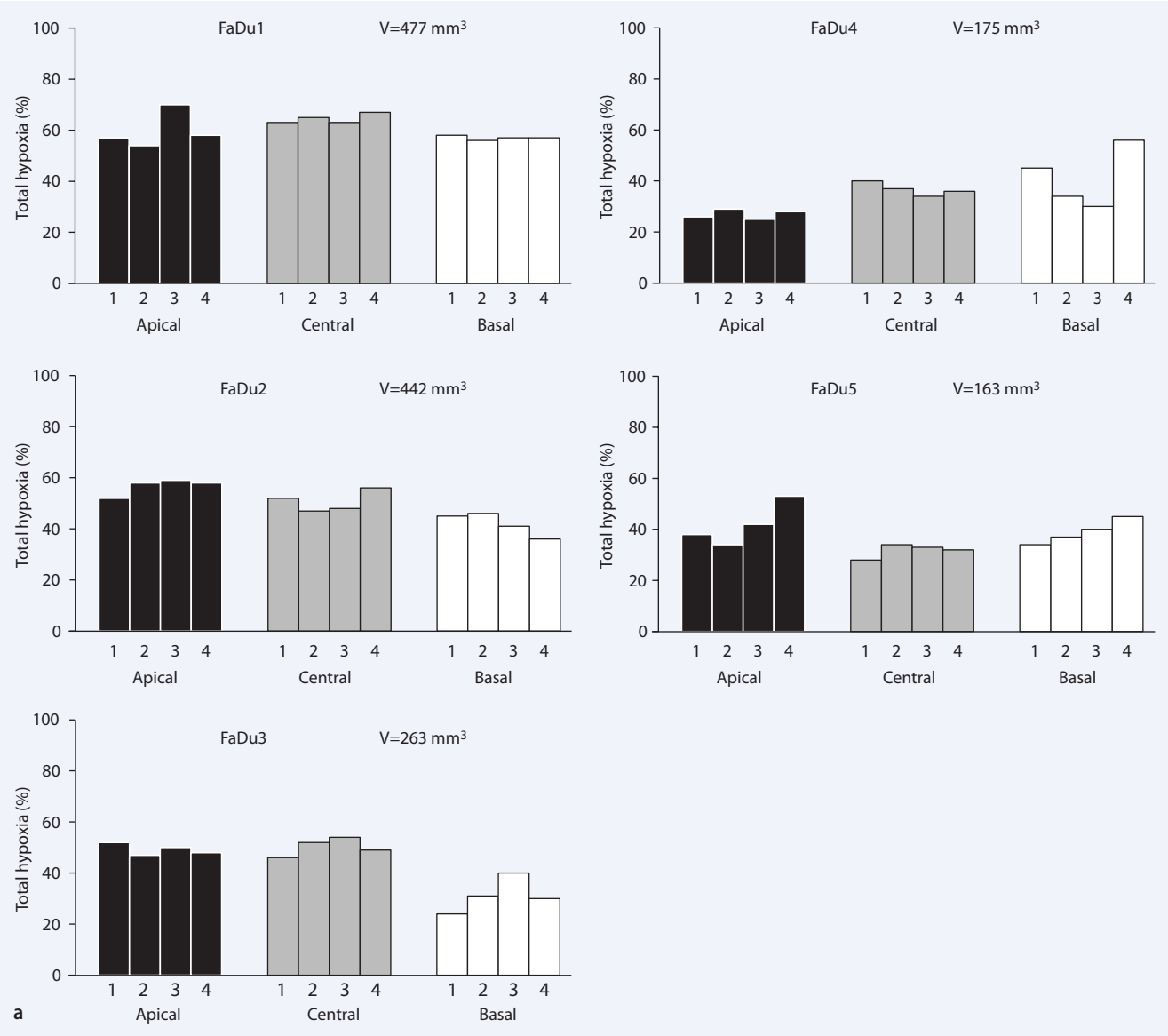

Fig. 4 ▲ Fractions of **a** total, **b** chronic, and **c** acute hypoxia in serial cryosections of vital tumor tissue. For further explanation see the legend of Fig. 2

(farthest from the muscle layer, next to the subcutis) in the smaller tumors (FaDu4 and FaDu5). Interestingly, in the apical block, there was a gradual increase in vital tissue from larger to smaller tumors. The fractions of vital tissue pooled over all tumors were comparable in the three tissue blocks. In other words, pooling data from tumors of unequal volumes and from various tissue areas leads to loss of information on distinct intra- and inter-tumor heterogeneities.

Fractions of total, chronic, and acute hypoxia

The fractions of total, chronic, and acute hypoxia in vital tumor tissue were fairly similar in the four serial sections of the individual tissue blocks (**Fig. 4**). In addition, the fractions of chronic hypoxia (38.2 ± 1.3%) were consistently higher than those of acute hypoxia (7.1 ± 0.4%). However, there were significant differences between the apical, central, and basal blocks of individual tumors (**Fig. 5,6,7**). The overall mean revealed a relatively constant fraction of total and chronic hypoxia in all three blocks (**Fig. 5,6**), whereas the overall mean for acute hypoxia was significantly lower in the basal block than in the apical and central blocks (**Fig. 7**).

After pooling data from all three tissue blocks, significant increases in the fractions of total, chronic, and acute hypoxia were observed from small to large tumors ($p \leq 0.01$ for the two largest tumors compared to the two smallest tumors; **Fig. 8**). Data pooled from the small tumors (FaDu4 and FaDu5) demonstrated a slight *increase* in the fractions of total, chronic, and acute hypoxia in the basal, compared to the apical or central blocks

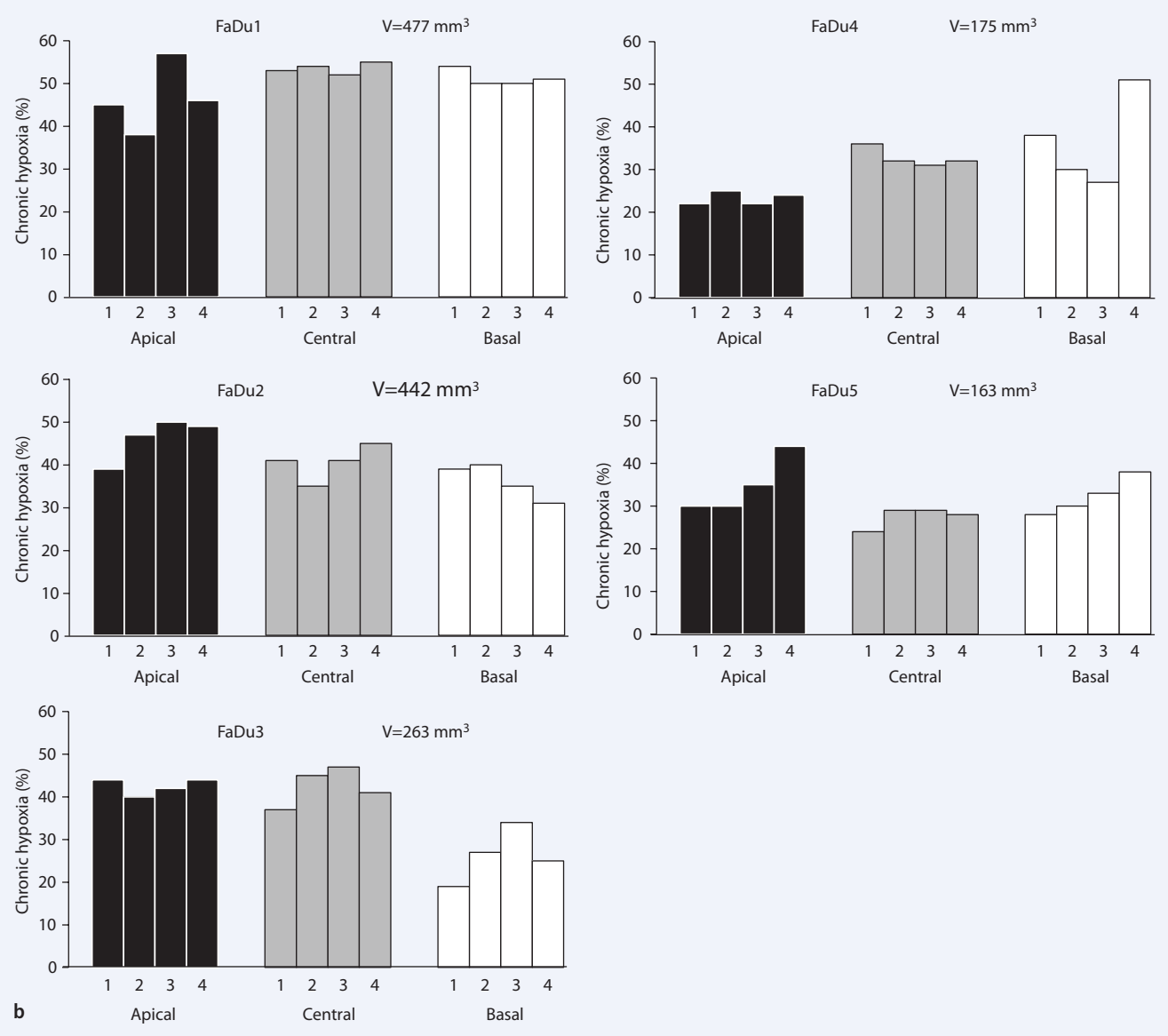

Fig. 4 ▲ Continued

(■ **Fig. 9**). Data pooled from the large and mid-sized tumors (FaDu1, FaDu2, and FaDu3) revealed a *decrease* in the fractions of total, chronic, and acute hypoxia in the basal, compared to the apical or central blocks (■ **Fig. 10**), which was significant for total and acute hypoxia ($p \leq 0.01$) Here again, information on significant intra- and intertumor heterogeneity is lost when the fractions of total, chronic, or acute hypoxia are pooled over a single tumor or tumors of different volumes.

Discussion

The goal of this study was to determine intra- and intertumor heterogeneities in the oxygenation status of xenografted FaDu squamous cell carcinomas of different volumes based on (immuno-)fluorescent techniques and quantitative assessment of total hypoxia and hypoxia subtypes in microcirculatory supply units. To our knowledge, this is the first systematic study showing distinct quantitative differences in the fraction of hypoxia subtypes in different layers of experimental tumors of different sizes.

Using the above mentioned approach, we could confirm earlier studies on experimental tumors using the polarographic oxygen microsensor technique or spectrophotometry for measuring microvascular oxyhemoglobin (HbO_2) saturation, which showed increasing tissue hypoxia with progressing tumor volumes. In iso- or allografted mouse [35] and rat tumors [20, 28, 32] as well as in xenografted human tumors [31], hypoxic areas became significantly larger with growing tumor mass. In contrast, in the clinical setting, tumor oxygenation and the extent of hypoxia were weakly dependent only on the pathological tumor stage (pT stage [13]).

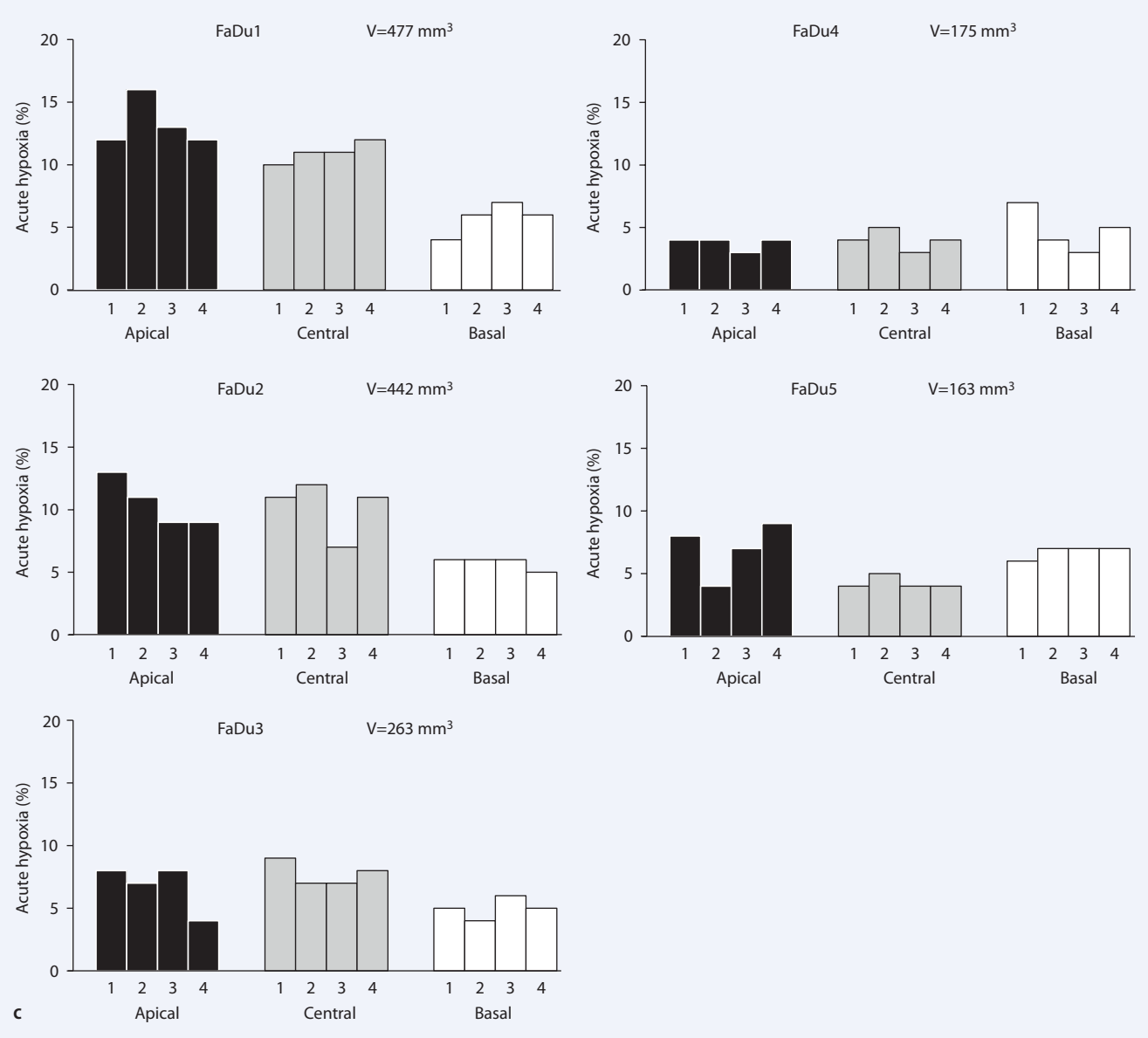

Fig. 4 ▲ Fortsetzung

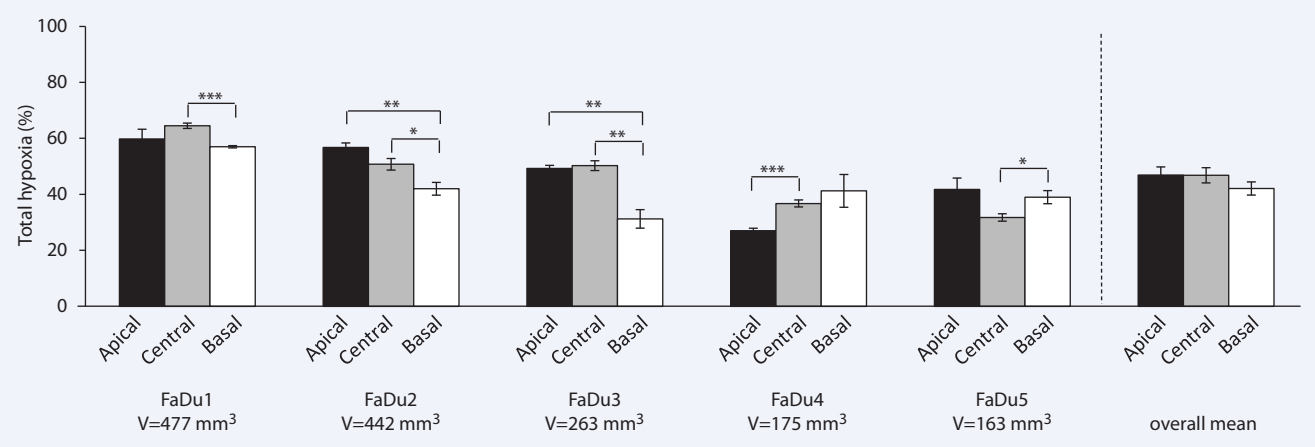

Fig. 5 ▲ Mean fractions of total hypoxia (± SEM) in vital tumor tissue. For further explanation see the legend of Fig. 3.
*p ≤ 0.05, **p ≤ 0.01, *** p ≤ 0.001

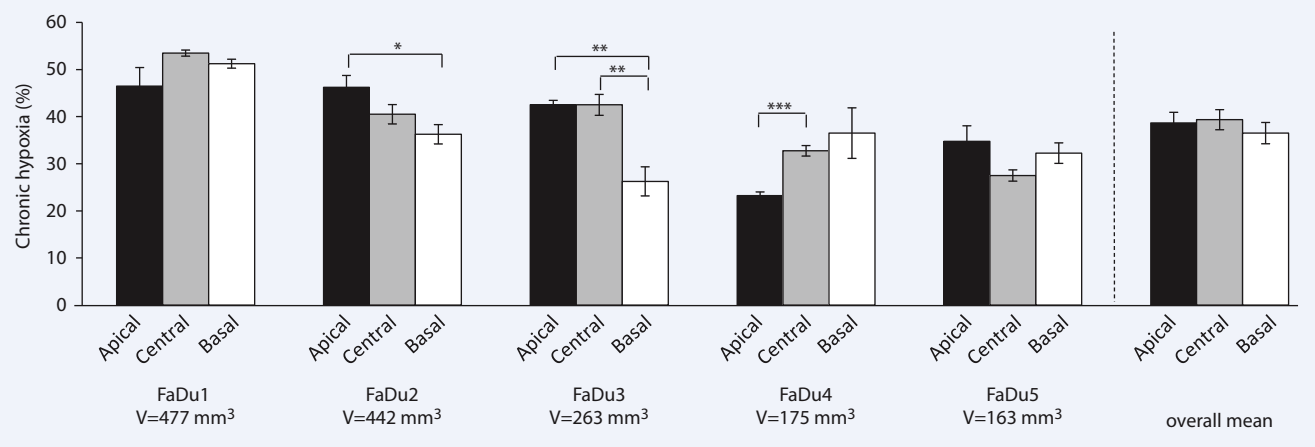

Fig. 6 ▲ Mean fractions of chronic hypoxia (± SEM) in vital tumor tissue. For further explanations see the legend of Fig. 3.
*p ≤ 0.05, **p ≤ 0.01, ***p ≤ 0.001

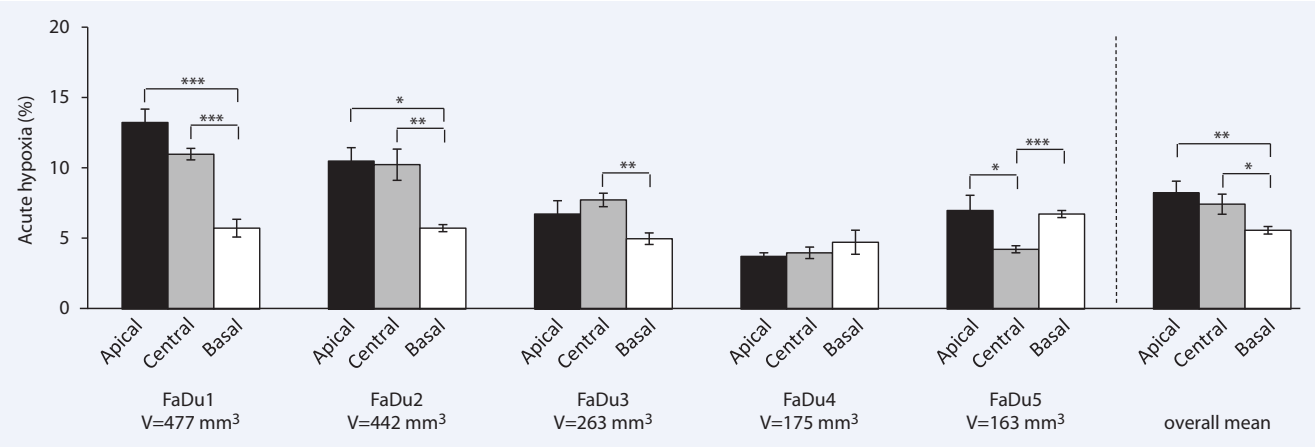

Fig. 7 ▲ Mean fractions of acute hypoxia (± SEM) in vital tumor tissue. For further explanations see the legend of Fig. 3.
*p ≤ 0.05, **p ≤ 0.01, ***p ≤ 0.001

Measurements failed to show any clear dependencies of hypoxia on clinical size or FIGO stage [13, 37]. Volume dependency of the tumor tissue oxygenation observed in the experimental setting, thus, can not be translated into the clinical setting without reservations. For this reason, most preclinical studies may serve only to detect and describe basic pathophysiological/biological and therapeutic patterns under well-defined and controlled boundary conditions that can not easily be translated to the clinical setting.

Pronounced heterogeneity in tissue oxygenation as seen in this study is a characteristic of both experimental tumors [28, 35, 39] and locally advanced cancers in the clinical setting [13, 21, 37, 40]. More centrally located hypoxic areas may prevail in abnormally large experimental tumors; however, there is no characteristic topological distribution of hypoxia within human tumors [12, 13, 39].

In addition, this study shows that large and mid-sized tumors are less hypoxic/necrotic in areas closest to the muscle layer, whereas the smaller tumors are more hypoxic/necrotic closest to the underlying skeletal musculature. Based on an earlier oxygenation study [32], we assume that smaller experimental tumors growing at the leg may receive their blood (vascular) supply mostly from the overlaying subcutis, whereas larger subcutaneous tumors (≥15% of the total body weight!) may be preferentially supplied from the muscle layer. Here again, certain limitations of subcutaneously growing tumors may become obvious.

Due to the heterogeneities described, random sampling is another problem in experimental and clinical oncology. Yaromina et al. [41] previously showed that estimation of the fraction of total hypoxia from a single section is similar to pooled data over several serial slices from the middle of the tumor. This observation is in line with our data, which shows that the fraction of total hypoxia was homogeneous between serial sections. On the other hand, we observed significant differences among the apical, central, and basal tissue blocks that were completely opposite depending on the tumor volume (**Fig. 5**). Such information will be lost when considering sections from the center of the tumor only.

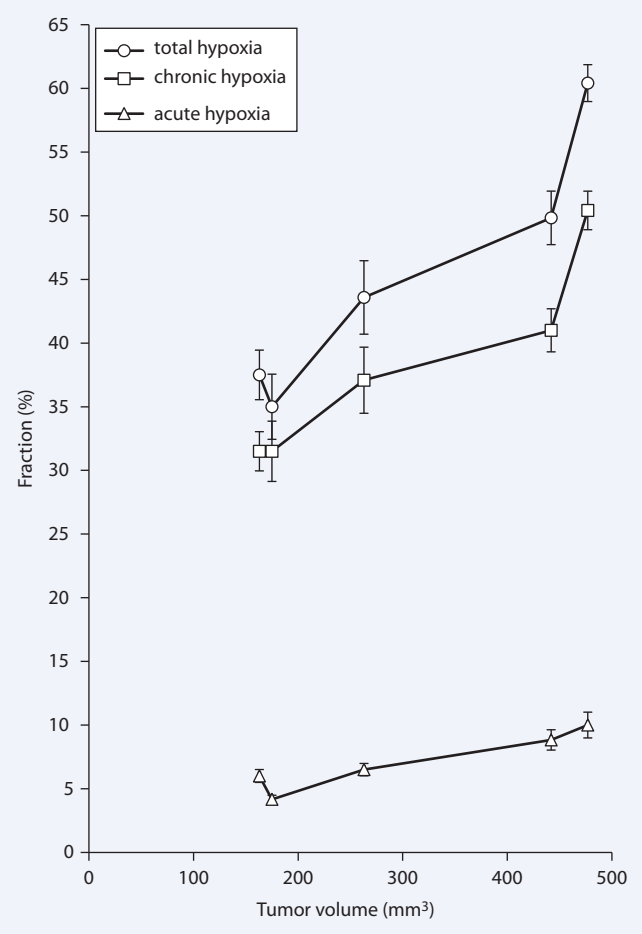

Fig. 8 ◀ Mean fractions (± SEM) of total, chronic, and acute hypoxia (pooled data) as a function of tumor volume

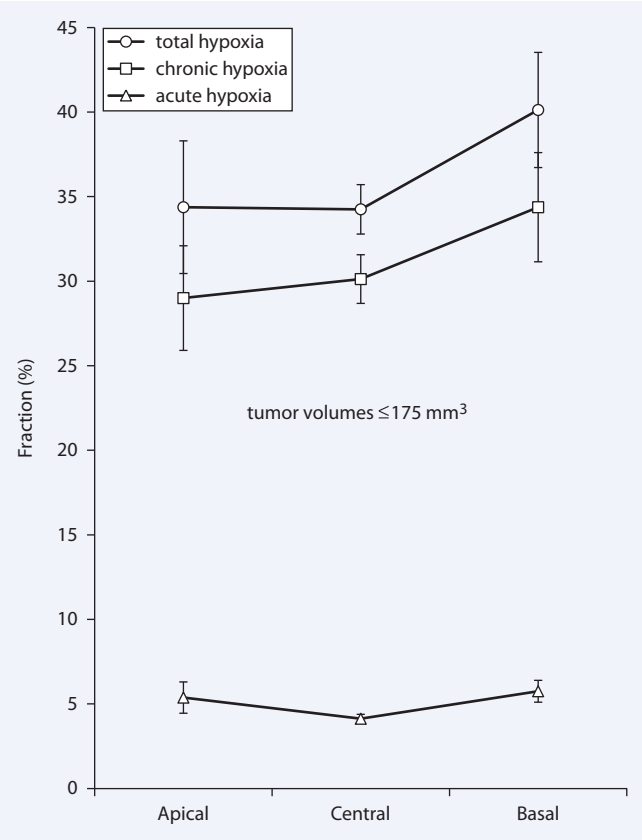

Fig. 9 ◀ Mean fractions (± SEM) of total, chronic, and acute hypoxia pooled over the smaller tumors (≤ 175 mm³) in the apical, central, and basal tissue blocks

Conclusion

The oxygenation status of FaDu tumors is heterogeneous and depends on the tumor volume. The average fractions of hypoxia from the central blocks correspond best to the average of the whole tumor. However, important information on intratumor heterogeneities is lost, especially when considering experimental, xenografted tumors of substantially different volumes. Therefore, we recommend assessing tumor oxygenation in multiple sections throughout different layers of the tumors.

Corresponding address

C. Bayer
Department of Radiotherapy and Radiation Oncology, Klinikum rechts der Isar, Technische Universität München
Ismaninger Str. 22, 81675 Munich
Germany
christine.bayer@lrz.tum.de

Conflict of interest. The corresponding author states that there are no conflicts of interest.

Acknowledgments. This work was supported by the BMBF (Bundesministerium für Bildung und Forschung; 01EZ0826).

References

1. Arabi M, Piert M (2010) Hypoxia PET/CT imaging: implications for radiation oncology. QJ Nucl Med Mol Imaging 54:500–509
2. Arteel GE, Thurman RG, Yates JM, Raleigh JA (1995) Evidence that hypoxia markers detect oxygen gradients in liver: pimonidazole and retrograde perfusion of rat liver. Br J Cancer 72:889–895
3. Astner ST, Shi K, Vaupel P, Molls M (2010) Imaging of tumor physiology: impacts on clinical radiation oncology. Exp Oncol 32:149–152
4. Bache M, Kappler M, Said HM et al (2008) Detection and specific targeting of hypoxic regions within solid tumors: current preclinical and clinical strategies. Curr Med Chem 15:322–338
5. Bayer C, Maftei CA, Astner ST et al (2010) Subtypes of chronic and acute hypoxia in tumors according to different causative mechanisms. Strahlenther Onkol 186(Suppl 1):66
6. Bayer C, Shi K, Astner ST et al (2011) Acute versus chronic hypoxia: why a simplified classification is simply not enough. Int J Radiat Oncol Biol Phys 80:965–968
7. Bayer C, Shi K, Maftei C et al (2011) Assessment of chronic and acute hypoxia in head and neck cancer using microscopic and macroscopic imaging approaches. Strahlenther Onkol 187:602
8. Brown JM (1979) Evidence for acutely hypoxic cells in mouse tumours, and a possible mechanism of reoxygenation. Br J Radiol 52:650–656

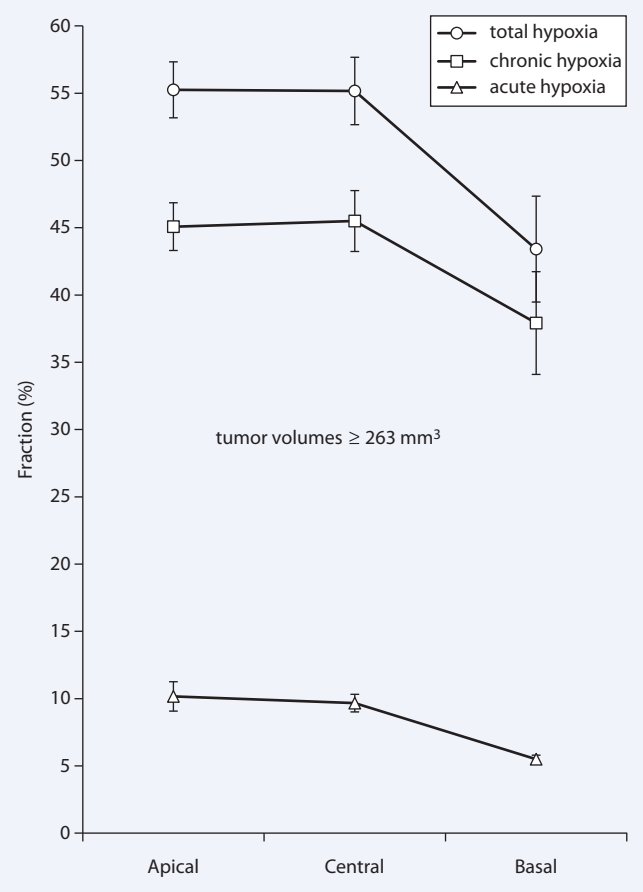

Fig. 10 ◀ Mean fractions (± SEM) of total, chronic, and acute hypoxia pooled over the larger tumors (≥ 263 mm^3) in the apical, central, and basal tissue blocks

9. Busk M, Horsman MR, Jakobsen S et al (2009) Can hypoxia-PET map hypoxic cell density heterogeneity accurately in an animal tumor model at a clinically obtainable image contrast? Radiother Oncol 92:429–436
10. Chaplin DJ, Durand RE, Olive PL (1986) Acute hypoxia in tumors: implications for modifiers of radiation effects. Int J Radiat Oncol Biol Phys 12:1279–1282
11. Chitneni SK, Palmer GM, Zalutsky MR, Dewhirst MW (2011) Molecular imaging of hypoxia. J Nucl Med 52:165–168
12. Grosu AL, Souvatzoglou M, Röper B et al (2007) Hypoxia imaging with FAZA-PET and theoretical considerations with regard to dose painting for individualization of radiotherapy in patients with head and neck cancer. Int J Radiat Oncol Biol Phys 69:541–551
13. Höckel M, Schlenger K, Knoop C, Vaupel P (1991) Oxygenation of carcinomas of the uterine cervix: evaluation by computerized O_2 tension measurements. Cancer Res 51:6098–6102
14. Ljungkvist AS, Bussink J, Rijken PF et al (2002) Vascular architecture, hypoxia, and proliferation in first-generation xenografts of human head-and-neck squamous cell carcinomas. Int J Radiat Oncol Biol Phys 54:215–228
15. Maftei CA, Bayer C, Astner ST et al (2011) Monitoring the fraction of total hypoxia and hypoxia subtypes in human squamous cell carcinomas during fractionated irradiation: evaluation using pattern recognition in microcirculatory supply units. Strahlenther Onkol 187(Suppl 1):25
16. Maftei CA, Bayer C, Shi K et al (2011) Quantitative assessment of hypoxia subtypes in microcirculatory supply units of malignant tumors using (immuno-)fluorescence techniques. Strahlenther Onkol 187:260–266
17. Maftei CA, Bayer C, Shi K et al (2011) Changes in the fraction of total hypoxia and hypoxia subtypes in human squamous cell carcinomas upon fractionated irradiation: evaluation using pattern recognition in microcirculatory supply units. Radiother Oncol 101:209–216
18. Maftei CA, Shi K, Bayer C et al (2011) Comparison of (immuno-) fluorescence data with serial [^{18}F]Fmiso PET/CT imaging for assessment of chronic and acute hypoxia in head and neck cancers. Radiother Oncol 99:412–417
19. Magat J, Jordan BF, Cron GO, Gallez B (2010) Noninvasive mapping of spontaneous fluctuations in tumor oxygenation using ^{19}F MRI. Med Phys 37:5434–5441
20. Manz R, Otte J, Thews G, Vaupel P (1983) Relationship between size and oxygenation status of malignant tumors. Adv Exp Med Biol 159:391–398
21. Mueller-Klieser W, Vaupel P, Manz R, Schmidseder R (1981) Intracapillary oxyhemoglobin saturation of malignant tumors in humans. Int J Radiat Oncol Biol Phys 7:1397–404
22. Nordsmark M, Bentzen SM, Rudat V et al (2005) Prognostic value of tumor oxygenation in 397 head and neck tumors after primary radiation therapy. An international multi-center study. Radiother Oncol 77:18–24
23. Reinhold HS, Blachiwiecz B, Blok A (1977) Oxygenation and reoxygenation in "sandwich" tumours. Bibl Anat 15:270–272
24. Rofstad EK, Maseide K (1999) Radiobiological and immunohistochemical assessment of hypoxia in human melanoma xenografts: acute and chronic hypoxia in individual tumors. Int J Radiat Biol 75:1377–1393
25. Stadler P, Becker A, Feldmann HJ et al (1999) Influence of the hypoxic subvolume on the survival of patients with head and neck cancer. Int J Radiat Oncol Biol Phys 44:749–754
26. Tatum J, Kelloff GJ, Gillies RJ et al (2006) Hypoxia: Importance in tumor biology, noninvasive measurement by imaging, and value of its measurement in the management of cancer therapy. Int J Radiat Biol 82:699–757
27. Thomlinson RH, Gray I (1955) The histological structure of some human lung cancers and the possible implications for radiotherapy. Br J Cancer 9:539–549
28. Vaupel P (1977) Hypoxia in neoplastic tissue. Microvasc Res 13:399–408
29. Vaupel P (2004) The role of hypoxia-induced factors in tumor progression. Oncologist 9(Suppl 5):10–17
30. Vaupel P (2009) Physiological mechanisms of treatment resistance. In: Molls M, Vaupel P, Nieder C et al (eds) The impact of tumor biology on cancer treatment and multidisciplinary strategies. Springer, Berlin-Heidelberg, pp 273–290
31. Vaupel P (2011) Acute and chronic hypoxia in the clinical setting: merely an academic discussion or do we need to distinguish between the two? Strahlenther Onkol 187:601
32. Vaupel P, Harrison L (2004) Tumor hypoxia: causative factors, compensatory mechanisms, and cellular response. Oncologist 9(Suppl 5):4–9
33. Vaupel P, Mayer A (2007) Hypoxia in cancer: significance and impact on clinical outcome. Cancer Metastasis Rev 26:225–239
34. Vaupel P, Mueller-Klieser W (1986) Cell line and growth site as relevant parameters governing tumor tissue oxygenation. Adv Exp Med Biol 200:633–643
35. Vaupel PW, Frinak S, Bicher HI (1981) Heterogeneous oxygen partial pressure and pH distribution in C3H mouse mammary adenocarcinoma. Cancer Res 41:2008–2013
36. Vaupel P, Höckel M, Mayer A (2007) Detection and characterization of tumor hypoxia using pO_2 histography. Antioxid Redox Signal 9:1221–1235
37. Vaupel P, Kluge M, Ambroz MC (1988) Laser Doppler flowmetry in subepidermal tumours and in normal skin of rats during localized ultrasound hyperthermia. Int J Hyperthermia 4:307–321
38. Vaupel P, Fortmeyer HP, Runkel S, Kallinowski F (1987) Blood flow, oxygen consumption, and tissue oxygenation of human breast cancer xenografts in nude rats. Cancer Res 47:3496–503
39. Vaupel P, Schlenger K, Knoop C, Höckel M (1991) Oxygenation of human tumors: evaluation of tissue oxygen distribution in breast cancers by computerized O_2 tension measurements. Cancer Res 51:3316–3322
40. Wendling P, Manz R, Thews G, Vaupel P (1984) Heterogeneous oxygenation of rectal carcinomas in humans: a critical parameter for preoperative irradiation? Adv Exp Med Biol 180:293–300
41. Yaromina A, Hölscher T, Eicheler W et al (2005) Does heterogeneity of pimonidazole labelling correspond to the heterogeneity of radiation-response of FaDu human squamous cell carcinoma? Radiother Oncol 76:206–212
42. Yaromina A, Zips D, Thames HD et al (2006) Pimonidazole labelling and response to fractionated irradiation of five human squamous cell carcinoma (hSCC) lines in nude mice: the need for a multivariate approach in biomarker studies. Radiother Oncol 81:122–129
43. Yasui H, Matsumoto S, Devasahayam N et al (2010) Low-field magnetic resonance imaging to visualize chronic and cycling hypoxia in tumor-bearing mice. Cancer Res 70:6427–6436
44. Wang K, Yorke E, Nehmeh SA et al (2009) Modeling acute and chronic hypoxia using serial images of ^{18}F-FMISO PET. Med Phys 36:4400–4408
45. Zoula S, Rijken PF, Peters JP et al (2003) Pimonidazole binding in C6 rat brain glioma: relation with lipid droplet detection. Br J Cancer 88:1439–1444